KU Leuven
Biomedical Sciences Group
Faculty of Pharmaceutical Sciences
Laboratory for Radiopharmacy

^{18}F-labelling of biomolecules for PET

Frederik Cleeren

Jury:

Promoter:	Prof. Dr. Guy Bormans
Co-promoter:	Prof. Dr. Alfons Verbruggen
Chair:	Prof. Dr. Arthur Van Aerschot
Jury members:	Prof. Dr. Jef Rozenski
	Dr. Tjibbe De Groot
	Dr. William J. McBride
	Prof. Dr. Vladimir Tolmachev

Dissertation presented in partial fulfilment of the requirements for the degree of Doctor in Pharmaceutical Sciences

September, 2016

Monday, September 19, 2016, 5 p.m.

Auditorium Irish College

The Leuven Institute for Ireland in Europe

Janseniusstraat 1

3000 Leuven

Promoter: Prof. Dr. Guy Bormans
Co-Promoter: Prof. Dr. Alfons Verbruggen

Laboratory for Radiopharmacy
Faculty of Pharmaceutical Sciences
Herestraat 49, O&N II, box 821
B-3000 Leuven

TABLE OF CONTENTS

DANKWOORD

Een zestal jaar geleden startte ik mijn masterthesis op het labo van Radiofarmacie, onder begeleiding van de enthousiaste Maarten Ooms en met Guy als promotor. Dankzij hen werd ik gepassioneerd door de radiochemie. Nu, 4 jaar later, is het mijn beurt om mijn doctoraat te verdedigen. Ik had hier nooit gestaan zonder de steun en hulp van velen. Daarom wil ik graag de kans grijpen om enkele bijzondere mensen te bedanken.

Guy, bedankt voor de kans die je mij hebt gegeven om te doctoreren op het labo. Je hebt me een mooi en uitdagend onderzoeksproject aangeboden. Ik heb grote bewondering voor de manier waarop je telkens opnieuw tijd maakt voor jouw doctoraatstudenten, jouw deur staat altijd open. Je kwam telkens met nieuwe ideëen om problemen op te lossen en staat open voor discussie, ik heb de afgelopen jaren ontzettend veel van je geleerd. Ik wil je ook bedanken voor het kritisch nalezen van mijn thesis, manuscripten, presentaties en zoveel meer. Bedankt voor de kans om seminaries en cursussen te volgen en de mogelijkheid om naar verschillende congressen te gaan. Dankzij jou heb ik veel aangename en interessante mensen leren kennen. Ik heb je de voorbije jaren leren kennen als een zeer intelligent, creatief en sportief persoon. Op de congressen, labweekends en andere teambuilding-activiteiten was het steeds leuk om nog een “laatste” Hoegaarden te drinken met jou.

Fons, bedankt voor het het grondig nalezen van mijn thesis, abstracts en manuscripten. Je hebt hier telkens opnieuw tijd voor vrijgemaakt in jouw drukke agenda. Dankzij jouw kritische vragen tijdens labmeetings en presentaties heb ik veel bijgeleerd.

I would like to thank my jury members Prof. Dr. Arthur Van Aerschot, Prof. Dr. Jef Rozenski, Dr. Tjibbe De Groot, Dr. William J. McBride and Prof. Dr. Vladimir Tolmachev. Their critical evaluation and comments have certainly given this thesis an additional value.

My close colleague Dr. Joan Lecina deserves a sincere *thank you*. Thanks for all the help with synthesis of chelators, characterisation of compounds with NMR, never-ending iTLC spotting in the “hotel lab” and many discussions dealing with the Al^{18}F-project. In my opinion we are an excellent team. You inspire me with your enthusiasm and dedication and I hope we can continue working together in the future. You really added an extra value to this thesis and research project. Thanks! Emilie and Ahamed: thank you for the help with the synthesis of different compounds and for the nice scientific chats.

Of course, I would like to thank all the other post-docs, PhD students and assistants of the laboratory of Radiopharmacy: Sofie, Joost, Uta, Lieven, Koen, Bala, Maxime, Daisy, Rufi, Maarten, Dieter, Pieter,

Jan and Ivan. Thank you for the wonderful times, for creating a great working environment and for the nice moments we shared in (and outside) the lab.

Julie, Jana, Ann,Tine en Peter: een dikke merci voor het inplannen en voor de hulp met het uitvoeren van de talrijke dierexperimenten. Verder wil ik ook graag Bryan bedanken voor de hulp met de celexperimenten. Andrey en Michel, bedankt voor de hulp bij de analyse van PET-beelden. Daarnaast wil ik ook mijn twee thesisstudenten Joey en Inias bedanken voor de leuke tijd en hun inzet in het labo. Ik heb er fijne herinneringen aan. Chantal, bedankt voor de hulp bij de administratie en Rita, bedankt om het labo netjes en op orde te houden. Ik wil ook iedereen bedanken van het “BOT 3 team” voor de leuke tijd tijdens de practica.

Ik wil ook graag alle mensen van de dienst nucleaire geneeskunde bedanken en dan in het bijzonder Tjibbe, Marva, Bert en Kim. Bedankt voor het inplannen van de experimenten en voor de technische steun. Ondanks jullie drukke schema waren jullie altijd vriendelijk en klaar om te helpen als er problemen waren met de cyclotron of loodkluizen.

Furthermore, I would like to thank the people from the VUB for the support with the nanobody project. Especially Catarina and Anneleen, thanks for all the help and your suggestions during the last few years.

Ook mijn beide ouders wil ik graag bedanken voor alle kansen die ik van hen heb gekregen. Ik wil jullie graag bedanken dat ik altijd op jullie steun kon rekenen.

Er zijn nog zoveel meer mensen die ik zou willen bedanken: vrienden, familie. Bedankt allemaal voor de aanmoediging, de hulp en de steun.

Nathalie, jou wil ik hier zeker ook bedanken voor het vele geduld, begrip en de vele steun die ik van jou heb gekregen! De laatste vier jaar is er veel veranderd in ons leven: we zijn getrouwd, hebben samen prachtige reizen gemaakt en hebben ons eigen huis gebouwd. Ik ben blij dat je in mijn team zit. Ik zie u echt ongeloofelijk graag en ik kijk al uit naar de ongetwijfeld fantastische tijd die nog voor ons ligt. Bedankt voor alles liefje!

Kortom, bedankt allemaal!

Frederik

LIST OF ABBREVIATIONS

%ID	Percent injected dose
%ID/g	Percent injected dose per gram
β^+	Positron
γ	Gamma ray photon
2-PMPA	2-(phosphonomethyl)pentane-1,5-dioic acid
[^{18}F]DCFPyL	2-(3-{1-Carboxy-5-[(6-[^{18}F]fluoro-pyridine-3-carbonyl)-amino]-pentyl}-ureido)-pentanedioic acid
[^{18}F]FBEM	*N*-[2-(4-[^{18}F]fluorobenzamido)ethyl]maleimide
[^{18}F]FDG	2-[^{18}F]fluoro-2-deoxy-D-glucose
[^{18}F]F-Py-TFP	6-[^{18}F]fluoronicotinic acid 2,3,5,6-tetrafluorophenyl ester
[^{18}F]SFB	N-succinimidyl 4-[^{18}F]fluorobenzoate
[^{68}Ga]Ga-PSMA-HBED-CC	[^{68}Ga]Glu-NH-CO-NH-Lys-(Ahx)-[Ga-N,N'-bis[2-hydroxy-5-(carboxyethyl)benzyl]ethylenediamine-N,N'-diacetic acid]
{Al^{18}F}$^{2+}$	Aluminium monofluoride
BFC	Bifunctional Chelator
CIA	Collagen-Induced Arthritis
CRIg	The complement receptor of the Ig superfamily
CRIg$^{-/-}$	CRIg knock out
CT	Computed Tomography
CuAAC	Copper(I)-catalyzed Huisgen [2,3]-cycloaddition between alkynes and azides
DMSO	Dimethylsulfoxide
DTPA	Diethylene triaminepentaacetic acid
EC	Electron capture
ESI	Electrospray ionization
e^+	Positron
FDA	Food and Drug Administration
GMP	Good manufacturing procedures
HPLC	High performance liquid chromatography
HRMS	High resolution mass spectrometry

HSA	Human serum albumin
IEDDA	Inverse-electron-demand Diels-Alder
IC	Internal conversion
Ig	Immunoglobulin
IT	Isomeric transition
iTLC	Instant thin layer chromatography
iTLC-SG	Instant thin layer chromatography-silica gel
LC	Liquid chromatography
mAb	Monoclonal antibody
MES	2-(*N*-morpholino)ethanesulfonic acid
MPAA	Methyl phenyl acetic acid
MMR	Macrophage mannose receptor
mRNA	Messenger ribonucleic Acid
MRI	Magnetic resonance imaging
NMR	Nuclear magnetic resonance
NODA	1,4,7-triazacyclononane-1,4-diacetate
NOTA	1,4,7-triazacyclononane-1,4,7-triacetic acid
OATP	Organic anion-transporting polypeptide
p.i.	Post injection
PBS	Phosphate buffered saline
PET	Positron emission tomography
PMT	Photomultiplier tube
Prep-HPLC	Preparative-high performance chromatography
PSA	Prostate specific antigen
PSMA	Prostate specific membrane antigen
PTFE	Polytetrafluoroethylene, teflon
QC	Quality control
RA	Rheumatoid arthritis
RESCA	Restrained complexing agent
RESCA-mal	RESCA-maleimide

RESCA-Tz	RESCA-tetrazine
rt	Room temperature
RCY	Radiochemical yield
SA	Specific activity
Scfv	Single-chain variable fragment
SIFA	Silicon-fluoride acceptors
SPECT	Single photon emission computed tomography
SUV	Standardised uptake value
TAC	Time activity curve
TAM	Tumor-associated macrophages
TCO	*trans*-cyclooctene
TLC	Thin layer chromatography
TOF-HRMS	High resolution time-of-flight mass spectrometry
Tris-HCL	Tris(hydroxymethyl)aminomethane hydrochloride
Tz	Tetrazine
V_{HH}	Heavy chain only antibody
WT	Wild-type
β^+	Positron
v	Neutrino

CHAPTER I

GENERAL INTRODUCTION

1. MOLECULAR IMAGING

Molecular imaging is a rapidly developing discipline envisaging early detection, characterisation and real-time monitoring of disease in complex biological processes of living organisms. Classical anatomy based imaging techniques, such as static x-ray imaging, magnetic resonance imaging (MRI), X-ray computed tomography (CT), and ultrasound scans are limited to detect macroscopic and anatomical abnormalities. Molecular imaging however, visualises functionality and molecular changes occurring prior to anatomic changes of tissue and organs thus providing a clear diagnostic advantage.[1] *In vivo* visualisation of biological processes at the cellular and subcellular level, within living organisms, can aid in diagnosis, follow-up of disease and direct the proper course of treatment. Moreover, molecular imaging is an important tool in research and can speed up drastically the drug development process.[2] Single photon emission computed tomography (SPECT) and positron emission tomography (PET) are the two major molecular imaging modalities within nuclear medicine.[3]

2. RADIONUCLIDE IMAGING AND THERAPY

Radionuclides are elements with an excess of nuclear energy, making them unstable. These radioisotopes either have a heavy nucleus (Z>83) or possess an imbalance in proton/neutron ratio, or are in a metastable energy state and will undergo radioactive decay. The excess of energy in the nucleus of the unstable element can result in emission of either particles (α, $\beta^{+/-}$) and/or electromagnetic radiation (gamma ray photons (γ)) and as a secondary effect X-rays, conversion electrons and Auger electrons.[4] Radionuclides occur naturally or are artificially made using nuclear reactors, cyclotrons, particle accelerators or are generated by decay of other radionuclides and obtained from radionuclide generators.[5] A rapidly expanding number of radionuclides with a broad variety of half-lives, emission types and energies for application of radionuclide imaging studies are routinely produced. **Table 1** lists the properties of radionuclides used most commonly in nuclear medicine.

The availability of a wide range of radionuclides makes it possible to carefully pick the best matching radionuclide for a certain application.[7] Depending on the decay properties of the radionuclide, it can be used for PET, SPECT and/or therapeutic applications.[8] When choosing the most suitable radionuclide for a certain application, one should not only consider the decay properties and availability of the radionuclide, it is also of great importance that the physical half-life of the radionuclide matches the biological half-life of the vector molecule.[9] This biological half-life can be in the range of minutes (small organic molecules), hours (peptides, antibody fragments) or even days

(monoclonal antibodies). Longer-lived radioisotopes should be selected when an extended time is required to achieve optimal target tissue to background ratios.

Table 1: *Selection of radionuclides frequently used in nuclear medicine for diagnosis or therapy, their properties and source. EC = electron capture, IT = isomeric transition, IC = internal conversion* [4-7]

	Radionuclide	Half-life	Decay mode (abundance in %)	E (keV)	Max. ß$^+$-range in H_2O (mm)	Production method
Radiometals	^{68}Ga	68 min	ß$^+$ (90%) EC (10%)	ß$^+E_{max}$:1899	8.9	^{68}Ge/^{68}Ga generator
	^{99m}Tc	6 h	IT (89%)	γ:141		^{99}Mo/^{99m}Tc generator
	^{64}Cu	12.7 h	ß$^+$ (18%) EC (24%) ß$^-$ (37%)	ß$^+E_{max}$:653	2.4	Cyclotron, ^{64}Ni(p,n)^{64}Cu
	^{90}Y	2.7 d	ß$^-$	ß$^-E_{max}$:2280		Nuclear reactor, ^{90}Zr(n,p)^{90}Y
	^{111}In	2.8 d	EC	γ:172, 245		Cyclotron, ^{111}Cd(p,n)^{111}In
	^{67}Ga	3.3 d	EC	γ:93, 184, 300		Cyclotron, ^{68}Zn(p,2n)^{67}Ga
	^{89}Zr	3.3 d	ß$^+$ (23%) EC (77%)	ß$^+E_{max}$:897 γ:909	3.6	Cyclotron, ^{89}Y(p,n)^{89}Zr
	^{177}Lu	6.6 d	ß$^-$	ß$^-E_{max}$:497 γ:208		Nuclear reactor, ^{176}Lu(n,γ)^{177}Lu
	^{223}Ra	11.4 d	α	E_{max}:5850		^{227}Ac/^{223}Ra generator
Radiohalogens	^{18}F	109.8 min	ß$^+$ (97%) EC (3%)	ß$^+E_{max}$:634	2.3	Cyclotron, ^{18}O(p,n)^{18}F
	^{124}I	4.2 d	ß$^+$ (23%) EC (77%)	ß$^+E_{max}$:1535, 2138 γ:602, 722, 1691	6.9, 10.2	Cyclotron, ^{124}Te(p,n)^{124}I
	^{131}I	8.0 d	ß$^-$	ß$^-E_{max}$:606 γ:80, 284, 364, 637		Nuclear reactor, ^{235}U(n,f)^{131}Te --> ^{131}I
	^{125}I	60.1 d	EC	γ:35 Te-X (IC):27		Nuclear reactor, ^{124}Xe(n,γ)^{125}Xe --> ^{125}I
Others	^{15}O	2.0 min	ß$^+$	ß$^+E_{max}$:1732	8.0	Cyclotron, ^{14}N(d,n)^{15}O
	^{13}N	10.0 min	ß$^+$	ß$^+E_{max}$:1198	5.1	Cyclotron, ^{16}O(p,α)^{13}N
	^{11}C	20.3 min	ß$^+$	ß$^+E_{max}$:960	3.9	Cyclotron, ^{14}N(p,α)^{11}C

Important to note is that several elements have multiple radioactive isotopes that are useful for diagnostic or therapeutic purposes. Isotopes of a given element have identical chemistry, thus, a single radiopharmaceutical agent can be radiolabelled with different radioisotopes of the same element (e.g. $^{86/90}$Y), while maintaining the same biological behaviour and distribution *in vivo*.[7] This class of radiopharmaceuticals is called theranostic agents.

Most radionuclides used in nuclear medicine belong to one of two subgroups (**Table 1**). Radiometals and radiohalogens are radioactive isotopes of metallic elements or halogens respectively, and both can be applied for biological applications as such. Radiometals are often used as a complex with a suitable chelator (ligand) that is used as such (e.g. most ^{99m}Tc-complexes) or covalently linked to a biologically active targeting molecule, making an active radiopharmaceutical agent. In contrast, radiohalogens are mostly incorporated in a targeting molecule by standard carbon-halogen bond formation.[10]

3. CHELATION CHEMISTRY

Each (radio)metal ion has different chemical properties, including coordination number, coordination geometry and ligand donor atom preferences (e.g. N,O,S, hard/soft). Therefore, it is important to find the optimal match between chelator and (radio)metal. The properties of an ideal chelator for preparation of a radiopharmaceutical are that it can efficiently bind the (radio)metal in high yields (quantitative reaction) and within a short reaction time in aqueous medium at low temperature (conditions compatible with heat-sensitive molecules). In general, macrocyclic chelators are known to form more kinetically inert complexes than acyclic chelators.[7] However, crucial properties where most acyclic chelators excel and most macrocycles suffer are the coordination kinetics and radiolabelling efficiency. Fast kinetics of (radio)metal incorporation (association, k_{ass}) often also mean fast (radio)metal release (dissociation, k_{dis}). The rate of dissociation *in vivo* is what directs the kinetic inertness of a radiometal complex, and these off-rates are highly influenced by the high dilution factor when a radiopharmaceutical (often only micrograms) is diluted into the blood pool (**Figure 1**). Therefore, the stability and kinetic inertness of the chelate should be experimentally determined *in vitro* as well as *in vivo*. The consequence of radiometal loss from a radiopharmaceutical *in vivo* depends on the properties and biological behavior of the specific radiometal ion in question. For example, $^{67/68}Ga^{3+}$, $\{Al^{18}F\}^{2+}$ and $^{89}Zr^{4+}$ are known to accumulate in bone, whereas $^{64}Cu^{2+}$ is known to accumulate in the liver.[7]

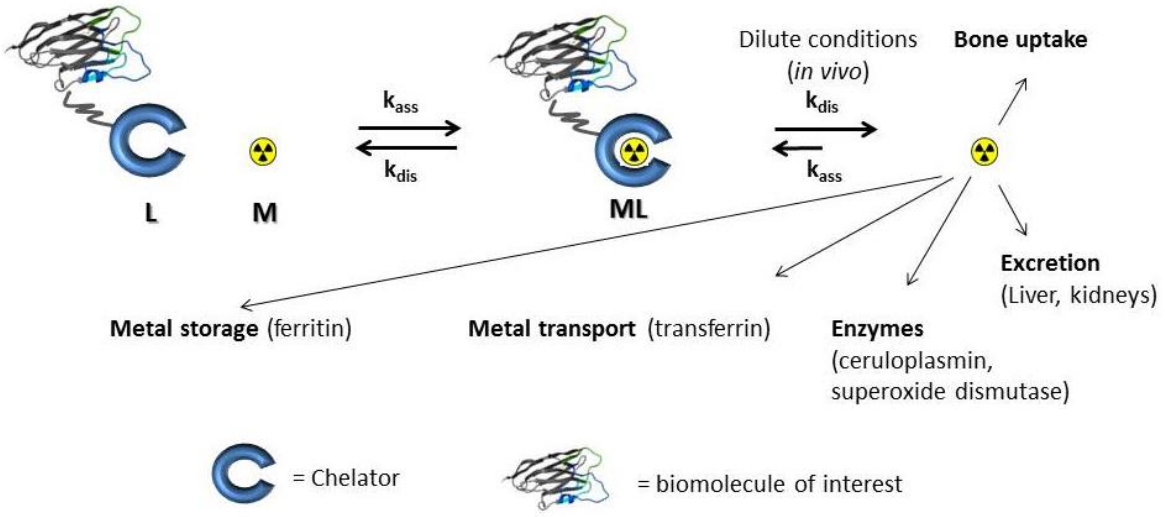

Figure 1: *Metal ion coordination kinetics and enhanced in vivo dissociation (k_{dis}) kinetics due to extremely dilute conditions. Possible routes of radiometal ions in vivo (adapted from Eric W Price and Chris Orvig)*[7]

4. POSITRON EMISSION TOMOGRAPHY

PET provides a non-invasive, sensitive and quantitative visualisation of biochemical and physiological phenomena *in vivo*, which can be used to study the function of cells, receptors, neurotransmitters, genes and drug pharmacokinetics.[11] High quality three-dimensional images are quantified relative to the total injected activity of radiotracer, usually labelled with short-lived positron-emitting radionuclides.[12] Positron emitters are unstable due to a proton excess in their nucleus. Here, a spontaneous process called β^+-decay is triggered in which one of the protons in the nucleus is converted to a neutron, a positron (e^+), and a neutrino (ν). The atomic number of the daughter nucleus is decreased with one unit compared to the parent nuclide.

$$p^+ \rightarrow n + e^+ + \nu$$

The emitted positron, also known as the anti-particle of an electron (e^-), travels a short distance (0-10 mm, depending on its kinetic energy and density of the tissue) during which it loses kinetic energy. When the positron is decelerated, it collides with a random nearby electron of the surrounding tissue to yield a positronium. This positronium almost immediately annihilates resulting into two anti-parallel 511-keV photons. Detection of such events is achieved using circular arrays of bismuth germanium oxide or cerium-doped lutetium oxyorthosilicate scintillation detectors. When the opposing gamma rays simultaneously reach two scintillation detector crystals they cause a flash of light (scintillation), the energy of which is used to release electrons at a photocathode which are then multiplied by a photomultiplier tube (PMT). By combining the information of millions of annihilations using mathematical techniques, it is possible to visualise the distribution of the radionuclide in the

body (**Figure 2**).[9] The maximal positron range (unique for each radionuclide) and the inherent characteristics of the crystals and PMTs determine the final resolution of the clinical PET image, which is typically 4-6 mm in each space direction. However, spatial resolution of newer clinical systems (dedicated for brain imaging) has been improved up to 2.5 mm and in small animal PET imaging systems a resolution of 0.8-1.5 mm can be achieved.

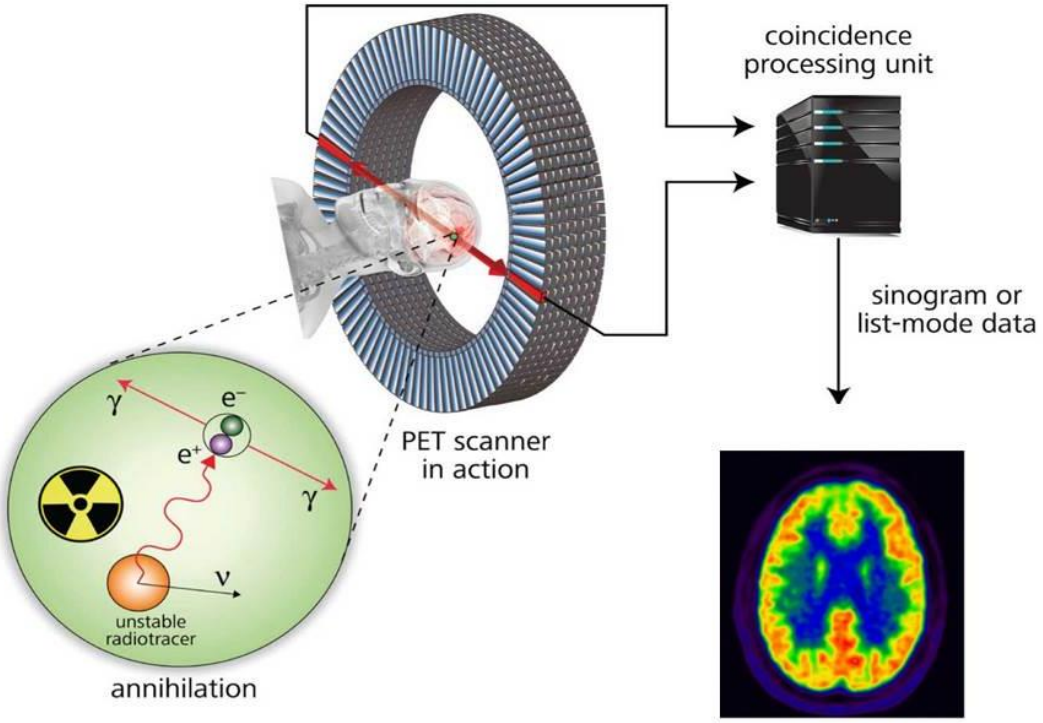

Figure 2: *Schematic illustration of the origin of PET-gamma rays and detection by a PET camera*

The use of PET in combination with anatomy based imaging techniques such as CT (PET/CT) and MRI (PET/MRI) offers the advantage of a simultaneous assessment of both anatomical and functional processes. These hybrid imaging techniques provide unique opportunities for an accurate localisation of pathological changes in certain diseases.[12]

Nuclear medicine is rapidly becoming the first choice for detecting early signs of disease, small tumors and even infections.[1] Compared to SPECT, PET imaging offers indisputably superior images that are characterised by (1) higher spatial resolution, (2) better imaging contrast, (3) less scatter, and (4) better attenuation correction.[13] Furthermore, PET-radioisotopes such as carbon-11 and fluorine-18 can be incorporated with little to no change in biological behaviour from their non-labelled counterparts.[5,14] The drawbacks of PET are predominantly its high costs and the need to produce short half-life positron-emitters using a particle accelerator (cyclotron), except for ^{68}Ga, which is obtained from a ^{68}Ge/^{68}Ga-generator.[11]

Figure 3: *PET/MRI apparatus located at UZ Leuven*

5. FLUORINE-18: THE RADIONUCLIDE OF CHOICE FOR PET

Among β^+-emitting radioisotopes, the halogen fluorine-18 is the most commonly used due to its optimal chemical properties and almost ideal nuclear decay characteristics. The low maximum energy (0.635 MeV) of its positron emissions enables high resolution PET images as a result of the short range tissue penetration prior to annihilation.[1,15] The half-life of 109.8 min is short enough to avoid prolonged irradiation of subjects, yet still long enough to allow multistep synthesis, extended *in vivo* investigations and commercial distribution to remote imaging centres without an on-site cyclotron.[5,14] Additionally, $^{18}F^-$ is readily manufactured in high radioactive quantities from highly enriched ^{18}O-water ($[^{18}O]H_2O$). However, ^{18}F-radiopharmaceuticals have a high production cost. One should not only consider the costs of radiochemists, cyclotron, lead shielded hot cells, remote handling and synthesis equipment and PET scanners, but also the cost of implementation and maintenance of a good manufacturing practice (GMP) quality system. The success and medical importance of one single ^{18}F-labelled radiopharmaceutical, namely 2-[^{18}F]fluoro-2-deoxy-D-glucose ([^{18}F]FDG), have led to the installation of many of these expensive infrastructures all over the world (**Figure 4**). Consequently, fluorine-18 is now readily available in more and more hospitals and research centres and the infrastructure is in place to expand its application far beyond [^{18}F]FDG.[7]

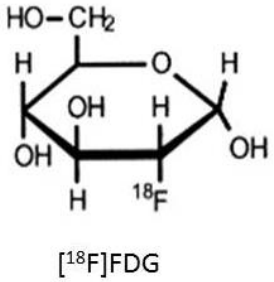

[18F]FDG

Figure 4: *Picture of lead shielded hot cells located at the GMP facility in UZ Leuven and chemical structure of 2-[18F]fluoro-2-deoxy-D-glucose ([18F]FDG)*

The production of ^{18}F-PET tracers can be summarised in three steps. The first step is the production of fluorine-18 with a cyclotron. The second step entails the incorporation of fluorine-18 in the vector molecule to obtain the radiopharmaceutical, followed by purification. Finally, the PET-tracer is submitted to a battery of quality-control (QC) tests before it is released to be administered to patients.

6. PRODUCTION OF FLUORINE-18

The first step in de production of ^{18}F-PET tracers is the generation of fluorine-18. Radionuclides that decay by positron emission can be produced by addition of a proton to a stable nucleus. However, both proton and nucleus are positively charged and the resulting coulomb repulsion will require the proton to possess a high kinetic energy. The proton is charged and can thus be accelerated in a cyclotron in order to acquire this kinetic energy. In the ion source of the cyclotron, positioned at the centre of the vacuum chambre, H^- and H^+ ions are formed by flowing hydrogen gas through a plasma of electrons. The H^- ions are extracted from the ion source and accelerated using an alternating high voltage applied on two electrodes (D's).[4] To avoid collisions of the accelerated H^- particle with gas molecules, the acceleration chamber of the cyclotron is kept under high vacuum. Magnets (above and below the dees) generate a static magnetic field perpendicular to the electrode plane which forces the H^- particles to follow a spiral path. Both the centripetal force and the magnetic (Lorentz) force determine the trajectory of the H^- ions. During each acceleration cycle, the kinetic energy of the H^- ions and as a consequence also the radius of the spiral path increases and eventually the accelerated ions will reach the maximal radius and thus maximal energy. The electrons are now

stripped from the H^- ions by passage through a thin carbon foil ("stripper"). The resulting positively charged protons, subjected to a centrifugal magnetic Lorentz force are deflected out of the cyclotron to strike the target, filled with $[^{18}O]H_2O$ where the $^{18}O(p,n)^{18}F$ nuclear reaction takes place.[15] **Figure 5** shows an internal view and schematic representation of a cyclotron.

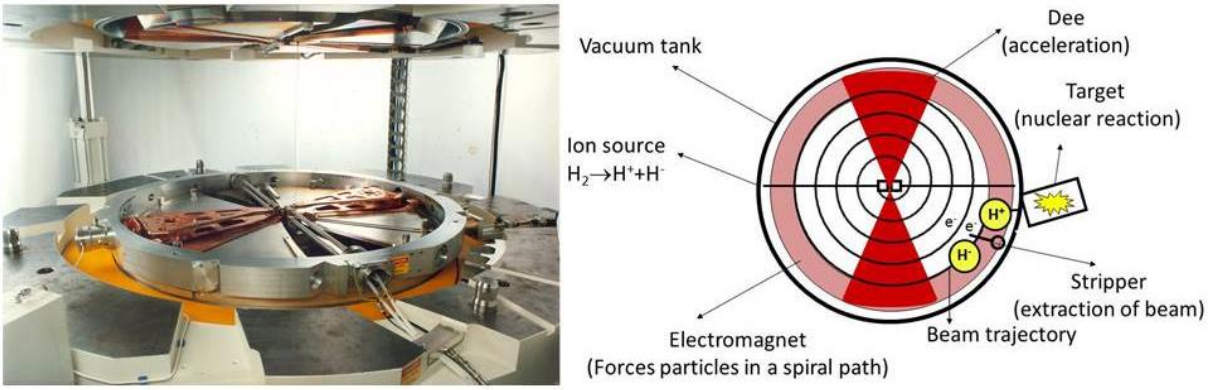

Figure 5: *Internal view and schematic representation of a cyclotron (adapted from Verbruggen A. and Bormans G.)*[4]

7. RADIOFLUORINATION OF VECTOR MOLECULES

7.1 Radiolabelling by carbon-fluorine bond formation

7.1.2 Standard fluorine-18 labelling

In order to achieve high radiochemical yields, high specific activity (SA) and considering the relative short physical half-life of fluorine-18, the radiolabelling process must be quick and involve as few reaction steps as possible. In addition, the incorporation of the radionuclide is ideally the last step in the process. Labelling organic molecules with ^{18}F is performed by reactions in which ^{18}F is either electrophilic or nucleophilic in nature.[10]

The major shortcoming of electrophilic substitution with $[^{18}F]F_2$ gas is the low specific activity of the final compound. Moreover, $[^{18}F]F_2$ gas is a non-specific reactive agent that requires specialised equipment and often a mixture of unwanted by-products is obtained.

In most cases, ^{18}F is attached to a small organic molecule by binding to one of its carbon atoms via an aliphatic or aromatic nucleophilic substitution reaction.[10] The nucleophilic method can potentially yield higher specific radioactivity than the electrophilic approach because it can be used with no-carrier-added fluoride $[^{18}F]F^-$.

As mentioned higher, fluorine-18 in the form of fluoride is obtained as an aqueous solution by proton irradiation of $[^{18}O]H_2O$. However, aqueous environment severely decreases the nucleophilicity of fluoride ions due to the formation of strong hydrogen bonds and a tightly bound hydration sphere.

To increase nucleophilicity, several time-consuming drying steps, anhydrous aprotic solvents and high temperatures need to be applied.[16] Even after these drying procedures, the nucleophilicity of the fluoride ions is lower compared to that of other halides. Therefore, a highly reactive electrophilic substrate, containing an excellent leaving group, is often required to obtain satisfactory radiochemical yields. The most used leaving groups for aliphatic nucleophilic substitution are sulfonic acid esters such as mesylate, tosylate or triflate moieties. These electrophiles can react readily with a wide variety of functional groups that are more nucleophilic than fluoride. Therefore, protection of functional groups is often required, introducing the need for post-labelling deprotection and in that way increasing the number of reaction steps. In the case of biomolecules, incorporating potent leaving groups is problematic because of the overabundance of nucleophilic groups present in the amino acid side chains. Finally, after the successful incorporation of fluorine-18 in a vector molecule, a purification step is required. This can be done by using either preparative high performance liquid chromatography (HPLC) or solid phase extraction cartridges. Although preparative HPLC is more time consuming than solid phase extraction, it is more selective and efficient in separating the final compound from impurities such as fluoride-18, precursor molecules or other (radioactive) impurities.

For radiolabelling of heat-sensitive peptides or biomolecules, labelling techniques using suitable radiometals such as ^{99m}Tc and ^{111}In for SPECT or ^{68}Ga and ^{64}Cu for PET, have been developed.[1,3] Nevertheless, ^{18}F with its growing availability and its nearly ideal physical properties, is also a very attractive radionuclide for radiolabelling biomolecules.[15] However, only a limited number of methods are available for introducing fluorine-18 into complex and sensitive biomolecules in a rapid and efficient way. A solution to overcome the complications caused by the low nucleophilicity of $^{18}F^-$ in aqueous media is the use of fluorine-18 labelled prosthetic groups.

7.1.2 Fluorine-18 labelled prosthetic groups

Fluorine-18 labelled prosthetic groups (or secondary labelling agents) are small and simple fluorine-18 containing molecules that facilitate the radiolabelling process of complex molecules. ^{18}F-prosthetic groups are generally coupled to proteins via conjugation with amines, carboxyl or thiol groups, followed by purification.[17] This approach avoids exposing the biomolecule to harsh conditions but intrinsically requires time consuming synthesis procedures that often include several HPLC purification steps.[18] Some well-known prosthetic groups are N-succinimidyl 4-[^{18}F]fluorobenzoate ([^{18}F]SFB)[19] and 6-[^{18}F]fluoronicotinic acid 2,3,5,6-tetrafluorophenyl ester ([^{18}F]F-Py-TFP).[20]

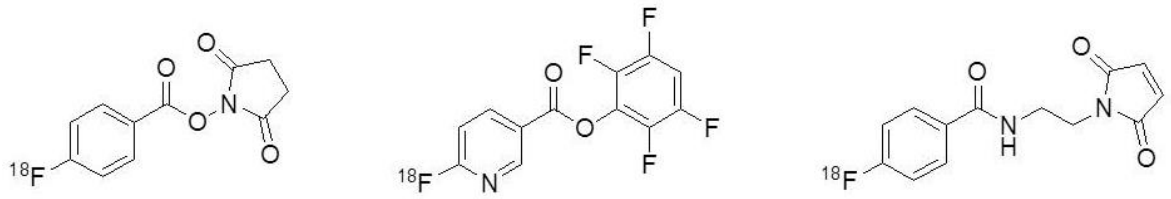

Figure 6: *Structural formulas of N-succinimidyl 4-[^{18}F]fluorobenzoate ([^{18}F]SFB)[19], 6-[^{18}F]fluoronicotinic acid 2,3,5,6-tetrafluorophenyl ester ([^{18}F]F-Py-TFP)[20] and* N*-[2-(4-[^{18}F]fluorobenzamido)ethyl]maleimide ([^{18}F]FBEM)[21]*

Despite its widespread use, the radiosynthesis of [^{18}F]SFB is cumbersome and several purification steps are needed. The advantage of [^{18}F]F-Py-TFP is that it can be labelled in a one-step reaction and purification can be performed using solid phase extraction cartridges. Both fluorine-18 labelled active esters [^{18}F]SFB and [^{18}F]F-Py-TFP can be conjugated to biomolecules via the amine of the side-chain of lysines. Fluorine-18 labelled prosthetic groups containing a maleimide moiety (e.g. *N*-[2-(4-[^{18}F]fluorobenzamido)ethyl]maleimide ([^{18}F]FBEM))[21] can be coupled in a site-specific way with a biomolecule *via* a maleimide-thiol reaction.

7.1.3 ^{18}F-Click chemistry

An exciting recent development in bio-conjugation strategies for radiolabelled imaging agents has been the deployment of the copper(I)-catalyzed Huisgen [2,3]-cycloaddition between alkynes and azides (CuAAC), which is widely referred to as the 'click reaction'.[22] Click reactions are defined more broadly as those that meet the necessary criteria of being selective, high yielding, and having fast reactions kinetics. Numerous ^{18}F-labelled PET radiotracers have been prepared *via* CuAAC and to a lesser extent through Staudinger ligation. However, slow reaction kinetics of the Staudinger ligation and the requirement for a cuprous catalyst limit the utility of the method.[23] Cu(I) ions are generally cytotoxic, causing oxidative degradation of DNA molecules and proteins, *via* formation of hydroxyl radicals *in vivo*.[24] Additionally the possibility that the Cu(I) catalyst can bind to biomolecules may lead to various problems, such as blocking or reducing the biological activity, as well as the rate of the CuAAC reaction. Moreover, Cu(I) ions can compete in chelation when metallic radionuclides (^{64}Cu, ^{68}Ga) are used and as metal catalysts tend to clog HPLC columns, they can cause difficulties in product purification.[25] The above reasons have led to the search for alternative fast and copper-free click chemistry concepts applicable to radiochemistry.[26] This approach can be based on a bioorthogonal inverse-electron-demand Diels-Alder (IEDDA) "click" reaction between tetrazines (Tz) and *trans*-cyclooctene derivatives (TCO) or a strain promoted Cu-free Huisgen click reaction.[27]

The advantage is that neither azides nor alkenes, tetrazines or trans-cyclooctene react with other functional groups commonly present in biomolecules. Hence, there is no need for protective group chemistry and the removal of Cu or other catalysts. Other advantages of the TCO/Tz strategy include fast reaction times, almost quantitative yields, no need for elevated temperatures, biocompatible reaction conditions and high selectivity.[28] However, one should keep in mind that the first step in the process is derivatisation of the biomolecule of interest with a "Click A" group via standard conjugation methods. Ideally this conjugation reaction should be site-specific. After this conjugation step the derivatised biomolecules can be fully characterised and stored in aliquots. Subsequently, the fluorine-18 labelled "click B" group can be added to the derivatised biomolecule to obtain the fluorine-18 labelled biomolecule in nearly quantitative yields. Another advantage is that different "Click B" groups, derivatised with other radionuclides or dyes, can be conjugated with the same biomolecule of interest for versatile applications in molecular imaging and therapy (**Figure 7**). A final purification step is often required to remove excess of "click B" compound after the conjugation reaction.

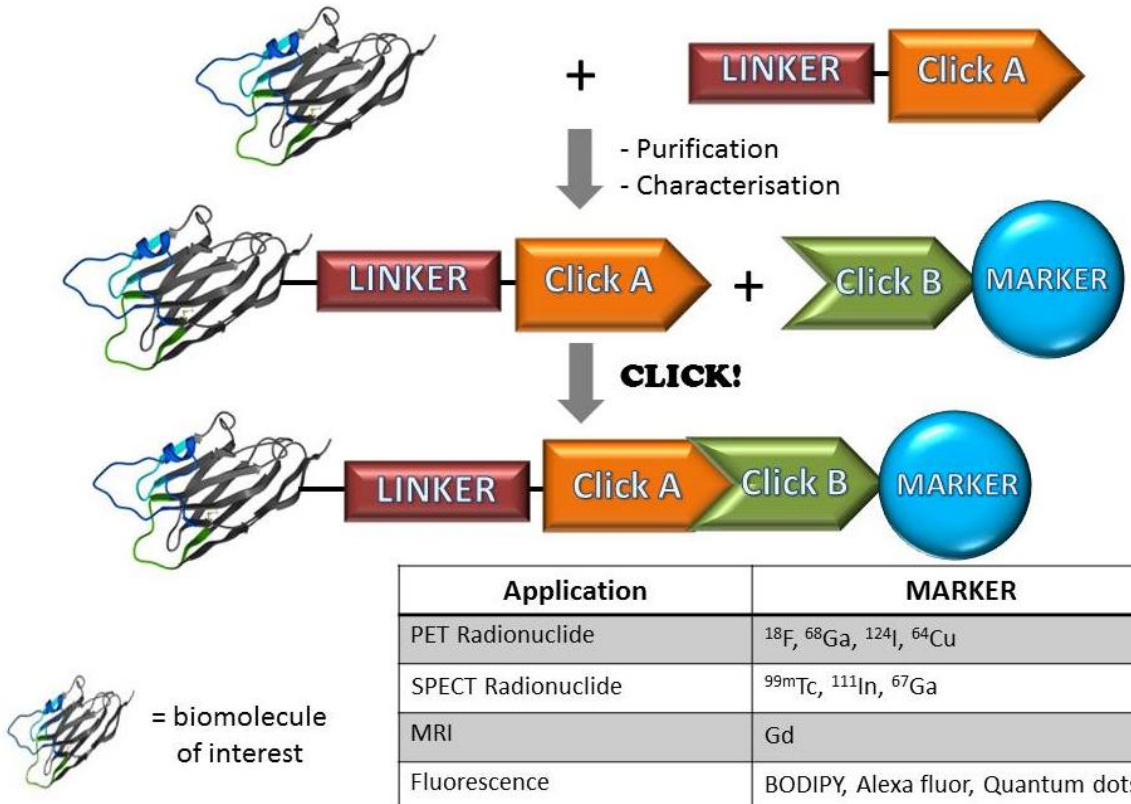

Application	MARKER
PET Radionuclide	^{18}F, ^{68}Ga, ^{124}I, ^{64}Cu
SPECT Radionuclide	^{99m}Tc, ^{111}In, ^{67}Ga
MRI	Gd
Fluorescence	BODIPY, Alexa fluor, Quantum dots
Therapy	^{90}Y, ^{131}I, ^{177}Lu

Figure 7: *Schematic representation of "click chemistry" in molecular imaging and therapy*

7.1.4 Pretargeting approach for PET

In cancer research, *in vivo* pretargeted PET imaging has emerged as an effective two-step approach that combines the high affinity and selectivity of antibodies with the rapid pharmacokinetics and favourable dosimetry of smaller molecules radiolabelled with short-lived radionuclides (e.g. fluorine-18).[29] The pretargeting approach involves the sequential administration of an antibody, derivatised with a suitable "Click A" group, and a low molecular mass radiolabelled moiety ("Click B"). Crucially, the radiolabelled "Click B" group is administered after a predetermined lag period (3-4 days) to allow the antibody sufficient time to accumulate at the target site (e.g. cancer cells). Additionally, the period between the two injections should be long enough so that residual antibody can be cleared from the circulation to achieve good target-to-background ratios.[30] This approach can be based on the bioorthogonal IEDDA "click" reaction between tetrazines and *trans*-cyclooctene derivatives. Pretargeting is a very appealing approach that can be used for therapeutic applications as well if the "click B" group is labelled with a therapeutic radionuclide. However, pretargeting is a more complex approach compared to the use of directly radiolabelled tracer agents for imaging or radiotherapy. Many hurdles still have to be overcome and it will require careful optimisation in order to be successfully translated into a clinical setting.

7.2 Inorganic approaches for labelling biomolecules with fluorine-18

Besides conventional carbon-fluorine radiolabelling methods, different inorganic approaches can be used for labelling of biomolecules with fluorine-18. Several non-carbon elements favour strong bonds (*i.e.* high bond enthalpy) with fluorine, preserve high kinetic stability of the fluorine containing compounds formed and have a lower activation energy for their formation in comparison to carbon-fluorine bonds.[10] These chemical properties were the basis for a new field in ^{18}F-radiochemistry. Currently, boron, silicon and aluminium are three elements under investigation. The strength of the inorganic approach is that it can entail only one, potentially very fast, radiochemical reaction step, which can be easily automated for routine production. Furthermore, time-consuming and rather complex drying steps are avoided since the reaction can take place in, at least partially, aqueous media.[10]

7.2.1 Boron and silicon

Boron-fluorine bonds are some of the most thermodynamically stable covalent bonds known (>730 KJ/mol). The high silicon-fluorine bond energy (>570 KJ/mol) has also drawn attention to its potential for ^{18}F-labelling.[31] Radiofluorination of trifluoroboronates (RBF_3^-) and fluorosilane/fluorosilanol (silicon-fluoride acceptors, SIFA) is performed through either leaving group displacement or isotopic exchange (**Figure 8**). However, hydrolysis of trifluoroboronates to their corresponding boronic acids

($RB(OH)_2$) can be problematic in an aqueous environment. In the case of silicon, the limited stability of the Si-F bond *in vivo* is a major problem but the inconvenience can be adequately reduced by using lipophilic bulky alkyl groups which gives rise to steric hindrance that preserves the silicon-fluorine bond.[31] The most recent generation of exchange carriers, $AmBF_3^-$ and SIFA*lin*, bear a quaternary ammonium cation which reduces the (undesired) lipophilicity of SIFA and increases the stability of RBF_3^- (**Figure 8**).[32,33] Both [^{18}F]SIFA and R[^{18}F]BF_3^- techniques have been mainly used for radiolabelling of peptides and could eventually result in a kit-like radiolabelling approach. However, at this moment there is still room for improvement regarding the specific activity, the pharmacokinetics and the *in vivo* stability of the radiolabelled constructs.

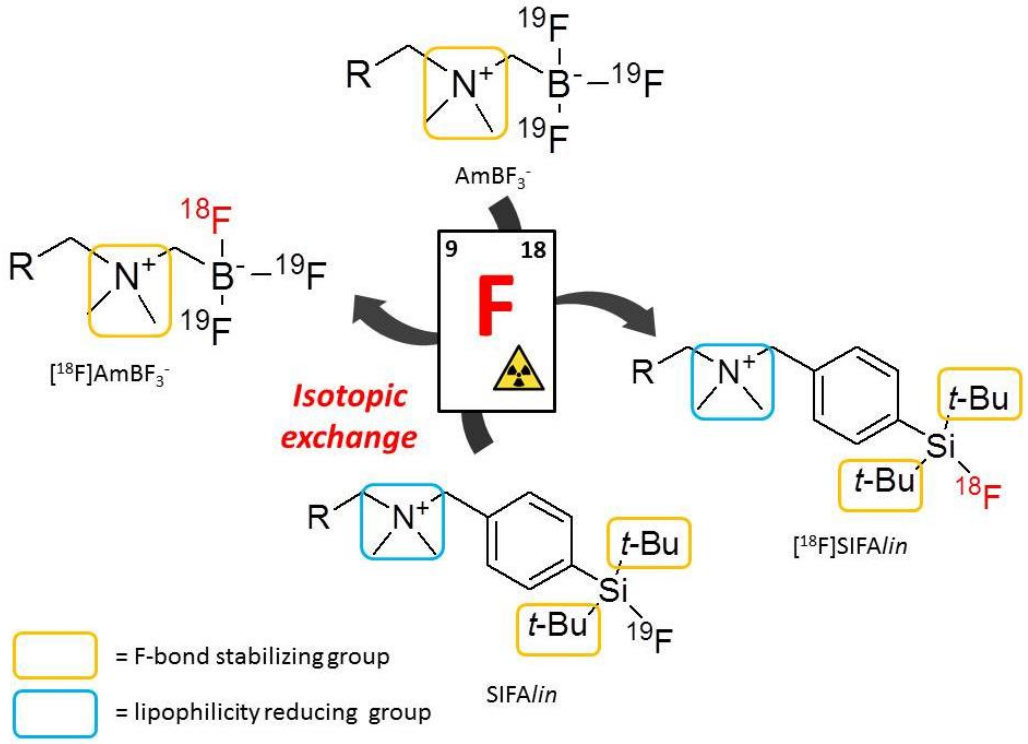

Figure 8: *Schematic overview of isotopic exchange reactions with $AmBF_3^-$ and SIFAlin (adapted from Bernard-Gauthier et al.)*[31]

7.2.2 Aluminium

Al^{18}F-chelation is a relatively new approach and has gained a lot of attention, using only minute amounts of biomolecule (nmol range). In this method, $^{18}F^-$ is firmly bound to Al^{3+} (>670 KJ/mol) to form an aluminium fluoride moiety. At low fluoride concentration, Al^{3+} forms monofluoride species ($\{AlF\}^{2+}$). When the concentration of fluoride increases, aluminium fluoride species constitute the series AlF_n^{3+-n}, where n ranges from one to six. $\{AlF\}^{2+}$ can be chelated by a suitable chelator and this metal chelating agent becomes a bifunctional chelator (BFC) when it accommodates another reactive functional group for stable attachment to biomolecules.[7] Aluminium forms octahedral complexes, therefore a pentadentate ligand is desired, leaving only one binding site open for the fluorine-18 ion.

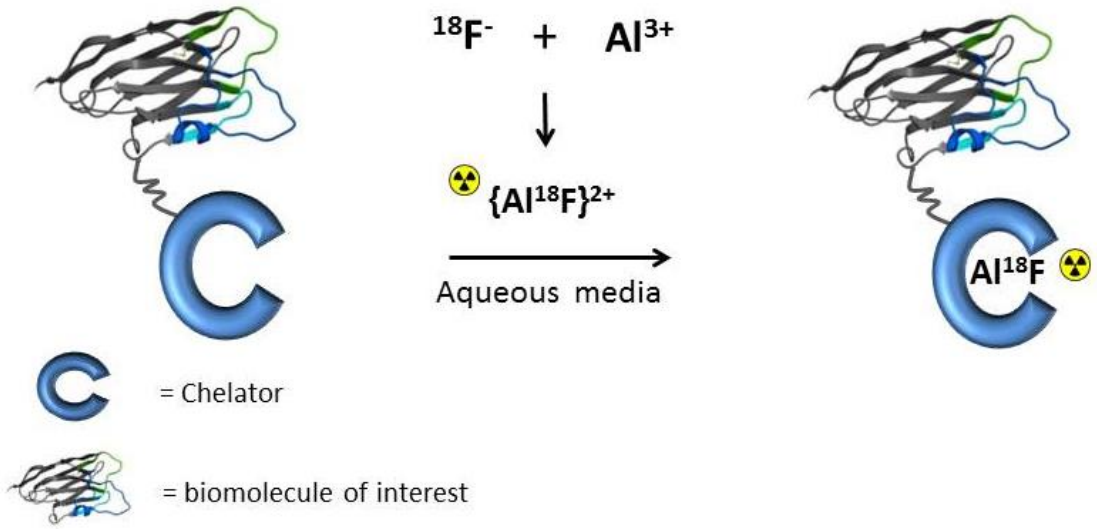

Figure 9: *One-step radiolabelling with fluorine-18 via the $Al^{18}F$-method*

McBride *et al.* were the first to explore the $Al^{18}F$-method. As proof of principle they radiolabelled a peptide, suitable for a bispecific antibody pretargeting method, with $\{AlF\}^{2+}$.[34] Initially, the authors examined diethylene triaminepentaacetic acid (DTPA, **Figure 10**), an acyclic octadentate ligand, as a potential chelator for $\{AlF\}^{2+}$. They observed a promising radiochemical yield using a low amount of DTPA-peptide, however the formed complexes were not sufficiently stable for *in vivo* applications.[35] The authors pointed out that the biggest challenge is finding a stable $Al^{18}F$-ligand that remains intact for several hours *in vivo*.

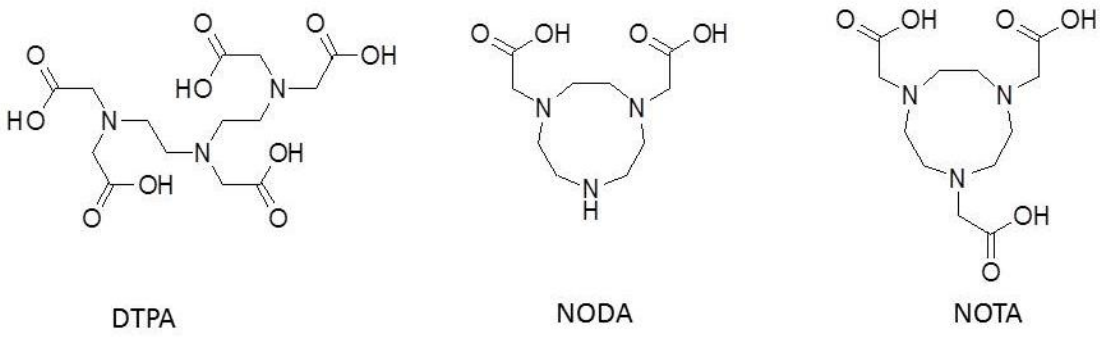

Figure 10: *Chemical structure of diethylene triaminepentaacetic acid (DTPA), 1,4,7-triazacyclononane-1,4-diacetate (NODA) and 1,4,7-triazacyclononane-1,4,7-triacetic acid (NOTA)*

The most promising chelators tested until now are the pentadentate (N_3O_2-donor) ligand 1,4,7-triazacyclononane-1,4-diacetate (NODA, **Figure 10**) and the hexadentate (N_3O_3-donor) ligand 1,4,7-triazacyclononane-1,4,7-triacetic acid (NOTA, **Figure 10**).[36] It has been demonstrated that the most stable aluminium complexes are based on multidentate ligands with negatively charged oxygen donor groups. X-ray crystal structures of $Al^{18}F$-complexes revealed that Al^{3+} is located at the centre of a slightly distorted octahedral complex and bound to fluorine pointing to an axial position.[35,37]

Labelling studies of NODA-benzyl derivatives showed that the presence of groups adjacent to the ligand can have a significant interaction with the complexation. A carbonyl group on the NODA-ring spaced more than three or four carbons had little influence on its labelling potency (78-86%), whereas a carbonyl near-at-hand could form an additional coordination group that reduced the labelling yield drastically (11-24%). This demonstrated that in the presence of a competing intra-molecular metal binding ligand atom (forming a hexadentate ligand), Al^{3+} could be coordinated by all six donor atoms and $^{18}F^-$ is then displaced from the initially formed $\{Al^{18}F\}^{2+}$ complex.

The last years, a wide range of peptides have been labelled using the $Al^{18}F$-method by several groups.[38] Not only relative small peptides such as $\alpha_v\beta_3$ integrin-binding peptides, but also larger peptides, such as exendin-4 and affibodies, were successfully labelled with $\{AlF\}^{2+}$. The first clinical study using a ^{18}F-labelled peptide was published in 2013.[39] Although these macrocyclic chelators show a lot of potential, the high temperatures required for the complexation reaction (≥100 °C) is still the main shortcoming that limits widespread application of this radiolabelling approach.

In an attempt to use the $Al^{18}F$-method for radiolabelling of heat-sensitive biomolecules, Bhalla and coworkers reported late stage $^{18}F^-$ incorporation via halide exchange ($Cl^-/^{18}F^-$) of preformed metal complexes at room temperature.[40] However, this elegant approach requires high amounts of precursor to obtain satisfactory radiochemical yields. Finally the $Al^{18}F$-strategy has been applied to label heat-sensitive antibody Fab' fragments *via* a two-step process using the $Al^{18}F$-labelled prosthetic group $Al^{18}F$-NODA-MPAEM.[41]

8 REFERENCES

(1) Naumova, A. V, Modo, M., Moore, A., Murry, C. E., and Frank, J. a. (2014) Clinical imaging in regenerative medicine. *Nat. Biotechnol. 32*, 804–818.

(2) Lee, C., and Farde, L. (2006) Using positron emission tomography to facilitate CNS drug development *Trends Pharmacol. Sci.27*, 310–316.

(3) Rahmim, A., and Zaidi, H. (2008) PET versus SPECT: strengths, limitations and challenges. *Nucl. Med. Commun. 29*, 193–207.

(4) Verbruggen, A., and Bormans, G. (2015) Cursus Radiofarmaca.

(5) Serdons, K., Verbruggen, A., and Bormans, G. M. (2009) Developing new molecular imaging probes for PET. *Methods 48*, 104–111.

(6) Florimonte, L., Dellavedova, L., and Maffioli, L. S. (2016) Radium-223 dichloride in clinical practice : a review. *Eur J Nucl Med Mol Imaging*.

(7) Price, E. W., and Orvig, C. (2014) Matching chelators to radiometals for radiopharmaceuticals. *Chem. Soc. Rev. 43*, 260–290.

(8) Wadas, T. J., Wong, E. H., Weisman, G. R., and Anderson, C. J. (2010) Coordinating Radiometals of Copper , Gallium , Indium , Yttrium , and Zirconium for PET and SPECT Imaging of Disease. *Chem. Rev. 110*, 2858–2902.

(9) Tolmachev, V., and Stone-elander, S. (2010) Biochimica et Biophysica Acta Radiolabelled proteins for positron emission tomography : Pros and cons of labelling methods. *BBA Gen. Subj. 1800*, 487–510.

(10) Smith, G. E., Sladen, H. L., Biagini, S. C. G., and Blower, P. J. (2011) Inorganic approaches for radiolabelling biomolecules with fluorine-18 for imaging with positron emission tomography. *Dalton Trans. 40*, 6196–6205.

(11) Weissleder, R. (2002) Scaling down imaging: molecular mapping of cancer in mice. *Nat. Rev. cancer 2*, 1–8.

(12) Wadsak, W., and Mitterhauser, M. (2010) Basics and principles of radiopharmaceuticals for PET / CT. *Eur. J. Radiol. 73*, 461–469.

(13) Bateman, T. M. (2012) Advantages and disadvantages of PET and SPECT in a busy clinical practice. *J. Nucl. Cardiol. 19*, 3–11.

(14) Huyvetter, M. D., Xavier, C., Caveliers, V., Lahoutte, T., Muyldermans, S., and Devoogdt, N. (2014) Radiolabeled nanobodies as theranostic tools in targeted radionuclide therapy of cancer. *Expert Opin. Drug Deliv. 11*, 1939–1954.

(15) Le Bars, D. (2006) Fluorine-18 and medical imaging: Radiopharmaceuticals for positron emission tomography. *J. Fluor. Chem. 127*, 1488–1493.

(16) Richter, S., and Wuest, F. (2014) ^{18}F-Labeled Peptides: The Future Is Bright. *Molecules 19*, 20536–20556.

(17) Basuli, F., Li, C., Xu, B., Williams, M., Wong, K., Coble, V. L., Vasalatiy, O., Seidel, J., Green, M. V., Griffiths, G. L., Choyke, P. L., and Jagoda, E. M. (2015) Synthesis of fluorine-18 radio-labeled serum albumins for PET blood pool imaging. *Nucl. Med. Biol. 42*, 219–225.

(18) Cumming, R. C., Olberg, D. E., and Sutcliffe, J. L. (2014) ^{18}F-radiolabeling of peptides from [^{18}F]fluoride using a single microfluidics device. *R. Soc. Chem. 4*, 49529–49534.

(19) Thonon, D., Goblet, D., Goukens, E., Kaisin, G., Paris, J., Aerts, J., Lignon, S., Franci, X., Hustinx, R., and Luxen, A. (2011) Fully Automated Preparation and Conjugation of N-Succinimidyl 4-[^{18}F]Fluorobenzoate ([^{18}F]SFB) with RGD Peptide Using a GE FASTlab^{TM} Synthesizer. *Mol. Imaging Biol. 13,* 1088-1095

(20) Olberg, D. E., Arukwe, J. M., Grace, D., Hjelstuen, O. K., Solbakken, M., Kindberg, G. M., and Cuthbertson, A. (2010) One step radiosynthesis of 6-[(^{18})F]fluoronicotinic acid 2,3,5,6-tetrafluorophenyl ester ([(^{18})F]F-Py-TFP): a new prosthetic group for efficient labeling of biomolecules with fluorine-18. *J. Med. Chem. 53*, 1732–1740.

(21) Kiesewetter, D. O., Jacobson, O., Lang, L., and Chen, X. (2011) Automated radiochemical synthesis of [^{18}F]FBEM : A thiol reactive synthon for radiofluorination of peptides and proteins This publication. *Appl. Radiat. Isot. 69*, 410–414.

(22) John C. Jewetta and Carolyn R. Bertozzi. (2010) Cu-free click cycloaddition reactions in chemical biology. *Chem Soc Rev. 39*, 1272–1279.

(23) Carroll, L., Evans, H. L., Aboagye, E. O., and Spivey, A. C. (2013) Biomolecular Chemistry imaging – progress and prospects. *Org. Biomol. Chem. 11*, 5772–5781.

(24) Mirfeizi, L., Campbell-verduyn, L., Dierckx, R. A., Feringa, B. L., and Elsinga, P. H. (2013) Application of Click Chemistry for PET. *Curr. Org. Chem. 17*, 2108–2118.

(25) Sletten, E. M., and Bertozzi, C. R. (2009) Bioorthogonal Chemistry : Fishing for Selectivity in a Sea of Functionality *Angew. Chem. Int*. Ed*., 48,* 6974–6998.

(26) Nwe, K., and Brechbiel, M. W. (2009) Growing Applications of "' Click Chemistry '" for Bioconjugation in Contemporary Biomedical Research. *Cancer Biother. Radiopharm. 24*, 289–302.

(27) Selvaraj, R., Giglio, B., Liu, S., Wang, H., Yuan, H., Chintala, S. R., Yap, L., Conti, P. S., Joseph, M., Li, Z., and Hill, C. (2015) Improved metabolic stability for ^{18}F PET probes rapidly constructed via tetrazine trans-cyclooctene ligation. *Bioconjug Chem. 26*, 435–442.

(28) Pretze, M., Pietzsch, D., and Mamat, C. (2013) Recent Trends in Bioorthogonal Click-Radiolabeling Reactions Using Fluorine-18. *Molecules 18*, 8618–8665.

(29) Devaraj, N. K. and W. R. (2011) Biomedical Applications of Tetrazine Cycloadditions. *Acc Chem Res. 44*, 816–827.

(30) Slugovc, A.-C. K. and C. (2013) Inverse electron demand Diels–Alder (iEDDA)-initiated conjugation: a (high) potential click chemistry scheme. *Chem. Soc. Rev. 42*, 5131–5142.

(31) Bernard-Gauthier, V., Bailey, J. J., Liu, Z., Wängler, B., Wängler, C., Jurkschat, K., Perrin, D. M., and Schirrmacher, R. (2015) From Unorthodox to Established: The Current Status of ^{18}F-Trifluoroborate- and ^{18}F-SiFA-Based Radiopharmaceuticals in PET Nuclear Imaging. *Bioconjug. Chem. 27*, 267–279.

(32) Pourghiasian, M., Liu, Z., Pan, J., Zhang, Z., Colpo, N., Lin, K., Perrin, D. M., and Bénard, F. (2015) Bioorganic & Medicinal Chemistry F-AmBF_3 -MJ9 : A novel radiofluorinated bombesin derivative for prostate cancer imaging. *Bioorg. Med. Chem. 23*, 1500–1506.

(33) Litau, S., Niedermoser, S., Vogler, N., Roscher, M., Schirrmacher, R., Fricker, G., Wängler, B., and Wängler, C. (2015) Next Generation of SiFAlin-Based TATE Derivatives for PET Imaging of SSTR-Positive Tumors: Influence of Molecular Design on in Vitro SSTR Binding and in Vivo Pharmacokinetics. *Bioconjug. Chem. 26*, 2350–2359.

(34) McBride, W. J., Sharkey, R. M., Karacay, H., D'Souza, C. A., Rossi, E. A., Laverman, P., Chang, C.-H., Boerman, O. C., and Goldenberg, D. M. (2009) A novel method of ^{18}F radiolabeling for PET. *J. Nucl. Med. 50*, 991–998.

(35) D'Souza, C. a, McBride, W. J., Sharkey, R. M., Todaro, L. J., and Goldenberg, D. M. (2011) High-yielding aqueous ^{18}F-labeling of peptides via Al^{18}F chelation. *Bioconjug. Chem. 22*, 1793–1803.

(36) McBride, W. J., Sharkey, R. M., and Goldenberg, D. M. (2013) Radiofluorination using aluminum-fluoride (Al^{18}F). *EJNMMI Res. 3*, 36–47.

(37) Shetty, D., Choi, S. Y., Jeong, J. M., Lee, J. Y., Hoigebazar, L., Lee, Y.-S., Lee, D. S., Chung, J.-K., Lee, M. C., and Chung, Y. K. (2011) Stable aluminium fluoride chelates with triazacyclononane derivatives proved by X-ray crystallography and ^{18}F-labeling study. *Chem. Commun. 47*, 9732–9734.

(38) Laverman, P., McBride, W. J., Sharkey, R. M., Goldenberg, D. M., and Boerman, O. C. (2014) Al(18) F labeling of peptides and proteins. *J. Labelled Comp. Radiopharm. 57*, 219–223.

(39) Ding, H., Xu, Y., Wang, L., Lang, L., Xie, Q., and Yang, M. (2013) First Experience of ^{18}F-Alfatide in Lung Cancer Patients Using a New Lyophilized Kit for Rapid Radiofluorination. *j. nucl. med. 54*, 691–698.

(40) Bhalla, R., Darby, C., Levason, W., Luthra, S. K., McRobbie, G., Reid, G., Sanderson, G., and Zhang, W. (2014) Triaza-macrocyclic complexes of aluminium, gallium and indium halides: fast ^{18}F and ^{19}F incorporation via halide exchange under mild conditions in aqueous solution. *Chem. Sci. 5*, 381–391.

(41) McBride, W. J., D'Souza, C. A., Sharkey, R. M., and Goldenberg, D. M. (2012) The radiolabeling of proteins by the [^{18}F]AlF method. *Appl. Radiat. Isot. 70*, 200–204.

OBJECTIVES AND OVERVIEW OF THE THESIS

Positron emission tomography (PET) is a sensitive, non-invasive imaging technology that produces three-dimensional images showing the dynamic *in vivo* concentration of radiotracers, which are usually labelled with short-lived positron emitting radioisotopes. Among β^+-emitting radioisotopes, the halogen fluorine-18 is the most commonly used due to its optimal chemical properties and almost ideal nuclear decay characteristics. The $Al^{18}F$-method is a relatively new approach that allows the radiofluorination of biomolecule-bound chelators in a one-step procedure and in aqueous media. This method avoids the laborious and time-consuming multistep procedures that are used routinely in labelling of biomolecules with fluorine-18. Although many previous studies demonstrated the versatility of the $Al^{18}F$ approach to radiolabel peptides, the approach has limited applicability for heat sensitive biomolecules due to high temperatures required for the complexation reaction (≥ 100 °C) when used with macrocyclic complexing agents such as NOTA and NODA. Therefore, an alternative chelator that eliminates the heating step is desired as it could result in a kit-based radiolabelling method in aqueous media.

In **Chapter II** we developed new acyclic pentadentate ligands which, unlike NODA, display a less rigid structure to reduce the activation energy of the complexation reaction. The area of improvement includes radiolabelling at moderate temperatures (≤40 °C), whilst maintaining sufficient *in vivo* stability. The stability of the new $Al^{18}F$-complexes was tested and in order to obtain a better understanding of the different factors influencing the formation and stability of the $Al^{18}F$-complexes, we carried out more in-depth experiments with ligand H_3L3. As a proof of concept, we successfully developed the urea-based PSMA inhibitor [^{18}F]AlF-Glu-NH-CO-NH-Lys(Ahx)L3 ([^{18}F]AlF-PSMA-L3) and performed an *ex vivo* biodistribution in healthy mice to evaluate the pharmacokinetics of the $Al^{18}F$-labelled compound.

Although the acyclic chelator H_3L3 proved to be a good lead candidate for labelling of heat-sensitive biomolecules with fluorine-18, there was still room for improvement regarding the stability of $Al^{18}F$-complexes. Therefore, in **Chapter III** we designed new restrained complexing agents (RESCA1-5) for application of the $Al^{18}F$ strategy at room temperature in an attempt to improve the stability of the resulting $Al^{18}F$-complexes. Restrained complexing agent 1 (RESCA1) is an acyclic pentadentate ligand with an N_2O_3 coordinative set and this new chelator allows radiolabelling of heat-sensitive biomolecules via the $Al^{18}F$-method in one radiolabelling step at moderate temperature. The new AlF chelator, RESCA1, provides an efficient, generic approach to label heat-sensitive biomolecules with fluorine-18 for PET applications. As a proof of concept, RESCA1 was conjugated to the heat-sensitive

protein human serum albumin (HSA) and the construct was labelled with $\{Al^{18}F\}^{2+}$ at ambient temperature. *Ex vivo* biodistribution and microPET studies in healthy rats were performed to assess the *in vivo* stability of $Al^{18}F$-RESCA1-HSA.

Prostate-specific membrane antigen (PSMA) is overexpressed in a majority of primary and metastatic prostate cancer patients and is a very promising target for specific prostate cancer imaging and therapy. In **chapter IV** we have developed two new $Al^{18}F$-labelled urea-based PSMA inhibitors, [^{18}F]AlF-PSMA-NODA-MPAA and [^{18}F]AlF-PSMA-RESCA1. Cell uptake and internalisation experiments with LNCaP ($PSMA^+$) and PC-3 ($PSMA^-$) cells, e*x vivo* biodistribution studies in healthy mice and microPET studies in prostate tumour bearing mice were performed to evaluate the prostate cancer PET-imaging properties of the $Al^{18}F$-tracers. The results were compared with those of [^{18}F]AlF-PSMA-L3 and [^{68}Ga]Ga-HBEDD-CC-PSMA, currently the most widely used PSMA-radioligand.

Nanobodies are promising tools in molecular imaging and have many advantages in comparison with full-size antibodies. Fluorine-18 is the radionuclide of choice for radiolabeling of nanobodies in view of their short biological half-life. In **Chapter V** we aimed to demonstrate that RESCA1 provides an efficient approach to radiolabel nanobodies with fluorine-18 at ambient temperature. We derivatised nanobodies targeting the CRIg receptor with RESCA1, labelled it with $\{Al^{18}F\}^{2+}$ and evaluated the stability of the tracer *in vitro*. Furthermore, we developed a generic radio-HPLC-HRMS system for the analysis and quality control of radiolabelled nanobodies. *Ex vivo* biodistribution studies in healthy mice and microPET studies in $CRIg^{-/-}$ mice were performed to evaluate the pharmacokinetics and specificity of the $Al^{18}F$-labelled nanobody, respectively.

Finally, the overall discussion of this dissertation and the future prospects of the project are provided in **chapter VI**.

CHAPTER II

New chelators for low temperature Al^{18}F-labelling of biomolecules

Cleeren F[1], Lecina J[1], Billaud E.M.F, Ahamed M., Verbruggen A[1] and Bormans G[1]

Laboratory for Radiopharmacy, University of Leuven, Leuven, Belgium

Bioconjugate Chem., **2016**, *27* (3), 790–798

Supplemental information: http://pubs.acs.org/doi/suppl/10.1021/acs.bioconjchem.6b00012

ABSTRACT

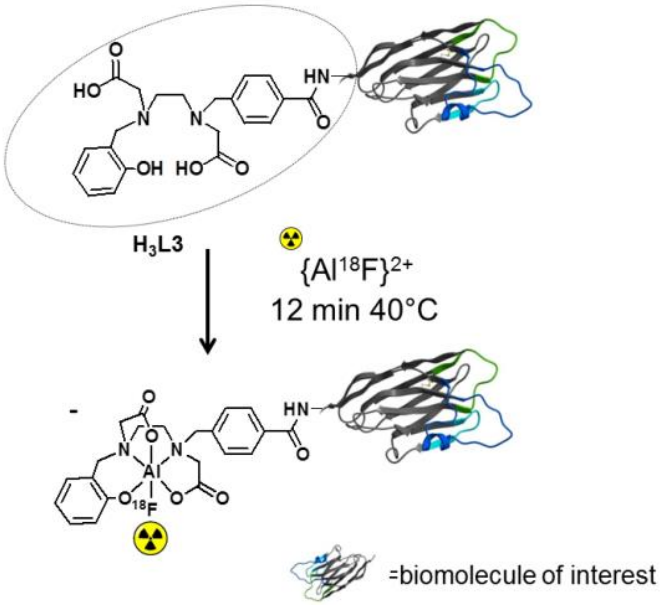

The $Al^{18}F$ labelling method is a relatively new approach that allows radiofluorination of biomolecules such as peptides and proteins in a one-step procedure and in aqueous solution. However, the chelation of the $\{Al^{18}F\}^{2+}$ core with the macrocyclic chelators NOTA or NODA requires heating to 100-120 °C. Therefore, we have developed new polydentate ligands for complexation of $\{Al^{18}F\}^{2+}$ with good radiochemical yields at a temperature of 40 °C. The stability of the new $Al^{18}F$-complexes was tested in phosphate buffered saline (PBS) pH 7.4 and in rat plasma. The stability of the $[^{18}F]$AlF-L3 complex was found to be comparable to that of the previously reported $[^{18}F]$AlF-NODA complex up to 60 minutes in rat plasma. Moreover, the biodistribution of $[^{18}F]$AlF-L3 in healthy mice showed absence of *in vivo* defluorination since no significant bone uptake was observed, whereas the major fraction of activity at 60 min p.i. was observed in liver and intestines, indicating hepatobiliary clearance of the radiolabelled ligand. The acyclic chelator H_3L3 proved to be a good lead candidate for labelling of heat-sensitive biomolecules with fluorine-18. In order to obtain a better understanding of the different factors influencing the formation and stability of the complex, we carried out more in-depth experiments with ligand H_3L3. As a proof of concept, we successfully conjugated the new AlF-chelator with the urea-based PSMA inhibitor Glu-NH-CO-NH-Lys to form Glu-NH-CO-NH-Lys(Ahx)L3 and a biodistribution study in healthy mice was performed with the $Al^{18}F$-labelled construct. This new class of AlF-chelators may have a great impact on PET radiochemical space as it will stimulate the rapid development of new fluorine-18 labelled peptides and other heat-sensitive biomolecules.

1. INTRODUCTION

Positron emission tomography (PET) is a sensitive, non-invasive imaging technology that produces three-dimensional images showing the *in vivo* concentration of radiotracers, which are usually labelled with short-lived positron emitting radioisotopes such as ^{15}O, ^{13}N, ^{11}C, ^{68}Ga, ^{18}F, ^{64}Cu, ^{89}Zr and ^{124}I.[1] Fluorine-18 is the most frequently used PET radionuclide as it combines several advantages like favourable decay properties ($t_{1/2}$ =109.8 min, ~ 97% ß$^+$-emission, 635 keV maximum positron energy), low β^+-trajectory (< 2 mm in water), small atom size and moreover, it is readily produced in large quantities (>400 GBq/batch) with a cyclotron. The half-life is long enough to allow multistep synthesis, transportation to remote hospitals without an on-site cyclotron and it is short enough to avoid extended irradiation of patients.[2]

The $Al^{18}F$ labelling method is a relatively new approach that allows radiofluorination of biomolecules such as peptides and proteins in a one-step procedure and in aqueous medium.[3,4] This method avoids laborious multistep procedures often required when secondary labelling agents are used to radiolabel biomolecules with fluorine-18.[5,6,7] Conventional radiofluorination strategies involve carbon-fluorine bond formation in anhydrous aprotic solvents. In contrast, the $Al^{18}F$-strategy involves the formation of aluminium monofluoride ($\{Al^{18}F\}^{2+}$) which is trapped by a suitable chelator –mostly bound to a biomolecule- in aqueous medium. McBride *et al.* published the first study using a chelator for $\{Al^{18}F\}^{2+}$ labelling in 2009.[4] The most promising chelators tested until now are the hexadentate ligand 1,4,7-triazacyclononane-1,4,7-triacetic acid (NOTA)[8,9] and the pentadentate ligand 1,4,7-triazacyclononane-1,4-diacetic acid (NODA)(**Figure 1**).[10,11]

Although these macrocyclic chelators show a lot of promise for radiolabelling peptides with fluorine-18, the chelation of the $\{Al^{18}F\}^{2+}$ core with NOTA or NODA requires heating to 100-120 °C. These harsh reaction conditions are problematic when the chelator is coupled to heat-sensitive biomolecules.[12] Therefore it would be desirable to have an improved chelator that allows efficient chelation of $\{Al^{18}F\}^{2+}$ at moderate temperature (<40 °C). This could ultimately allow development of a kit-based, room temperature fluorine-18 radiolabelling method for heat-sensitive biomolecules. Although there are reports from Bhalla and coworkers on late stage $^{18}F^-$ incorporation via halide exchange ($Cl^-/^{18}F^-$) of preformed metal complexes at room temperature and also a recent attempt from Malik et al. on radiofluorination of a prostate cancer imaging agent *via* $\{Al^{18}F\}^{2+}$ chelation at ambient temperature, new chelators for the $Al^{18}F$ method are warranted.[13,14]

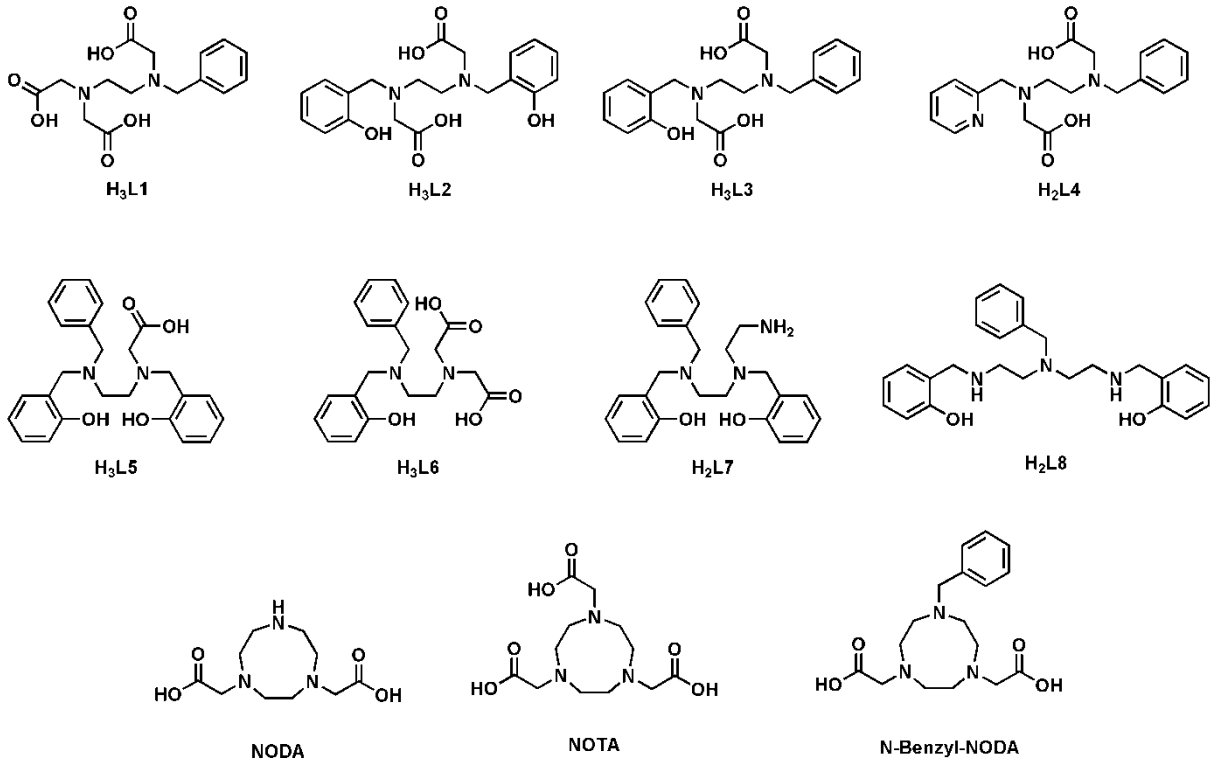

Figure 1: *Chemical structures of H_3L1-8, NODA, NOTA and N-benzyl-NODA*

In the present study, we synthesised new polydentate ligands that allow chelation of $\{Al^{18}F\}^{2+}$ at moderate temperatures (<40 °C). These new chelators, unlike NODA and NOTA, consist of a flexible structure to reduce the activation energy of the complexation reaction. Macrocyclic chelators exhibit a high stability once the metal complex is formed, but they generally require high temperatures to rearrange the ligand structure in order to accommodate the $\{Al^{18}F\}^{2+}$ moiety.[15] However, replacing the macrocyclic by a more flexible acyclic structure can compromise the stability of the complex. To avoid this, the original coordinative set of NODA (N_3O_2) was modified, replacing one nitrogen by an oxygen atom (N_2O_3). Indeed, negatively charged oxide donor atoms are more effective Al-chelators than nitrogen and sulphur among others.[16] Therefore, novel chelators H_3L1-8 (**Figure 1**) were synthesised. These novel derivatives have been evaluated as such (*i.e.* without being conjugated to biomolecules) to fully assess the $\{Al^{18}F\}^{2+}$-core chelation efficiency and the *in vivo* and *in vitro* stability of the corresponding fluorine-18 labelled chelates. Furthermore, in order to gain a better understanding of the different factors influencing the formation and stability of the complex, we carried out more in-depth experiments with ligand H_3L3. In addition, as a proof of concept, we conjugated the ligand H_3L3 with a urea-based inhibitor of the prostate-specific membrane antigen (PSMA), Glu-NH-CO-NH-Lys,[17] to form Glu-NH-CO-NH-Lys(Ahx)H_3L3 and performed a biodistribution study in healthy mice with the $Al^{18}F$-labelled construct. PSMA is overexpressed in a majority of primary and metastatic prostate cancers and can be considered as a promising target for specific prostate cancer imaging and therapy.[18-19] Although the urea-based inhibitor of PSMA can tolerate

high temperature radiolabelling procedures, the proposed method can straightforwardly be applied to radiolabel heat-sensitive biomolecules, such as the 55-kDa fragment antigen-binding (FAB), the 28-kDa single-chain variable fragment (scFv) or 15-kDa antibody fragments derived from heavy-chain only antibodies (VHH or nanobodies).[12]

2. MATERIALS AND METHODS

2.1 General

All reagents and solvents were purchased from Sigma-Aldrich (Bornem, Belgium), Fluka (Bornem, Belgium), Fisher (Doornik, Belgium) or Acros Organics (Geel, Belgium). Fluorine-18 was produced on site using a cyclotron (IBA Cyclone 18/9, IBA, Louvain-la-Neuve, Belgium) by irradiation of $H_2{}^{18}O$ with 18-MeV protons. Radioactivity was measured using an ionisation chamber based activity meter (Capintec Radioisotope Calibrator CRC-721, Ramsey, NJ, USA).

Identification of the molecular ion mass of various compounds was achieved using a Dionex Ultimate 3000 LC System (Thermo Fisher Scientific, Sunnyvale, USA) coupled in series to an ultra-high resolution time-of-flight mass spectrometry (TOF-HRMS) (MaXis impact, Bruker, Bremen, Germany), equipped with orthogonal electrospray ionisation (ESI) interface. Acquisition and processing of data were conducted using HyStar and Compass DataAnalysis (version 3.2, Bruker), respectively. Calculated monoisotopic mass values were obtained using Compas IsotopePattern (version 3.2, Bruker). Thin layer chromatography (TLC) was used for rapid analysis of reaction mixtures. The TLC plates were silica-based (Silica gel 60 plates, Merck, Darmstadt, Germany).

Preparative high performance liquid chromatography (prep-HPLC) was carried out with a system consisting of a Merck-Hitachi L-6200 pump and an XTerra preparative C18 10 µm 10 mm x 250 mm column (Waters, Milford, USA). The mobile phase consisted of a gradient of water and acetonitrile, eluted at a flow rate of 5 mL/min. The eluate was analysed for its UV absorbance (Merck Hitachi L-4200 UV-VIS detector) at 254 nm.

Chemical structure elucidation was performed using proton-nuclear magnetic resonance (^{1}H-NMR) at 400 MHz, carbon-nuclear magnetic resonance (^{13}C-NMR) at 101 MHz and fluorine-nuclear magnetic resonance (^{19}F{^{1}H}-NMR) at 376 MHz on a Bruker AVANCE 400 MHz spectrometer (5 mm probe, Bruker AG, Fällanden, Switzerland).

Instant thin layer chromatography-silica gel (iTLC-SG) papers (Varian, Diegem, Belgium) were developed in an elution chamber using a mixture of acetonitrile and water (75:25, v/v). Autoradiography was performed using phosphor storage screens (super-resolution screen, Perkin

Elmer, Waltham, USA). Screens were read in a Cyclone Plus system (Perkin Elmer) and analysed using Optiquant software (Perkin Elmer).

2.2 Complexation of $\{Al^{18}F\}^{2+}$

2.2.1 $\{Al^{18}F\}^{2+}$solution

$[^{18}F]F^-$ was separated from $[^{18}O]H_2O$ by trapping on a SepPak Light Accel plus QMA anion exchange cartridge (Cl^- form; Waters). The cartridge was washed with water (3 mL) and $[^{18}F]F^-$ (148-333 MBq) was eluted from the cartridge with an aqueous solution of sodium chloride 0.9% (0.3 mL). The obtained $[^{18}F]F^-$ solution (50 µl) was added to 22.5 µL of 2 mM aluminum chloride ($AlCl_3$) in sodium acetate buffer (0.1 M, pH 4). The solution was incubated at rt for 5 min to form $\{Al^{18}F\}^{2+}$.

2.2.2 Synthesis and purification of [$Al^{18}F$]-complexes

A solution of each ligand (1 mL, 150 µM) in sodium acetate buffer (0.1 M, pH 4) was added to separate vials which contained a freshly prepared $\{Al^{18}F\}^{2+}$ solution. The closed vials were heated in an oil bath at different temperatures for 12 min and the radiochemical yields (RCY's) were determined by iTLC-SG (H_3L1 and H_3L3 n=3, H_3L2, H_3L4-8 and N-benzyl-NODA n=1).

The resulting mixtures were purified using a Sep-Pak Plus Alumina-N-Cartridge (Waters, pre-rinsed with an aqueous solution of sodium chloride 0.9% (5 mL)). After loading of the crude reaction mixture, the cartridge was eluted with an aqueous solution of sodium chloride 0.9% (3 mL). The eluate was collected and each of the purified [$Al^{18}F$]-complexes was analysed using iTLC-SG and/or radio-HPLC-HRMS (Acquity UPLC BEH C_{18}, 1.7 µm, 2.1 mm x 150 mm, Waters) with gradient elution at a flow rate of 0.6 mL/min A: H_2O B: ACN, 0-2 min 5% B, 2 to 8 min 5% B to 95% B, 8-10 min 95% B, 10 to 12 min 95% B to 5% B).

2.3 Stability tests of $[^{18}F]$AlF-L1-4 and $[^{18}F]$AlF-*N*-benzyl-NODA in phosphate buffered saline (PBS) and rat plasma

$Al^{18}F$-complexes were synthesised and purified as described above by heating the mixtures at 40 °C for 12 min ($[^{18}F]$AlF-L1-3) or at 110 °C for 12 min ($[^{18}F]$AlF-L4 and $[^{18}F]$AlF-*N*-benzyl-NODA). A volume of 200 µL of each solution of purified [$Al^{18}F$]-complex was added to PBS (1 mL, 0.1 M pH 7.4) or rat plasma (1 mL). These mixtures were incubated at 37 °C and analysed by iTLC-SG at 10, 30, 60, 120, 180 and 240 min after the start of the incubation. Plasma samples were denatured by addition of the plasma solution (50 µL) to acetonitrile (50 µL). The mixture was stirred and centrifuged (1300 g, 3 min). Finally the supernatant was analysed using iTLC-SG.

2.4 Biodistribution studies

Quantification of radioactivity for biodistribution studies was performed using an automated gamma-counter equipped with a 3-inch NaI(Tl) well crystal coupled to a multichannel analyzer, mounted in a

sample changer (Perkin Elmer 1480 Wizard 3q). Counts were corrected for background radiation, physical decay and counter dead time.

Animals were housed in individually ventilated cages in a thermo-regulated (~22 °C), humidity-controlled facility under a 12h-12h light-dark cycle, with access to food and water *ad libitum*. All animal experiments were conducted according to the Belgian code of practice for the care and the use of animals, after approval from the university animal ethics committee.

The biodistribution studies of [^{18}F]AlF-L3, [^{18}F]AlF-Glu-NH-CO-NH-Lys(Ahx)L3 and {$Al^{18}F$}$^{2+}$ were carried out in healthy male Naval Medical Research Institute (NMRI) mice (body weight: 30-40 g) at 10 and 60 min post injection (p.i.) (*n* = 4/time point). Mice were injected with the [^{18}F]AlF-L3 complex (2 MBq) or with {$Al^{18}F$}$^{2+}$ (5.55 MBq) or with [^{18}F]AlF-Glu-NH-CO-NH-Lys(Ahx)L3 (2 MBq) with or without coadministration of 2 mg/kg 2-PMPA *via* a tail vein under anesthesia (2.5% isoflurane in O_2 at 1 L/min flow rate) and sacrificed by decapitation at above specified time points. Blood and major organs were collected in tared tubes and weighed. The radioactivity in blood, organs and other body parts was counted using the automated γ-counter. For calculation of total radioactivity in blood, bone and muscle, tissue mass was assumed to be, respectively, 7, 12 and 40% of the total body mass.[28,29]

2.5 [^{18}F]AlF-L3: additional experiments

2.5.1 Effect of pH

A solution of H_3L3 (1 mL, 150 µM) was prepared in sodium acetate buffer (0.1 M) at different pH values ranging from pH 3 to pH 5.5. The buffer solution was added to a vial which contained a freshly prepared {$Al^{18}F$}$^{2+}$ solution. The vials were heated at 40 °C for 12 min and the RCYs were determined by iTLC-SG (n=3).

2.5.2 Effect of reaction volume

Different stock solutions (900, 750, 600, 300, 150 µM) of H_3L3 in sodium acetate buffer (0.1 M, pH 4) were prepared. Respectively 165, 200, 250, 500 and 1000 µl of the H_3L3 stock solutions were added to 73 µl of freshly prepared {$Al^{18}F$}$^{2+}$ solution. With this protocol reaction volumes ranging from 238 µl to 1073 µl were obtained, without changing the concentration of the ligand. The vials were heated at 40 °C for 12 min and the RCYs were determined by iTLC-SG.

2.5.3 Effect of organic solvents

Different stock solutions of H_3L3 (150 µM) in sodium acetate buffer (0.1 M, pH 4) were prepared containing acetonitrile or ethanol, ranging from 0 to 80%. 1 ml of each solution was added to a vial containing 73 µl of freshly prepared {$Al^{18}F$}$^{2+}$ solution. The vials were heated at 40 °C for 12 min and the RCYs were determined by iTLC-SG.

2.5.4 Effect of relative amount of $^{19}F^-$

After cyclotron production, [^{18}F]F^- was separated from [^{18}O]H_2O as described higher and [^{18}F]F^- (3500-5500 MBq) was eluted from the anion exchange cartridge with an aqueous solution of sodium chloride 0.9% (0.5 mL). The solution of [^{18}F]fluoride was further diluted 1000 times with a solution of sodium chloride 0.9%. The highly diluted solution of [^{18}F]fluoride (50 µl, 350-550 kBq) and 20, 40, 80 or 160 µl of Na^{19}F solution (1 mM) was added to 22.5 µl of 2 mM aluminum chloride ($AlCl_3$) in sodium acetate buffer (0.1 M, pH 4). Sodium acetate buffer (0.1 M, pH 4) was added to obtain a total volume of 233 µl. A solution of H_3L3 (1 mL, 150 µM) in sodium acetate buffer (0.1 M, pH 4) was added to the vials which contained the freshly prepared {Al$^{18/19}$F}$^{2+}$ solutions. The vials were heated at 40 °C for 12 min and the RCYs were determined by iTLC-SG.

2.5.5 Effect of H_3L3 to Al^{3+} ratio

Different stock solutions of $AlCl_3$ (2000, 1000, 500, 100, 50, 25 and 10 µM) in sodium acetate buffer (0.1 M, pH 4) were prepared. From these solutions 22.5 µl was added to [^{18}F]F^- solution (50 µl) and the mixtures were incubated at rt for 10 min to form {Al^{18}F}$^{2+}$. Different stock solutions of H_3L3 in sodium acetate buffer (0.1 M, pH 4) were prepared: 150, 100, 75, 50 and 25 µM. The freshly prepared {Al^{18}F}$^{2+}$ solutions were added to 1 mL of the H_3L3 stock solutions. With this protocol H_3L3 to Al^{3+} ratios ranging from 652 to 0.54 were obtained. The vials were heated at 40 °C for 12 min and the RCYs were determined by iTLC-SG.

2.5.6 Stability of [^{18}F]AlF-L3 in different buffers ranging from pH 2 to pH 8

200 µl of the purified Al^{18}F-L3 solution was added to 1 mL of sodium phosphate buffer (0.1 M, pH 2 or pH 3), sodium acetate buffer (0.1 M, pH 4, pH 5 or pH 6), PBS buffer (0.1 M, pH 7) or Tris-HCl buffer (0.1 M, pH 8). These mixtures were incubated at room temperature and analyzed by iTLC-SG at 30 and 60 min after the start of the incubation.

2.6 Remote controlled radiosynthesis and purification of Al^{18}F-labelled Glu-NH-CO-NH-Lys(Ahx)L3

[^{18}F]fluoride was produced (40 GBq) and trapped on a SepPak Light Accel plus QMA anion exchange cartridge as described above. The [^{18}F]F^- was eluted from the cartridge with an aqueous solution of sodium chloride 0.9% (0.25 mL) and added to 5 µl of 20 mM aluminum chloride ($AlCl_3$) in sodium acetate buffer (0.1 M, pH 4.5). The solution was incubated at rt for 5 min to form {Al^{18}F}$^{2+}$. A solution of Glu-NH-CO-NH-Lys(Ahx)L3 (0.115 mL, 2.58 mM) was added and the reaction vial was heated at 40 °C for 12 min. After dilution with water (0.5 mL), the crude reaction mixture was purified with semi-preparative HPLC (XBridge C_{18}, 5 µm, 4.6 mm x 150 mm, Waters) using the following method. Solvent A (ammonium acetate 0.05M pH 5.5) and solvent B (EtOH), flow rate 1 ml/min. The elution gradient was 100% A to 80% A over 0-25 min. UV detection of the eluate was performed at 254 nm. The

[^{18}F]AlF-Glu-NH-CO-NH-Lys(Ahx)L3 peak was isolated and identification was performed by radio-HPLC (XBridge C_{18}, 3.5 µm, 3.0 mm x 100 mm, Waters) using gradient elution at a flow rate of 0.8 ml/min (A: ammonium acetate 0.05M pH 5.5 B: acetonitrile, 0 to 25 min 0% B to 20% B) and by ESI-MS ((m/z): found, 873.3261 $[M]^-$ calculated for $C_{39}H_{51}AlFN_6O_{14}$ 873.3257).

3. RESULTS & DISCUSSION

McBride and others have reported the Al^{18}F-labelling method using bis-carboxylate derivatives of 1,4,7-triazacyclononane for a "one-pot" radiolabelling of a diverse range of biomolecules.[8,20] However, the need for elevated temperatures (100-120 °C) limits its widespread applicability because of the thermal instability of many (high MW) biomolecules.[12] Therefore, we designed new acyclic ligands with an N_2O_3 coordinative set or N_3O_2 bis-phenol structure (**Figure 1**).

3.1 Synthesis

The ligands H_3L1-4 have an ethylenediamine-*N*,*N*'-diacetic acid scaffold in common, but the tertiary amines are substituted with different groups (benzyl, 2-hydroxybenzyl, 2-pyridylmethyl, acetic acid). H_3L1 was synthesised in two steps with 50% overall yield (see Supporting information, **S1**), starting from *N*-benzylethylenediamine, by nucleophilic substitution of ethyl bromoacetate, followed by saponification of the ethyl esters. H_3L2-4 were synthesised with overall yields ranging from 20 to 48% using a similar pathway (see Supporting information, **S2-S4**), starting from ethylenediamine or *N*-benzylethylenediamine: first, a reductive amination of the primary amines with an aldehyde (salicylaldehyde or 2-pyridine carboxaldehyde), followed by nucleophilic substitution using *tert*-butyl bromoacetate, and finally deprotection of the *tert*-butyl esters. H_3L5 and H_2L7 have a common synthetic pathway (see Supporting information, **S5** and **S7**), starting from *N*-Boc-ethylenediamine. After a reductive amination to incorporate the 2-hydroxybenzyl substituent, nucleophilic substitution of benzyl bromide by the same nitrogen atom, followed by removal of the Boc-protecting group afforded intermediate 9. This compound was then subjected to another reductive amination using salicylaldehyde to yield the key compound 10. This key compound was then used to synthesise H_3L5 by nucleophilic substitution using bromoacetic acid, and also to synthesise H_2L7 by nucleophilic substitution using 2-(Boc-amino)ethyl bromide followed by deprotection of the primary amine. H_3L5 and H_2L7 were produced with 42% and 9% overall yields over 5 and 6 steps, respectively. H_3L6 is a structural isomer of H_3L3. It was synthesised in two steps (see Supporting information, **S6**) starting from compound 10, an intermediate in the syntheses of H_3L5 and H_2L7. *Tert*-butyl bromoacetate was used for nucleophilic disubstitution of the primary amine, and subsequent deprotection of the *tert*-butyl esters afforded H_3L6 with 30% overall yield. H_2L8 has a scaffold based on 1,4,7-triazaheptane. The benzyl and 2-hydroxybenzyl *N*-substituents were introduced by nucleophilic substitution using

benzyl bromide and reductive amination using salicylaldehyde. H_2L8 was prepared in two steps, with 50% overall yield (see Supporting information, **S8**).

3.2 Complexation of $\{Al^{18}F\}^{2+}$

The effectiveness of the novel chelators for complexation of $\{Al^{18}F\}^{2+}$ was tested. The new ligands were incubated with $\{Al^{18}F\}^{2+}$ at different temperatures (from rt to 110 °C) for 12 min and the radiochemical yields (RCYs) were determined by instant thin layer chromatography (iTLC) (**Figure 2**). It was observed that only ligands containing the fragment ethylenediamine-*N*,*N*'-diacetic acid (H_3L1-L4) were able to efficiently chelate aluminium fluoride. Ligands without this arrangement of functional groups (H_3L5-8) did not complex aluminium fluoride with good RCY under the conditions tested (see Supporting information, **Table S1**). This was corroborated when the reactivities of the two structural isomers H_3L3 and H_3L6 were compared. While the first ligand chelated $\{Al^{18}F\}^{2+}$ at moderate temperatures (77% at 40 °C), H_3L6 was not able to complex $\{Al^{18}F\}^{2+}$ efficiently, even at 110 °C only a low RCY of 8% was observed. Moreover, a thorough analysis of the results revealed that a pentadentate ligand with three carboxylic acids and without a phenol moiety is more reactive than a pentadentate ligand with only two carboxylic acids and a phenol. This combination of donating groups (H_3L1) resulted in a RCY of more than 90%, even at rt. This observation can be explained by the pH of the reaction mixture as an acidic pH (4-4.5) is required for chelation to prevent hydrolysis of aluminium fluoride in solution,[21] which would cause a significant drop in RCY. At pH 4 the carboxylic acids (pKa 3-4) are partially deprotonated and available to form an ionic bond with the aluminium ion, phenols on the other hand have a higher pKa (9-10) and are almost fully protonated at pH 4.5 and thus significantly less available to chelate $\{Al^{18}F\}^{2+}$.

Chelators H_3L2 and H_3L3 displayed a substantial increase of the RCY when the reaction was carried out at 40 °C as compared to room temperature (20-25 °C). Nevertheless, raising the temperature to 60, 80 or 110 ºC did not further improve the RCY. Similar temperature dependence was observed for H_2L4, but in this case the higher RCYs were observed from 60 °C on. This demonstrates that a phenol (H_3L2-3) is more suitable to complex $\{Al^{18}F\}^{2+}$ than a pyridine nitrogen atom (H_2L4) under these mild reaction conditions. Under the pH conditions required for the chelation of $\{Al^{18}F\}^{2+}$ (*i.e.* pH 4-5), the nitrogen atom on the pyridine ring is protonated, resulting in a positive charge that could hinder the complexation of $\{Al^{18}F\}^{2+}$ at low temperature.

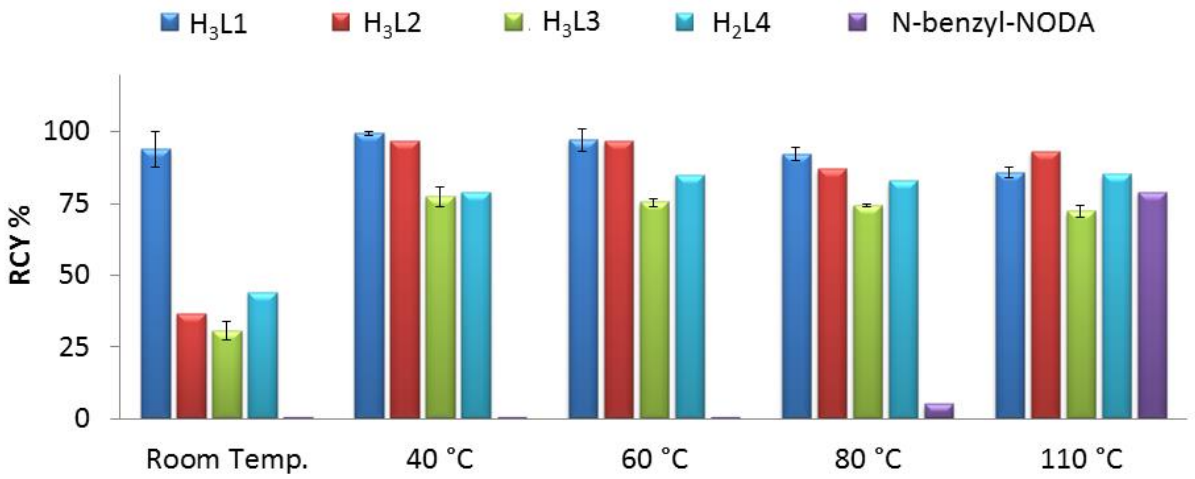

Figure 2: *Al^{18}F-complexation efficiency of H_3L1-4 and N-benzyl-NODA at different temperatures (150 nmoles ligand, 46 nmoles $AlCl_3$, sodium acetate buffer 0.1 M pH 4, 12 min). X-axis displays the reaction temperature, while the Y-axis displays the radiochemical yield as percentage of starting fluorine-18 radioactivity (H_3L1 and H_3L3: n=3; H_3L2, H_2L4 and N-benzyl-NODA: n=1)*

All studied metal complexes were successfully purified using Sep-Pak Plus Alumina-N-cartridges, following a previously reported procedure.[11] An example of iTLC analysis of Al^{18}F-L3, before and after alumina-N-cartridge purification is shown in **Figure S1** (see Supporting information). The purified Al^{18}F-complexes were characterised with radio-HPLC-HRMS and the proposed structures of the complexes are presented in **Figures S2-S5** (see Supporting information). As derived from the molecular ion mass, the AlF-complexes formed with ligands H_3L1-3 have a negative overall charge whereas H_2L4 forms a neutral complex with $\{Al^{18}F\}^{2+}$.The stable complexes Al^{19}F-L_n and Al^{19}F-*N*-benzyl-NODA were also prepared and identified with HPLC-HRMS (see Supporting information). Al^{19}F-L1, Al^{19}F-L3 and Al^{19}F-*N*-benzyl-NODA were further identified with ^{1}H and ^{13}C NMR (see Supporting information, **Figure S6-8**).

3.3 *In vitro* and *in vivo* stability studies

The stability of [^{18}F]AlF-L1-4 and [^{18}F]AlF-*N*-benzyl-NODA in phosphate buffered saline (PBS) (0.1 M, pH 7.4) at 37 °C and in rat plasma at 37 °C is shown in **Figure 3**. The stability of Al^{18}F-L3 was comparable to that of [^{18}F]AlF-*N*-benzyl-NODA up to 60 minutes of incubation. After 60 minutes the percentage of intact [^{18}F]AlF-L3 starts to decrease slowly, indicating demetallation and/or defluorination. After 240 min of incubation, 70% and 66% of [^{18}F]AlF-L3 was still intact in PBS and in rat plasma, respectively. The percentage of intact [^{18}F]AlF-*N*-benzyl-NODA after 240 min was respectively 88% and 87% in PBS and in rat plasma. Regarding complexes [^{18}F]AlF-L1, [^{18}F]AlF-L2 and [^{18}F]AlF-L4, substantial degradation occurred between 10 and 30 min of incubation. As expected, the degradation occurred faster in rat plasma than in PBS, possibly because in rat plasma competing metals and different endogenous chelators (for example *apo*-transferrin[15]) are present that can hamper the stability of the AlF-complexes. The limited stability of [^{18}F]AlF-L1 is probably due to the

fact that either the complex is not rigid enough to retain the $\{Al^{18}F\}^{2+}$ moiety or the low basicity of the acetate groups makes the Al-O bond weaker (in comparison with phenol on H_3L3). In either case, the complex is more labile causing a faster demetallation. The instability of the complex with the hexadentate ligand [^{18}F]AlF-L2 can be explained by demetalation and/or defluorination in the presence of an uncoordinated donor atom. We hypothesise that at pH 7 the uncoordinated donor atom competes with fluoride to bind to aluminium, thus causing fast defluorination. The formation of a complex with a hexadentate ligand and the consequent defluorination could be explained by the chelation effect despite the fact that the Al-F bond is stronger than an Al-O bond. The instability of $Al^{18}F$-L4 confirms that phenols form more stable complexes with $\{Al^{18}F\}^{2+}$ than pyridines.

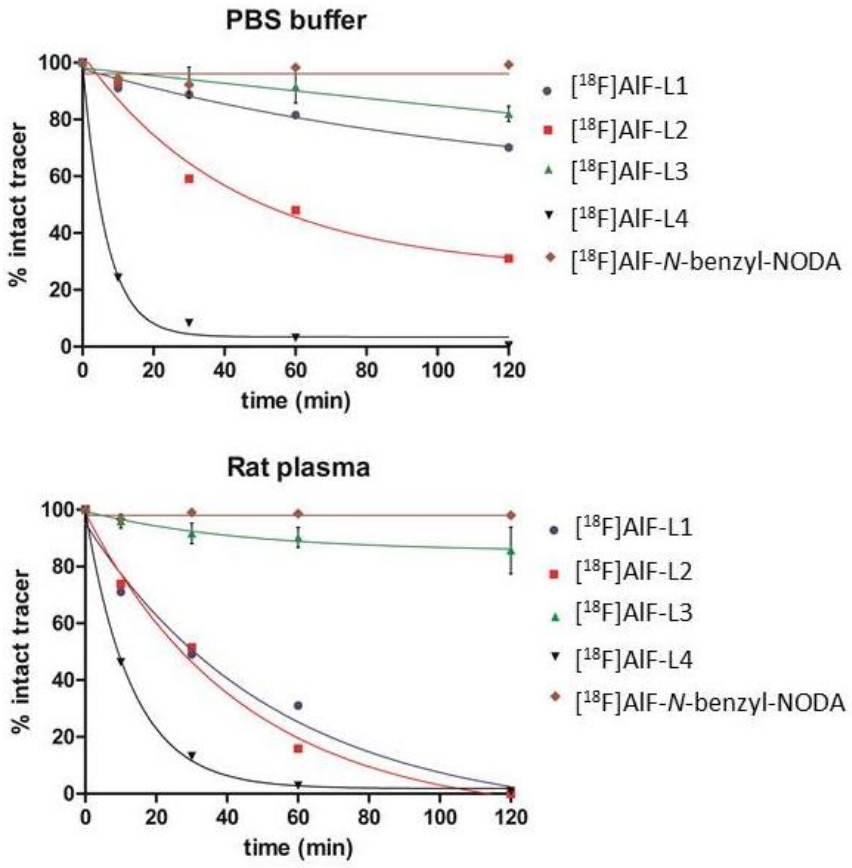

Figure 3: *Stability of [^{18}F]AlF-L1 (n=1), [^{18}F]AlF-L2 (n=1), [^{18}F]AlF-L3 (n=3), [^{18}F]AlF-L4 (n=1) and [^{18}F]AlF-N-benzyl-NODA (n=1) in PBS or rat plasma at 37 °C*

A biodistribution study with [^{18}F]AlF-L3 was carried out in healthy mice (**Figure 4**), and the results were compared to the distribution profile of $\{Al^{18}F\}^{2+}$. Free fluorine-18 as well as $\{Al^{18}F\}^{2+}$ are known to accumulate in bone.[22,23] As expected, there was extensive bone uptake for $\{Al^{18}F\}^{2+}$, with 60%ID (10 min p.i.) and 83%ID (60 min p.i.) and the excretion pathway for the metal fragment was mainly *via* the renal route. The biodistribution of [^{18}F]AlF-L3 demonstrated high *in vivo* stability, since no significant bone uptake was observed, which would indicate $\{Al^{18}F\}^{2+}$ or ^{18}F-fluoride release. The major fraction of activity at 60 min p.i. was observed in liver and intestines indicating hepatobiliary

clearance of the radiolabelled ligand. In comparison, [^{18}F]AlF-*N*-benzyl-NODA also was rapidly cleared from blood, showed low bone uptake but was mainly cleared renally.[11] It is difficult to predict whether the excretion pathway of the metal chelate will eventually influence the excretion of corresponding biomolecule conjugates. Probably, this effect needs to be taken into account when radiolabelling relatively small biomolecules, such as urea-based PSMA inhibitors for specific prostate cancer imaging.

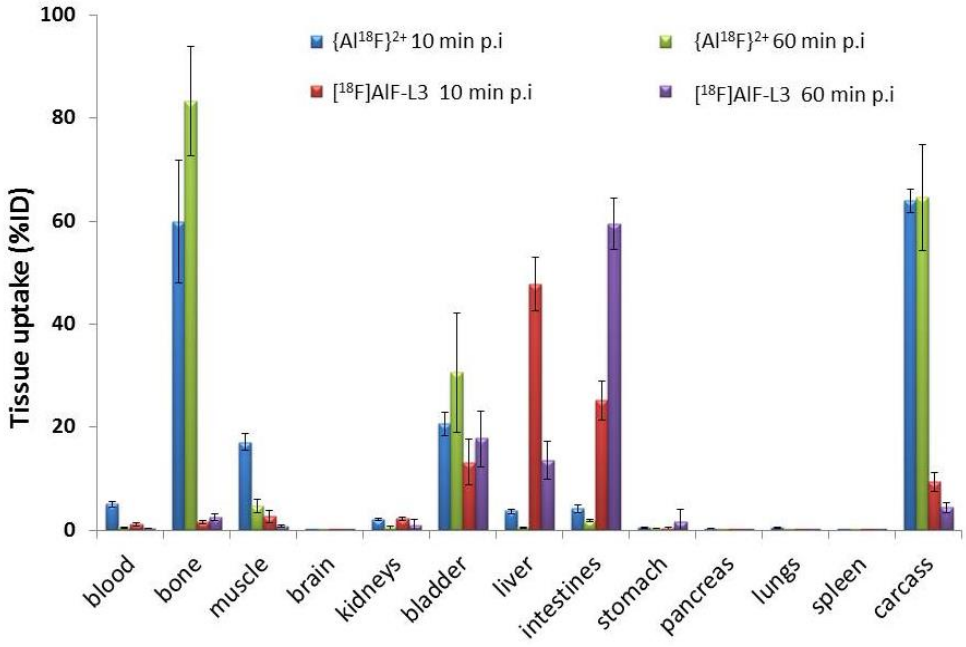

Figure 4: *Biodistribution of {Al^{18}F}$^{2+}$ and [^{18}F]AlF-L3 after iv injection in healthy male NMRI mice at 10 and 60 minutes p.i. (n=4/group). Results are presented as percentage of injected dose (%ID).*

3.4 Studies of different parameters influencing the complexation yield

The optimal pH range for labelling H_3L3 was found to be between 4 and 5, but even at pH 5.5 high RCYs were still observed, indicating that also acid-sensitive proteins can be labelled with the proposed method (**Figure 5A**). If the pH is too low, the preferred fluoride species in equilibrium is likely to be HF.[24] Moreover, the results suggest that the carboxylic acid groups need to be sufficiently deprotonated to efficiently chelate the {Al^{18}F}$^{2+}$ moiety since at pH 3-3.5 the RCY dropped significantly (<20%).

The reaction volume did not affect the radiochemical yield in the range of 238 µL to 573 µL (RCY > 90%). However, when the volume exceeded 1 mL the RCY decreased to 82%. Other groups already described improvement of {Al^{18}F}$^{2+}$ labelling yields in the presence of acetonitrile or ethanol.[15] We also observed an increase of the RCY from 77% to 95% in the presence of 20% of either ethanol or acetonitrile. Small amounts of organic solvent are compatible with biomolecules but excessive

percentages should be avoided to prevent denaturation. In conclusion, optimal results were obtained at pH 4.5-5, a total reaction volume less than 1 ml and in the presence of 20% acetonitrile or ethanol.

Purification and quality control of radiolabelled peptides is usually performed with RP-HPLC in acidic conditions e.g. using trifluoroacetic acid 0.1% w/v in the mobile phase (pH 2). However, most metal complexes are found to de-ligate fairly quickly at this pH.[15] Therefore the stability of [^{18}F]AlF-L3 was determined in different buffers ranging from pH 2 to pH 8. The results show that the [^{18}F]AlF-L3 complex is not stable at pH <4. After 60 min of incubation, the percentage of intact tracer dropped to 58%, 68% and 75% at pH 2, 3 and 4, respectively. In contrast, the [^{18}F]AlF-L3 complex was very stable (> 95%) for at least 60 min in the pH range from 5 to 8 (see Supporting information, **Figure S9**). Recovery of fluorine-18 in the form of fluoride is an important validation parameter in the quality control of fluorine-18 labelled radiopharmaceuticals because retention of [^{18}F]fluoride on HPLC columns may result in an overestimation of the radiochemical purity. Ory et al.[25] have shown that [^{18}F]fluoride recovery increases with increasing pH and thus it is recommended to use a mobile phase with a pH higher than 5 for silica-based C18 columns for both quality control and semi-preparative HPLC of fluorine-18 labelled PET radiopharmaceuticals. Consequently, for both reasons an appropriate buffer should be selected for HPLC purification and analysis of the Al^{18}F-complexes.

Another critical parameter for efficient labelling is the $^{18/19}F^-$-to-Al^{3+} ratio and the Al^{3+}-to-ligand ratio in the reaction mixture. The number of fluorine-18 atoms in a batch of [^{18}F]F^- is typically negligible (13 GBq corresponds to 0.2 nmoles of fluorine-18) in comparison with the number of fluorine-19 atoms. The main origin of fluorine-19 is the [^{18}O]water dispensing (loading) and delivery (unloading) system of the target, which often contains teflon (PTFE) tubings.[26] The specific activity of fluorine-18 tracers is usually in the range of 56-112 GBq/µmol. Hence, it should be kept in mind that there is a considerable amount of fluorine-19 present in a batch of [^{18}F]F^- (for example 3.7 GBq corresponds to 33-66 nmoles of fluorine for a specific activity of 56-112 GBq/µmol). To determine the effect of increasing amounts of fluorine on the chelation yield, increasing amounts of fluorine-19 (apart from the fluorine-19 present in 50 µL highly diluted (1/1000) [^{18}F]F^- solution) were added to a fixed amount of $AlCl_3$ (40 nmoles) and H_3L3 (150 nmoles). **Figure 5B** shows a decrease of labelling efficiency when higher amounts of fluorine-19 were added to the reaction mixture. This could be explained by the fact that not only $\{AlF\}^{2+}$ is formed, but with increasing amounts of fluorine-19 also other species, such as $\{Al^{18/19}F_2\}^+$ and $Al^{18/19}F_3$ can potentially be formed which are less efficiently chelated by H_3L3 and as a result the RCY drops.[27] The specific activity of fluorine-18 thus proves to be an important parameter for the Al^{18}F chelation yield.

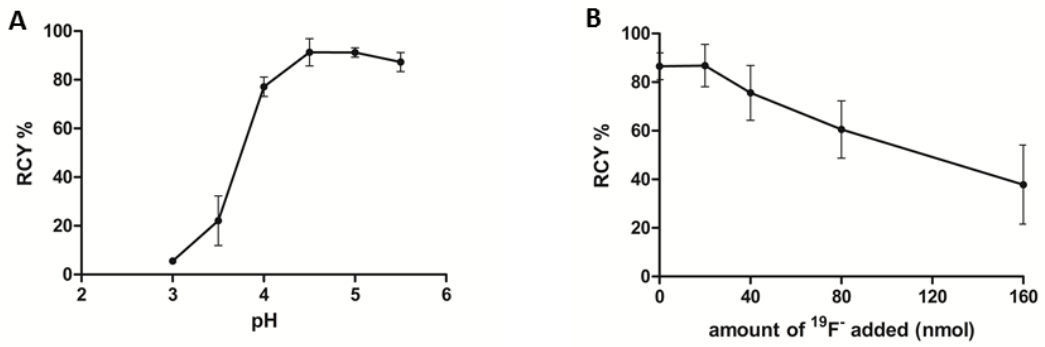

Figure 5: ***A:*** *Comparative labelling efficiencies of H_3L3 at different pH values (n=3)* ***B:*** *Effect of the amount of $^{19}F^-$ added to the reaction mixture on the RCY (%) of [^{18}F]AlF-L3 (n=3)*

In another experiment, a fixed amount of ^{18}F-fluoride spiked with ^{19}F-fluoride (30 nmoles) was used and variable amounts of $AlCl_3$ (20 nmoles to 320 nmoles) were added. Addition of more than 50 nmoles of $AlCl_3$ resulted in a significant drop of RCYs. Most likely AlOH-L3 is formed in these conditions and as a consequence there is less ligand available for chelation of $\{AlF\}^{2+}$. The optimal H_3L3 to Al^{3+} molar ratio was found to be 3:1 (see Supporting information, **Figure S10**).

3.5 Synthesis, radiosynthesis and preclinical evaluation of [^{18}F]AlF-labelled Glu-NH-CO-NH-Lys(Ahx)L3

The best method to assess the *in vivo* stability and kinetic inertness of a chelate is to attach it to a suitable vector so that the complex remains in circulation for a longer period of time.[15] The "naked" and negatively charged $Al^{18}F$-L3 complex is cleared relatively fast from the body, and does not persist *in vivo* long enough to encounter challenge to its structural integrity. Therefore, as a proof of concept, the ligand H_3L3 was derivatised and successfully conjugated with a hydrophilic urea-based inhibitor of PSMA, Glu-NH-CO-NH-Lys, to form Glu-NH-CO-NH-Lys(Ahx)L3 (see Supporting information, **S9**).[18] The process of radiosynthesis and purification with preparative radio-HPLC was performed using a home-built remotely controlled system. Glu-NH-CO-NH-Lys(Ahx)L3 was labelled with $\{Al^{18}F\}^{2+}$ in a non-optimized yield of 25% (12 min 40 °C, pH 4.5). The batch (8.14 GBq) was produced and purified to a radiochemical purity higher than 98%, in 35 min (starting after elution of fluorine-18 from the anion exchange QMA cartridge). The specific activity was 27 GBq/µmol, calculated on the starting amount of Glu-NH-CO-NH-Lys(Ahx)L3. Analytical HPLC of the final product was performed and high resolution mass spectrometry (HRMS) analysis corroborated the identity of the radiotracer (see Supporting information, **Figure S11**). It was shown that the PSMA-binding fragment as such cannot bind the $\{Al^{18}F\}^{2+}$ core under the conditions tested (see Supporting information, **Figure S12**). [^{18}F]AlF-Glu-NH-CO-NH-Lys(Ahx)L3 was stable (>95%) in saline at room temperature for at least three hours (see Supporting information, **Figure S13**).

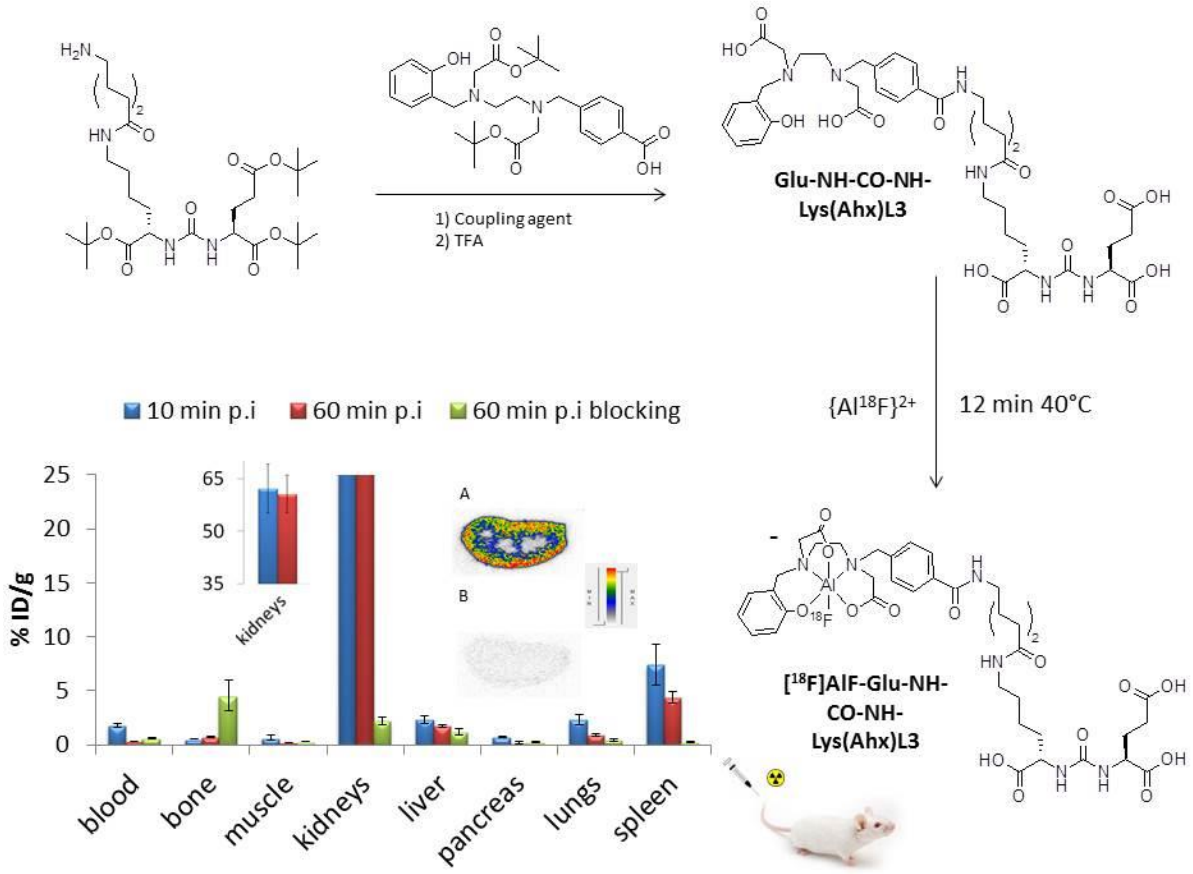

Figure 6: *Synthesis, Al^{18}F-labelling, in vitro autoradiography on kidney slices, and in vivo biodistribution in healthy mice of [^{18}F]AlF-labelled Glu-NH-CO-NH-Lys(Ahx)L3. Biodistribution (%ID/g) in healthy NMRI mice (n= 4 per time point) with or without coadministration of 2 mg/kg 2-PMPA (blocking agent) at 10 min or 60 min p.i. and autoradiography on kidney slices of healthy mice with (B) or without (A) blocking with 2-PMPA (100 µM).*

To assess the *in vivo* stability and to evaluate the distribution profile of the tracer, a biodistribution study was carried out in healthy mice (**Figure 6**). The compound demonstrated high *in vivo* stability, as no significant bone uptake was observed at 60 min p.i. (0.74 ± 0.07% ID/g). However, the hydrophilic tracer was cleared fast from plasma and PSMA negative tissue, therefore additional experiments with peptides that circulate longer in blood are needed to further evaluate the structural integrity of the [^{18}F]AlF-L3 complex *in vivo*. Radio-iTLC-SG analysis of mouse urine samples 60 min p.i. showed that >90% of activity was still present as an Al^{18}F-complex and not as free fluorine-18 or {Al^{18}F}$^{2+}$(see Supporting information, **Figure S14**). The retention at 60 min p.i. in organs with reported high expression of PSMA such as kidneys (121± 11% ID/g) and spleen (4± 0.5% ID/g) was nearly completely blocked when the non-structural related inhibitor 2-(phosphonomethyl)pentane-1,5-dioic acid (2-PMPA) was coinjected to block PSMA-specific binding. These results indicate high affinity and specific binding of [^{18}F]AlF-Glu-NH-CO-NH-Lys(Ahx)L3 for the PSMA receptor. The same effect was shown with in-vitro autoradiography on kidney slices of healthy

mice with or without blocking with 2-PMPA (**Figure 6**). The increased bone uptake at 60 min p.i. observed after coadministration of the blocking agent 2-PMPA is possibly the result of extended residence time in blood, which could indicate limited instability of the [^{18}F]AlF-L3 complex *in vivo*. In conclusion, the first preclinical results of [^{18}F]AlF-Glu-NH-CO-NH-Lys(Ahx)L3 look promising and this radiotracer will be further evaluated in mice bearing PSMA-positive tumors.

4. CONCLUSIONS

This study identified new chelators that allow efficient complexation of {Al^{18}F}$^{2+}$ using mild labelling conditions (temperature of 40 °C). These ligands display a less rigid structure than macrocyclic ligands such as NOTA and NODA, thus reducing the activation energy for the complexation reaction and consequently allowing low-temperature labelling. Optimal results were obtained at pH 4.5-5 and it has been shown that the specific activity of fluorine-18 proves to be an important parameter for the Al^{18}F chelation yield. [^{18}F]AlF-L3 complex demonstrated a stability in PBS and in rat plasma comparable to that of the previously reported Al^{18}F-*N*-benzyl-NODA complex, up to 60 minutes. Although *in vitro* incubation in rat plasma showed slow decomposition, biodistribution of [^{18}F]AlF-L3 showed absence of bone uptake indicating that *in vivo* defluorination or demetalation if any, is limited. As a proof of concept, the ligand H_3L3 was derivatised and successfully conjugated with a urea-based inhibitor of PSMA. [^{18}F]AlF-Glu-NH-CO-NH-Lys(Ahx)L3 was produced with high radiochemical purity in 35 min. The compound demonstrated high *in vivo* stability, proven by the absence of significant bone uptake, and the first preclinical results in healthy mice look promising.

In conclusion, the acyclic chelator H_3L3 demonstrated to be a good lead candidate for labelling of heat-sensitive biomolecules with fluorine-18. However, there is still room for improvement regarding the stability of the [^{18}F]AlF-L3 complex, so that the synthesis of improved derivatives is warranted. We are confident that this new class of AlF chelators may provide an efficient approach to label peptides and biomolecules with fluorine-18 at ambient temperature.

5. ACKNOWLEDGEMENTS

The authors would like to thank Ann Van Santvoort from the Department of Nuclear Medicine and Julie Cornelis, Ivan Sannen, Pieter Haspeslagh and Jana Hemelaers from the Laboratory for Radiopharmacy for their assistance. Compounds H_3L2, H_2L4 and H_2L5 were synthesised by Dr. Joan Lecina. Compounds H_3L6 and H_2L7 were synthesised by Dr. Emilie Billaud and compound Glu-NH-CO-NH-Lys(Ahx) was synthesised by Dr. Muneer Ahamed. All NMR experiments and interpretation of spectra were performed by Dr. Joan Lecina. This research has received support within the SBO project MIRIAD, funded from the IWT Flanders.

6. REFERENCES

(1) Rahmim, A., and Zaidi, H. (2008) PET versus SPECT: strengths, limitations and challenges. *Nucl. Med. Commun. 29*, 193–207.

(2) Serdons, K., Verbruggen, A., and Bormans, G. M. (2009) Developing new molecular imaging probes for PET. *Methods 48*, 104–111.

(3) Smith, G. E., Sladen, H. L., Biagini, S. C. G., and Blower, P. J. (2011) Inorganic approaches for radiolabelling biomolecules with fluorine-18 for imaging with positron emission tomography. *Dalton Trans. 40*, 6196–61205.

(4) McBride, W. J., Sharkey, R. M., Karacay, H., D'Souza, C. A., Rossi, E. A., Laverman, P., Chang, C.-H., Boerman, O. C., and Goldenberg, D. M. (2009) A novel method of ^{18}F radiolabeling for PET. *J. Nucl. Med. 50*, 991–998.

(5) Richter, S., Wuest, M., Bergman, C. N., Way, J. D., Krieger, S., Rogers, B. E., and Wuest, F. (2015) Rerouting the metabolic pathway of ^{18}F-labeled peptides: the influence of prosthetic groups. *Bioconjug. Chem. 26*, 201–212.

(6) Olberg, D. E., Arukwe, J. M., Grace, D., Hjelstuen, O. K., Solbakken, M., Kindberg, G. M., and Cuthbertson, A. (2010) One step radiosynthesis of 6-[$^{(18)}$F]fluoronicotinic acid 2,3,5,6-tetrafluorophenyl ester ([$^{(18)}$F]F-Py-TFP): a new prosthetic group for efficient labeling of biomolecules with fluorine-18. *J. Med. Chem. 53*, 1732–1740.

(7) Blykers, a., Schoonooghe, S., Xavier, C., D'hoe, K., Laoui, D., D'Huyvetter, M., Vaneycken, I., Cleeren, F., Bormans, G., Heemskerk, J. et al. (2015) PET Imaging of Macrophage Mannose Receptor-Expressing Macrophages in Tumor Stroma Using ^{18}F-Radiolabeled Camelid Single-Domain Antibody Fragments. *J. Nucl. Med. 56*, 1265–1271.

(8) McBride, W. J., Sharkey, R. M., and Goldenberg, D. M. (2013) Radiofluorination using aluminum-fluoride (Al^{18}F). *EJNMMI Res. 3*, 36-47

(9) Laverman, P., D'Souza, C. A., Eek, A., McBride, W. J., Sharkey, R. M., Oyen, W. J. G., Goldenberg, D. M., and Boerman, O. C. (2012) Optimized labeling of NOTA-conjugated octreotide with F-18. *Tumour Biol. 33*, 427–434.

(10) McBride, W. J., D'Souza, C. A., Sharkey, R. M., and Goldenberg, D. M. (2012) The radiolabeling of proteins by the [^{18}F]AlF method. *Appl. Radiat. Isot. 70*, 200–204.

(11) Shetty, D., Choi, S. Y., Jeong, J. M., Lee, J. Y., Hoigebazar, L., Lee, Y.-S., Lee, D. S., Chung, J.-K., Lee, M. C., and Chung, Y. K. (2011) Stable aluminium fluoride chelates with triazacyclononane derivatives proved by X-ray crystallography and ^{18}F-labeling study. *Chem. Commun. 47*, 9732-9734.

(12) De Meyer, T., Muyldermans, S., and Depicker, A. (2014) Nanobody-based products as research and diagnostic tools. *Trends Biotechnol. 32*, 263–270.

(13) Bhalla, R., Darby, C., Levason, W., Luthra, S. K., McRobbie, G., Reid, G., Sanderson, G., and Zhang, W. (2014) Triaza-macrocyclic complexes of aluminium, gallium and indium halides: fast ^{18}F and ^{19}F incorporation via halide exchange under mild conditions in aqueous solution. *Chem. Sci. 5*, 381-391.

(14) Malik, N., Baur, B., Winter, G., Reske, S. N., Beer, A. J., and Solbach, C. (2015) Radiofluorination of PSMA-HBED via $Al^{(18)}F^{(2+)}$ Chelation and Biological Evaluations In Vitro. *Mol. Imaging Biol.* 777–785.

(15) Price, E. W., and Orvig, C. (2014) Matching chelators to radiometals for radiopharmaceuticals. *Chem. Soc. Rev. 43*, 260–290.

(16) Yokel, R. a. (1994) Aluminum chelation: chemistry, clinical, and experimental studies and the search for alternatives to desferrioxamine. *J. Toxicol. Environ. Health*. *41*, 131-174

(17) Maresca, K. P., Hillier, S. M., Femia, F. J., Keith, D., Barone, C., Joyal, J. L., Zimmerman, C. N., Kozikowski, a. P., Barrett, J. a., Eckelman et al. (2009) A series of halogenated heterodimeric inhibitors of prostate specific membrane antigen (PSMA) as radiolabeled probes for targeting prostate cancer. *J. Med. Chem. 52*, 347–357.

(18) Eder, M., Schäfer, M., Bauder-Wüst, U., Hull, W. E., Wängler, C., Mier, W., Haberkorn, U., and Eisenhut, M. (2012) ^{68}Ga-complex lipophilicity and the targeting property of a urea-based PSMA inhibitor for PET imaging. *Bioconjug. Chem. 23*, 688–697.

(19) Mease, R. C., Foss, C. a, and Pomper, M. G. (2013) PET imaging in prostate cancer: focus on prostate-specific membrane antigen. *Curr. Top. Med. Chem.13,* 951-962

(20) Laverman, P., McBride, W. J., Sharkey, R. M., Goldenberg, D. M., and Boerman, O. C. (2014) $Al^{(18)}F$ labeling of peptides and proteins. *J. Labelled Comp. Radiopharm. 57*, 219–223.

(21) Yokel, R. A. (2002) Aluminum chelation principles and recent advances. *Coord. Chem. Rev. 228*, 97–113.

(22) Jadvar, H., Desai, B., and Conti, P. S. (2015) Sodium ^{18}F-fluoride PET/CT of bone, joint, and other disorders. *Semin. Nucl. Med. 45*, 58–65.

(23) Chatalic, K. L. S., Franssen, G. M., van Weerden, W. M., McBride, W. J., Laverman, P., de Blois, E., Hajjaj, B., Brunel, L., Goldenberg, D. M., Fehrentz et al. (2014) Preclinical comparison of $Al^{18}F$- and ^{68}Ga-labeled gastrin-releasing peptide receptor antagonists for PET imaging of prostate cancer. *J. Nucl. Med. 55*, 2050–2056.

(24) Martin, R. B. (1988) Ternary hydroxide complexes in neutral solutions of Al^{3+} and F^-. *Biochem. Biophys. Res. Commun. 155*, 1194–1200.

(25) Ory, D., Van den Brande, J., de Groot, T., Serdons, K., Bex, M., Declercq, L., Cleeren, F., Ooms, M., Van Laere, K., Verbruggen et al. (2015) Retention of [^{18}F]fluoride on reversed phase HPLC columns. *J. Pharm. Biomed. Anal. 111*, 209–214.

(26) Füchtner, F., Preusche, S., Mäding, P., Zessin, J., and Steinbach, J. (2008) Factors affecting the specific activity of [^{18}F]fluoride from a [^{18}O]water target. *Nuklearmedizin. 47*, 116–119.

(27) HEM, J. D. (1968) Aluminum Species in Water, *In Trace Inorganics In Water*. *4*, 98–114.

(28) Fritzberg, A. R., Whitney, W. P., Kuni, C. C., and Klingensmith, W. (1982) Biodistribution and renal excretion of ^{99m}Tc-N,N'-bis-(Mercaptoacetamido) ethylenediamine. Effect of renal tubular transport inhibitors. *Int. J. Nucl. Med. Biol. 9*, 79–82.

(29) Mitterhauser, M., Toegel, S., Wadsak, W., Lanzenberger, R. R., Mien, L.-K., Kuntner, C., Wanek, T., Eidherr, H., Ettlinger, D. E., Viernstein et al. (2007) Pre vivo, ex vivo and in vivo evaluations of [^{68}Ga]-EDTMP. *Nucl. Med. Biol. 34*, 391–407.

(30) Balsells, J., Carroll, P. J., and Walsh, P. J. (2001) Achiral tetrahydrosalen ligands for the synthesis of C2-symmetric titanium complexes: A structure and diastereoselectivity study. *Inorg. Chem. 40*, 5568–5574.

(31) Sundaravel, K., Dhanalakshmi, T., Suresh, E., and Palaniandavar, M. (2008) Synthesis, structure, spectra and reactivity of iron(III) complexes of facially coordinating and sterically hindering 3N ligands as models for catechol dioxygenases. *Dalton Trans.* 7012–7025.

(32) Baffert, C., Collomb, M., Deronzier, A., Kjærgaard-knudsen, S., Latour, J., Lund, K. H., Mckenzie, C. J., Mortensen, M., Preuss, L., and Thorup, N. (2003) Biologically relevant mono- and di-nuclear manganese II / III / IV complexes of mononegative pentadentate ligands *Dalton Trans*. 1765–1772.

CHAPTER III

RESTRAINED COMPLEXING AGENTS FOR AL^{18}F-LABELLING OF HEAT-SENSITIVE BIOMOLECULES

Cleeren F[1], Lecina J[1], Koole M[2], Verbruggen A[1] and Bormans G[1]

[1]*Laboratory for Radiopharmacy, University of Leuven, Belgium*
[2]*Department of Nuclear Medicine and Molecular Imaging, University of Leuven, Belgium*

ABSTRACT

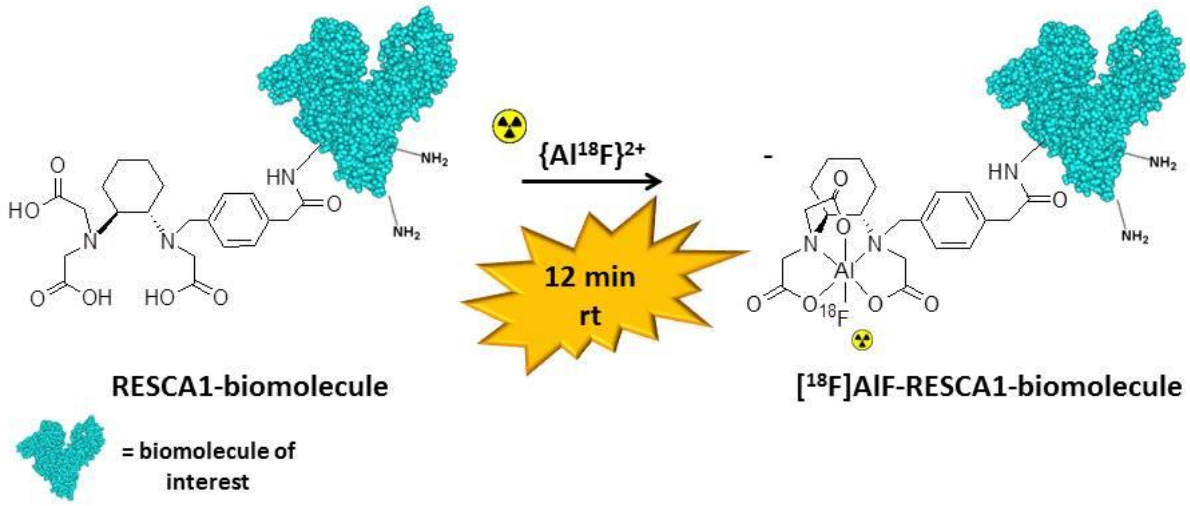

Most methods for radiolabelling biomolecules with fluorine-18 are laborious and require multistep procedures with moderate overall labelling yields. The $Al^{18}F$-labelling strategy involves chelation of aluminium mono[^{18}F]fluoride ($\{Al^{18}F\}^{2+}$) in aqueous medium by a suitable chelator conjugated to a biomolecule. Although many previous studies demonstrated the versatility of the $Al^{18}F$ approach to radiolabel peptides, the approach has limited applicability for heat sensitive biomolecules due to high temperatures required for the complexation reaction (≥ 100 °C) when used with macrocyclic complexing agents such as NOTA and NODA. Therefore, we designed new restrained complexing agents (RESCA1-5) for application of the $Al^{18}F$ strategy at room temperature. Restrained complexing agent 1 (RESCA1) is an acyclic pentadentate ligand with an N_2O_3 coordinative set and this new chelator allows radiolabelling of heat-sensitive biomolecules via the $Al^{18}F$-method in one radiolabelling step at moderate temperature. As a proof of concept, RESCA1 was conjugated to the heat-sensitive protein human serum albumin (HSA) and the construct was efficiently labelled with $\{Al^{18}F\}^{2+}$ at ambient temperature. [^{18}F]AlF-RESCA1-HSA showed excellent stability and favourable properties for PET blood pool imaging applications. The new AlF chelator provides an efficient, generic approach to label heat-sensitive biomolecules with fluorine-18 for PET applications.

1. INTRODUCTION

Positron emission tomography (PET) provides non-invasive, sensitive and specific imaging of biochemical and physiological phenomena *in vivo*, which can be used to study the function of cells, receptors, neurotransmitters, genes and drug pharmacokinetics.[1] Among β^+-emitting radioisotopes, the radiohalogen fluorine-18 is the most commonly used in PET due to its optimal chemical properties and almost ideal nuclear decay characteristics.[2] The low maximum energy (0.635 MeV) of its positron emission enables high resolution images as a result of the short range tissue penetration prior to annihilation. The half-life of 109.8 min is short enough to avoid prolonged irradiation of subjects, yet still long enough to allow multistep synthesis, extended *in vivo* investigations and, permits commercial distribution to remote imaging centres without an on-site cyclotron.[3]

The Al^{18}F-labelling strategy involves chelation in aqueous medium of aluminium mono[^{18}F]fluoride ({Al^{18}F}$^{2+}$) by a suitable chelator conjugated to a biomolecule.[4] Aluminium forms octahedral complexes, therefore a pentadentate ligand is desired, leaving one binding site open for the fluorine ion. The most frequently used chelator for Al^{18}F-labelling is the pentadentate ligand 1,4,7-triazacyclononane-1,4-diacetate (NODA).[5] Although this macrocyclic chelator shows a lot of potential, the high temperature required for the complexation reaction (≥100 °C) is still the main shortcoming that limits widespread application of this radiolabelling approach.[6] Therefore, an alternative chelator that eliminates the heating step is desired as it could result in a kit-based radiolabelling method. Kit preparation of ^{18}F-labelled PET tracers has the potential to partially substitute current technetium-99m tracers considering that (1) PET is a superior imaging technology over SPECT,[7] (2) recent problems with availability of technetium-99m generators due to molybdenum-99 disruptions is affecting the continuity of patient care worldwide,[8] and (3) growing availability of compact "dose-on-demand" cyclotrons.[9]

Recently, new polydentate ligands have been developed in our laboratory that can chelate {Al^{18}F}$^{2+}$ at moderate temperatures (≤40 °C). Successful labelling of two compounds, 2-[benzyl({2-[bis(carboxymethyl)amino]ethyl})amino]acetic acid (H_3L1) and 2-(benzyl(2-((carboxymethyl)(2-hydroxybenzyl)amino)ethyl)amino)acetic acid (H_3L3) was established (**Figure 1**).[10] These new chelators have less rigid structures, compared to NODA, reducing the activation energy required for complexation. Both H_3L1 and H_3L3 have excellent labelling properties but, unfortunately, Al^{18}F-L1 is not stable *in vitro*. On the other hand, Al^{18}F-L3 showed good stability in rat plasma up to 2 h but suffers from decomplexation after longer time-periods. Hence, there is still room for improvement regarding the stability of these newly developed {Al^{18}F}$^{2+}$-chelator complexes.

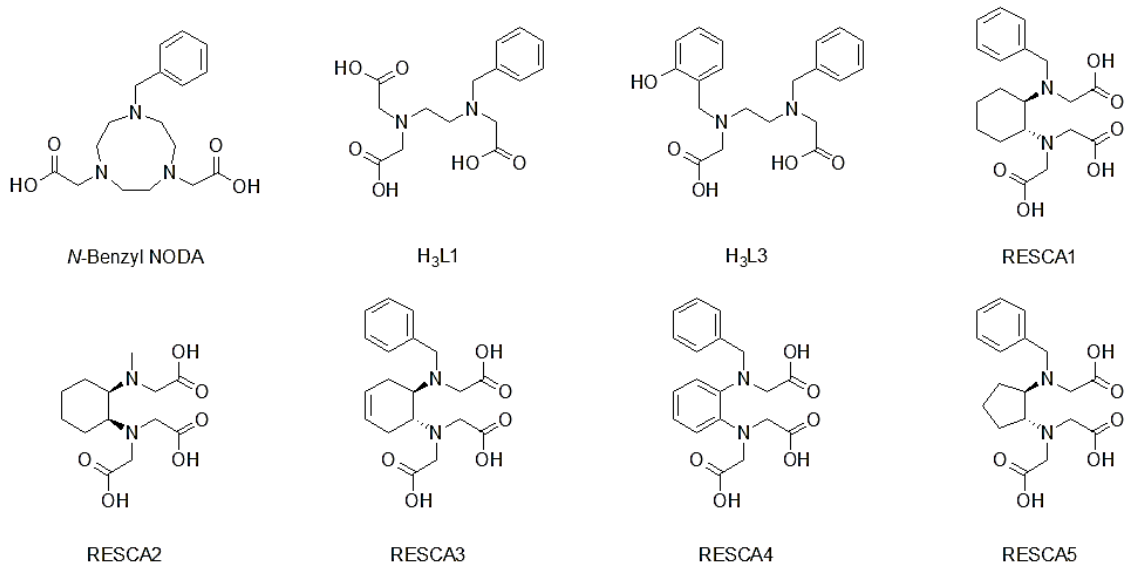

Figure 1: *Chemical structure of N-benzyl-NODA, H_3L1, H_3L3 and RESCA1-5*

The aim of the present study was to design new restrained complexing agents (RESCAs) which display a less rigid structure than the established macrocyclic AlF-ligands in order to reduce the activation energy of the complexation reaction. The area of improvement includes radiolabelling at moderate temperatures (≤40 °C), whilst maintaining sufficient *in vivo* stability. Novel chelators, RESCA1-5 (**Figure 1**), have been synthesised and the $\{Al^{18}F\}^{2+}$-core chelation efficiency and the *in vitro* and *in vivo* stability of the corresponding fluorine-18 labelled chelates has been evaluated as such (*i.e.* without being conjugated to biomolecules). Furthermore, in order to gain a better understanding of the different factors influencing the formation and stability of the complex, we carried out more in-depth experiments with ligand RESCA1. Labelling efficiency as a function of temperature, pH and $[Al^{3+}$/ligand]-ratio was studied in detail. As a proof of concept and to evaluate the stability and kinetic inertness of the chelate *in vivo*, RESCA1 was conjugated to human serum albumin (HSA) and the conjugate was labelled with $\{Al^{18}F\}^{2+}$.

2. MATERIALS & METHODS

2.1 General

All reagents and solvents were purchased from Sigma-Aldrich (Bornem, Belgium), Fluka (Bornem, Belgium), Fisher (Doornik, Belgium) or Acros Organics (Geel, Belgium). Fluorine-18 was produced on site using a cyclotron (IBA Cyclone 18/9, IBA, Louvain-la-Neuve, Belgium) by irradiation of $H_2{}^{18}O$ with 18-MeV protons. Radioactivity was measured using an ionisation chamber based activity meter (Capintec Radioisotope Calibrator CRC-721, Ramsey, NJ, USA).

Determination of the molecular ion mass of various compounds was achieved using a Dionex Ultimate 3000 LC System (Thermo Fisher Scientific, Sunnyvale, USA) coupled in series to an ultra-high resolution time-of-flight mass spectrometer (TOF-HRMS, MaXis impact, Bruker, Bremen, Germany), equipped with orthogonal electrospray ionisation (ESI) interface. Acquisition and processing of data were conducted using HyStar and Compass DataAnalysis (version 3.2, Bruker), respectively. Calculated monoisotopic mass values were obtained using Compas IsotopePattern (version 3.2, Bruker). Thin layer chromatography (TLC) was used for rapid analysis of reaction mixtures. The TLC plates were silica-based (Silica gel 60 plates, Merck, Darmstadt, Germany).

The synthesis and characterisation of compounds RESCA1-5 and RESCA-TFP is described in patent WO/2016/065435. Chemical structure elucidation was performed using proton-nuclear magnetic resonance spectrometry (^{1}H-NMR) at 400 MHz, carbon-nuclear magnetic resonance spectrometry (^{13}C-NMR) at 101 MHz and fluorine-nuclear magnetic resonance spectrometry (^{19}F-NMR) at 376 MHz on a Bruker AVANCE 400 MHz spectrometer (5 mm probe, Bruker AG, Fällanden, Switzerland).

Instant thin layer chromatography- silica gel (iTLC-SG) papers (Varian, Diegem, Belgium) were used with a mixture of acetonitrile and water (75:25, v/v) as the mobile phase. Autoradiography was performed using phosphor storage screens (super-resolution screen, Perkin Elmer, Waltham, USA). Screens were read in a Cyclone Plus system (Perkin Elmer) and analysed using Optiquant software (Perkin Elmer).

2.2 Complexation of $\{Al^{18}F\}^{2+}$

2.2.1 $\{Al^{18}F\}^{2+}$solution

$[^{18}F]F^-$ was separated from $[^{18}O]H_2O$ by trapping on a SepPak Light Accel plus QMA anion exchange cartridge (Cl^- form; Waters, Milford, USA). The cartridge was washed with water (3 mL) and $[^{18}F]F^-$ (148-333 MBq) was eluted with an aqueous solution of sodium chloride 0.9% (0.3 mL). The obtained $[^{18}F]F^-$ solution (50 µl) was added to 22.5 µL of 2 mM aluminium chloride ($AlCl_3$) in sodium acetate buffer (0.1 M, pH 4). The solution was incubated at room temperature (rt) for 5 min to form $\{Al^{18}F\}^{2+}$.

2.2.2 Synthesis and purification of [Al^{18}F]-complexes

A solution of each ligand (1 mL, 150 µM) in sodium acetate buffer (0.1 M, pH 4) was added to a vial which contained a freshly prepared $\{Al^{18}F\}^{2+}$ solution. The closed vials were heated in an oil bath at different temperatures for 12 min and the radiochemical yields (RCYs) were determined by iTLC-SG. The resulting mixtures were purified using a Sep-Pak Plus Alumina-N-cartridge (Waters, pre-rinsed with an aqueous solution of sodium chloride 0.9% (5 mL)). After loading of the crude reaction mixture, the cartridge was eluted with an aqueous solution of sodium chloride 0.9% (3 mL). The eluate was collected and each of the purified [Al^{18}F]-complexes was analysed using iTLC-SG and/or

radio-UPLC-HRMS (Acquity UPLC BEH C_{18} column, 1.7 µm, 2.1 mm x 150 mm, Waters) with gradient elution at a flow rate of 0.6 mL/min A: H_2O B: ACN, 0-2 min 5% B, 2 to 8 min 5% B to 95% B, 8-10 min 95% B, 10 to 12 min 95% B to 5% B).

2.3 *In vitro* stability tests of [^{18}F]AlF-RESCA1-5 in phosphate buffered saline (PBS) and rat plasma

$Al^{18}F$-complexes were synthesised and purified as described above by heating the mixtures at 40 °C for 12 min. A volume of 200 µL of each solution of purified [$Al^{18}F$]-complex was added to PBS (1 mL, 0.1 M pH 7.4) or rat plasma (1 mL). The mixtures were incubated at 37 °C and analysed by iTLC-SG at 10, 30, 60, 120, 180 and 240 min after the start of the incubation. Plasma samples were denatured by addition of the plasma solution (50 µL) to acetonitrile (50 µL). The mixture was stirred and centrifuged (1300 g, 3 min). Finally the supernatant was analysed using iTLC-SG.

2.4 [^{18}F]AlF-RESCA1: additional experiments on labelling efficiency

2.4.1 Influence of pH

A solution of RESCA1 (1 mL, 150 µM) in sodium acetate buffer (0.1 M, pH 3, 3.5, 4, 4.5, 5, 5.5), 2-(*N*-morpholino)ethanesulfonic acid (MES) buffer (0.1 M; pH 6 or 6.5) or tris(hydroxymethyl)aminomethane hydrochloride (tris-HCl) buffer (0.1 M; pH 7.5 or 8) was added to different vials containing 50 µL (3.7 MBq) of a freshly prepared $\{Al^{18}F\}^{2+}$ solution. The mixtures were incubated at 25 °C and radiochemical yields were determined by iTLC-SG at 12 min after the start of the incubation (n= 3). The pH values of the reaction mixtures were verified after sufficient decay.

2.4.2 Influence of the [Al^{3+}/ligand] ratios

An aqueous solution of [^{18}F]F^- (50 µL, 3.7 MBq) was added to 34, 23, 12, or 6 µL of 2 mM $AlCl_3$ in sodium acetate buffer (0.1 M, pH 4.5). The solutions were incubated at rt for 5 min to form $\{Al^{18}F\}^{2+}$. A solution of RESCA1 (1 mL; 150, 75, 50, or 25 µM) in sodium acetate buffer (0.1 M, pH 4.5) was added. The mixtures were incubated at 25°C and radiochemical yields were determined by iTLC-SG at 12 min after the start of the incubation (n=3).

2.5 Biodistribution and microPET studies

Quantification of radioactivity for biodistribution studies was performed using an automated gamma counter equipped with a 3-inch NaI(Tl) well crystal coupled to a multichannel analyser, mounted in a sample changer (Perkin Elmer 1480 Wizard 3q). Counts were corrected for background radiation, physical decay and counter dead time.

Animals were housed in individually ventilated cages in a thermo-regulated (~22 °C), humidity-controlled facility under a 12h-12h light-dark cycle, with access to food and water *ad libitum*. All animal experiments were conducted according to the Belgian code of practice for the care and the use of animals, after approval from the university animal ethics committee.

The biodistribution study of [^{18}F]AlF-RESCA1 was carried out in healthy male Naval Medical Research Institute (NMRI) mice (body weight: 30-40 g) at 10 and 60 min post injection (p.i.) (*n* = 4/time point). Mice were injected with the [^{18}F]AlF-RESCA1 complex (2 MBq) *via* a tail vein under anesthesia (2.5% isoflurane in O_2 at 1 L/min flow rate) and sacrificed by decapitation at above specified time points.

The biodistribution study of [^{18}F]AlF-RESCA1-HSA was carried out in healthy female Wistar rats (body weight: 187-225 g) at 1 h, 3 h and 6 h p.i. (*n* = 4/time point). Rats were injected with the [^{18}F]AlF-RESCA1-HSA complex (2-7.5 MBq) *via* a tail vein under anesthesia (2.5% isoflurane in O_2 at 1 L/min flow rate) and sacrificed by decapitation at above specified time points. Blood and major organs were collected in tared tubes and weighed. The radioactivity in blood, organs and other body parts was counted using the automated γ-counter. For calculation of total radioactivity in blood, bone and muscle, tissue mass was assumed to be, respectively, 7, 12 and 40% of the total body mass.[11,12] Results are presented as standardised uptake values (SUV). Blood data points in rats were fitted with a one component exponential equation to determine blood biological half-life. Small-animal whole-body PET imaging was performed on rats using a FOCUS^{TM} 220 microPET scanner (Concorde Microsystems, Knoxville, US) and PMOD software (v 3.2, PMOD Technologies, Zürich, Switzerland).

2.6 Synthesis of RESCA1-HSA

A solution of RESCA1-tetrafluorophenyl ester (RESCA1-TFP, 80 µL, 5.64 x 10^{-6} moles) in DMSO was added in a 15 molar excess to a solution of human serum albumin (1.5 ml, 3.7609 x 10^{-7} moles, CAF-DCF, Brussels, Belgium) in 0.05 M sodium bicarbonate pH 8.6 and the mixture was incubated for 2 h at rt. The conjugate was purified by gel filtration (PD-10 desalting column, GE Healthcare Bio-Science AB, Uppsala, Sweden) and the concentration of RESCA1-HSA was determined spectrophotometrically at 280 nm.

2.7 Radiosynthesis and purification of [^{18}F]AlF-RESCA1-HSA

[^{18}F]fluoride was produced (3.9 GBq) and trapped on a SepPak Light Accel plus QMA anion exchange cartridge as described above. [^{18}F]F^- was eluted from the cartridge with an aqueous solution of sodium chloride 0.9% (0.3 mL) and the eluate was diluted with water (2.7 mL). [^{18}F]F^- solution (250 µl, 1.25 GBq) was added to 25 µL of 2 mM aluminium chloride ($AlCl_3$) in sodium acetate buffer (0.1 M, pH 4.5). The solution was incubated at rt for 5 min to form $\{Al^{18}F\}^{2+}$. A solution of RESCA1-HSA (0.5 mL, 75 nmoles) in sodium acetate buffer (0.1 M, pH 4.6) was added to the freshly prepared $\{Al^{18}F\}^{2+}$

solution and was incubated at ambient temperature (20-22 °C) for 12 min. After incubation, the mixture was purified by gel filtration on a disposable PD-10 column (GE Healthcare), equilibrated with phosphate buffered saline. Radiochemical identity and purity were assessed by size-exclusion chromatography on a Superdex 200 10/300 GL column (GE Healthcare) using sodium phosphate buffer (0.01 M, pH 7.4, 0.14 M NaCl), as eluent at a flow rate of 0.5 mL/min. UV detection of the eluate was performed at 280 nm. The identity of the main compound was confirmed using non-radioactive HSA as reference material.

3. RESULTS AND DISCUSSION

The last years, a wide range of peptides have been labelled using the $Al^{18}F$-method by several groups.[13] Not only relative small peptides such as αvβ3 integrin-binding peptides, but also larger peptides, such as exendin-4 and affibodies, were successfully labelled with $\{AlF\}^{2+}$. The first clinical study using a peptide labelled with fluorine-18 using this method was published in 2013.[14] Although the macrocyclic chelators used in the published methods show a lot of potential, the high temperatures required for the complexation reaction (≥100 °C) is still a limitation for the widespread application of this radiolabelling approach. Therefore, the availability of a chelator that allows efficient chelation of $\{Al^{18}F\}^{2+}$ at moderate temperature (<40 °C) would be a major improvement. In an effort to develop such chelator, structural changes were investigated on promising pentadentate ligands, recently developed in our laboratory.[10]

One of these recently developed chelators, H_3L1, showed excellent chelation efficiency at rt (RCY ≥90%). However, almost complete dissociation of the $Al^{18}F$ complex was observed after 2 h incubation in rat plasma. In contrast, [^{18}F]AlF-L3 complex exhibited rat plasma stability comparable to that of $Al^{18}F$-N-benzyl-NODA up to 60 minutes, but at later time points significant defluorination was observed. Moreover, prominent bone uptake was observed in microPET studies with $Al^{18}F$-L3-PSMA, suggesting *in vivo* defluorination (**chapter IV**). Hence, there is still room for improvement regarding the stability of these $\{Al^{18}F\}^{2+}$-chelator complexes.

3.1 Synthesis

Brechbiel et al. reported that the incorporation of a *trans*-cyclohexyl moiety into the backbone of the ligand diethylenetriamine penta-acetic acid (DTPA) to form CyDTPA sterically hinders breakage of metal chelate rings.[16] As a result, the ^{212}Bi-complex with the ligand CyDTPA showed significantly increased stability in comparison with ^{212}Bi-DTPA as such. We explored whether incorporation of a *trans*-cyclohexyl moiety into H_3L1, to form restrained complexing agent 1 (RESCA1), would also increase steric rigidity of the AlF-complex, improving the orientation of the chelating groups and as a result improving the stability of the resulting AlF-complex. RESCA1 is an acyclic pentadentate ligand

with an N_2O_3 coordinative set and was efficiently synthesised in a three-step reaction starting from commercially available chemicals with an overall yield of 65%. The first results revealed that RESCA1 was as efficient as H_3L1 to chelate $\{Al^{18}F\}^{2+}$, with high reactivity (RCY ≥85%) at rt (**Figure 2**). Encouraged by these promising results and in an attempt to broaden the range of chelators, we decided to develop more derivatives of RESCA1 with refined changes in the backbone (RESCA 2-5, **Figure 1**). RESCA2 is the "cis" derivative of RESCA1 (*N*-methyl instead of *N*-benzyl substituent) and RESCA3 has a *trans*-cyclohexenyl moiety in the backbone. RESCA4 and RESCA5 have a phenyl ring and *trans*-cyclopentyl moiety in the backbone, respectively.

3.2 Complexation of $\{Al^{18}F\}^{2+}$

The novel chelators (RESCA1-5) were compared with H_3L1 and *N*-benzyl-NODA for efficiency of $\{Al^{18}F\}^{2+}$ chelation and stability of the corresponding complexes. The ligands were incubated with $\{Al^{18}F\}^{2+}$ at different temperatures (from rt to 110 °C) for 12 min and the RCYs were determined by iTLC **(Figure 2)**. It was observed that ligands RESCA1-5 showed efficient chelation of $\{Al^{18}F\}^{2+}$at all tested temperatures with RCYs higher than 60%. Chelators RESCA2 and RESCA4 displayed substantial increase of the RCY when the reaction was carried out at 40 °C as compared to room temperature (20-25 °C). The standard deviation on the results obtained with RESCA5 is relatively high, possibly indicating limited stability of the [^{18}F]AlF-RESCA5 complex during analysis.

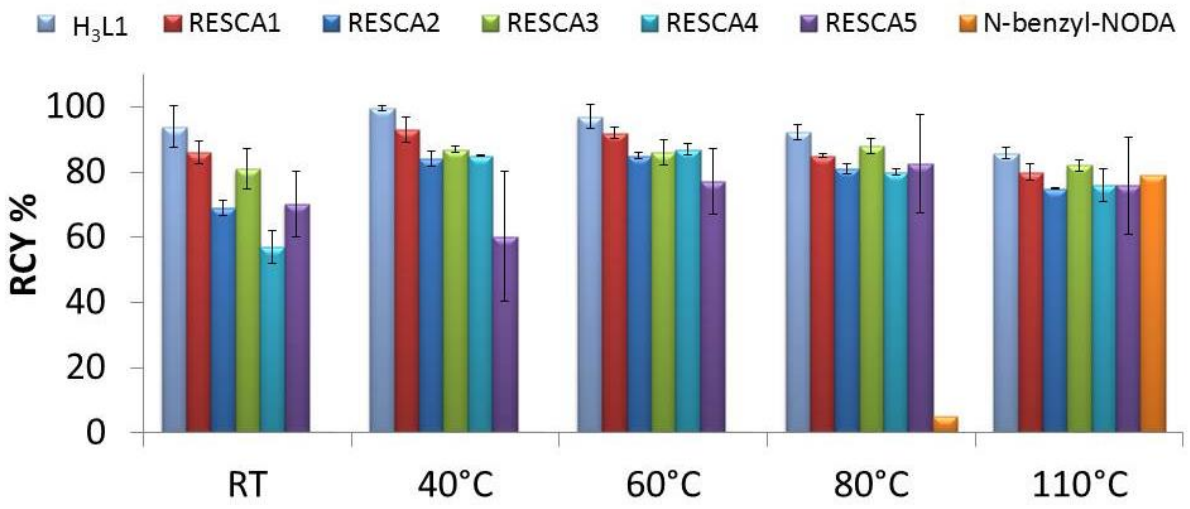

Figure 2: *$Al^{18}F$-complexation efficiency of H_3L1, RESCA1-5 and N-benzyl-NODA at different temperatures (150 nmoles ligand, 46 nmoles $AlCl_3$, sodium acetate buffer 0.1 M pH 4.5, 12 min). X-axis displays the reaction temperature, while the Y-axis displays the radiochemical yield as percentage of starting fluorine-18 radioactivity (H_3L1, RESCA1-5: n=3 and N-benzyl-NODA: n=1)*

All studied metal complexes were successfully purified (to > 98% purity) using Sep-Pak Plus Alumina-N-cartridges, following a previously reported procedure.[17] RESCA5 however was obtained with a purity of only 93%, determined by iTLC. The purified Al^{18}F-complexes were characterised with radio-HPLC-HRMS. As derived from the molecular ion mass, the AlF-complexes with ligands RESCA1-5 all

have a negative charge. The complex $Al^{19}F$-RESCA1 was prepared and identified with UPLC-HRMS and the structure of $Al^{19}F$-RESCA1 was further confirmed with ^{1}H- and ^{13}C-NMR.

3.3 *In vitro* stability of [^{18}F]AlF-RESCA1-5

Several factors are known to hamper the stability of an AlF-complex; (1) other metal ions (*e.g.* $Fe^{2/3+}$ and Ca^{2+}) readily present in plasma are able to compete with $\{AlF\}^{2+}$ for binding to the chelator[15], and (2) plasma proteins, such as the iron-binding blood plasma glycoprotein *apo*-transferrin, can potentially transchelate the $\{Al^{18}F\}^{2+}$ moiety out of the initial complex.[18] The stability of [^{18}F]AlF-L1, [^{18}F]AlF-RESCA1-5 and [^{18}F]AlF-*N*-benzyl-NODA in phosphate buffered saline (PBS) (0.1 M, pH 7.4) at 37 °C and in rat plasma at 37 °C is presented in **Figure 3**. [^{18}F]AlF-RESCA1 showed excellent stability in PBS and rat plasma, comparable to that reported for [^{18}F]AlF-*N*-benzyl-NODA, for at least 4 hours. After 240 min of incubation, 88% and 91% of $Al^{18}F$-RESCA1 was still intact in PBS and in rat plasma, respectively. The percentage of intact [^{18}F]AlF-*N*-benzyl-NODA after 240 min was respectively 88% and 87% in PBS and in rat plasma. It seems that the incorporation of the *trans*-cyclohexyl moiety into the backbone of ligand H_3L1 to form RESCA1 did not affect the reactivity to chelate $\{AlF\}^{2+}$ at room temperature. On the other hand, the kinetic inertness of the corresponding [^{18}F]AlF-RESCA1 complex was drastically improved compared to H_3L1, probably due to the increased steric rigidity and improved orientation of the chelating moieties. However, additional information on the structure of AlF-RESCA1 by X-ray diffraction studies is necessary to confirm above assumptions.

The “cis” derivative RESCA2, not only showed lower RCYs compared to RESCA1, also the stability of the corresponding AlF-complex was negatively affected with, as expected, a faster degradation in rat plasma than in PBS. After 240 min of incubation, 62% and 37% of [^{18}F]AlF-RESCA2 was intact in PBS and in rat plasma, respectively. These results confirm that the orientation of the chelating groups is not only of major importance for the reactivity but for the stability of the formed complex as well. The complex of $Al^{18}F$ with RESCA3 displayed good stability in PBS and rat plasma up to 60 minutes incubation. However, after 60 minutes the percentage of intact [^{18}F]AlF-RESCA3 started to decrease slowly, indicating demetallation and/or defluorination. After 240 min of incubation, 52% and 36% of $Al^{18}F$-RESCA3 was still intact in PBS and in rat plasma, respectively. This shows that small changes in the backbone (*trans*-cyclohexenyl ring instead of *trans*-cyclohexyl ring) seem to have a major effect on the stability of the formed complex. The instability of [^{18}F]AlF-RESCA4 could be explained by the reduced electrophilic properties of the nitrogen atoms due to the presence of the phenyl ring. It seems that changing the *trans*-cyclohexyl ring into a *trans*-cyclopentyl ring (RESCA5) results in inferior stability, probably due to unfavourable orientation of the chelating groups. Small changes in the backbone of RESCA1 resulted in minor to major loss of stability of the corresponding $\{AlF\}^{2+}$

complexes and thus, RESCA1 is the lead candidate for radiolabelling heat-sensitive biomolecules *via* the Al^{18}F-method.

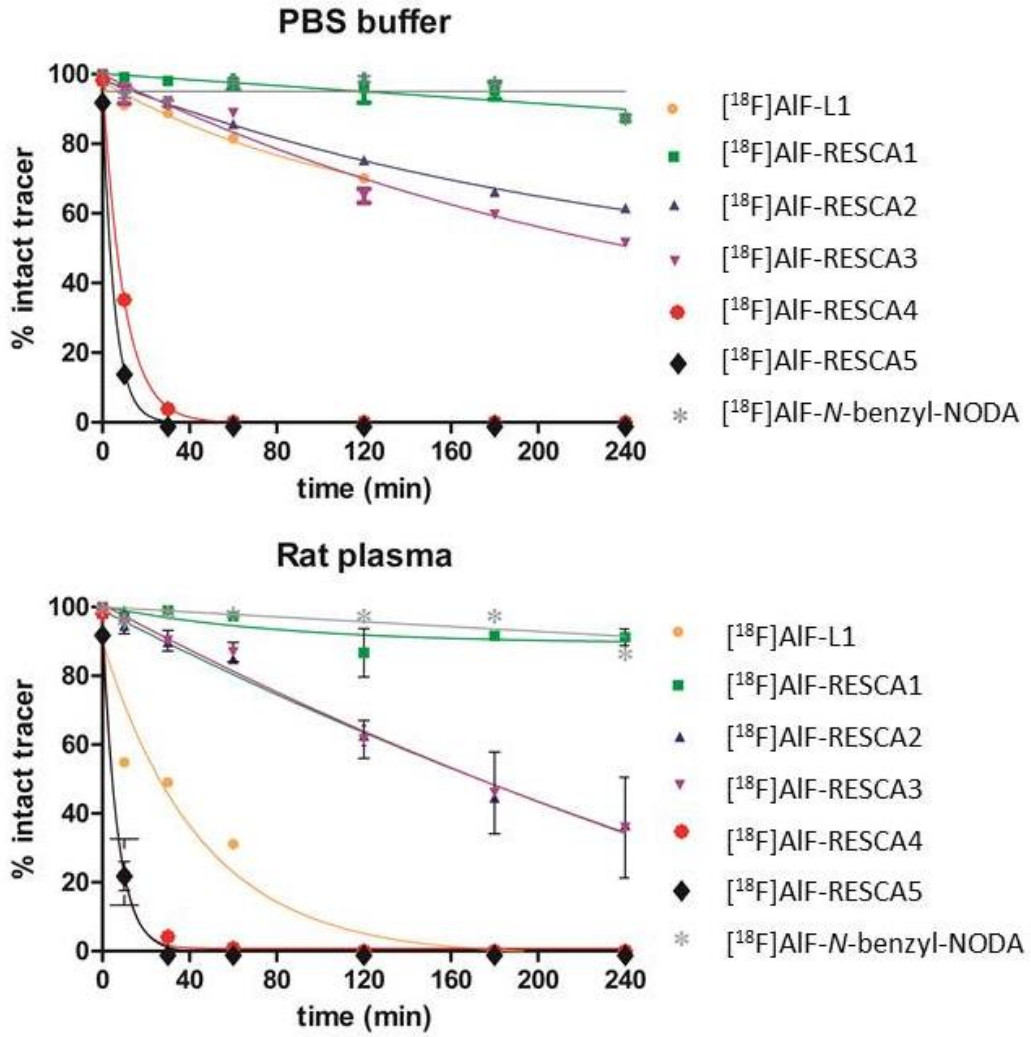

Figure 3: *In vitro stability of Al^{18}F-complexes in PBS and rat plasma. Stability of [^{18}F]AlF-L1 (n=1), [^{18}F]AlF-RESCA1-5 (n=3) and [^{18}F]AlF-N-benzyl-NODA (n=1) in PBS and rat plasma at 37 °C. Almost complete decomplexation (0.2% intact tracer) of [^{18}F]AlF-L1 in rat plasma is observed after 2 hours. [^{18}F]AlF-RESCA1 shows excellent stability in rat plasma, comparable to that of the reported [^{18}F]AlF-N-benzyl-NODA, for at least 4 hours.*

Purification and quality control of radiolabelled peptides is usually performed with RP-HPLC in acidic conditions, e.g. using trifluoroacetic acid 0.1% m/v in the mobile phase (pH 2).[19] However, metal complexes usually have lower stability at acidic pH.[15] Therefore the stability of [^{18}F]AlF-RESCA1 was determined in different buffers ranging from pH 2 to pH 8 and was found to be stable within this pH range. Mild degradation at the lowest investigated pH value (pH 2) was observed (91% and 88% was intact after 30 and 60 min, respectively). Consequently, an acidic buffer can be selected for HPLC purification and analysis of the [^{18}F]AlF-RESCA1-constructs.

3.4 *In vivo* stability of [^{18}F]AlF-RESCA1

To further explore the *in vivo* stability and evaluate the biodistribution of [^{18}F]AlF-RESCA1, a biodistribution study in NMRI mice was performed and results were compared to the biodistribution of free {Al^{18}F}$^{2+}$ (**Figure 4**). As expected, there was high bone uptake for {Al^{18}F}$^{2+}$ and the excretion pathway of the metal fragment was mainly *via* the renal route. In comparison, the biodistribution of [^{18}F]AlF-RESCA1 demonstrated high *in vivo* stability, as no significant bone uptake, which serves as an indicator of fluorine-18 release, was observed.

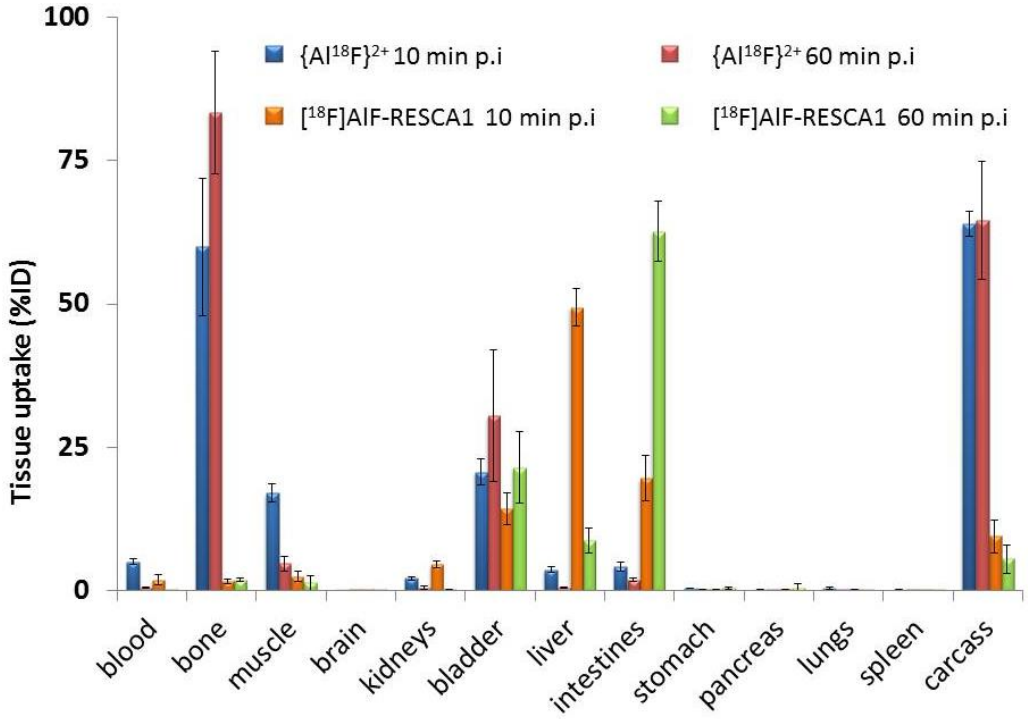

Figure 3: *Biodistribution of {Al^{18}F}$^{2+}$ and* [^{18}F]*AlF-RESCA1 after iv injection in healthy male NMRI mice at 10 and 60 min p.i. (n=4/group, 30-40 g). Results are presented as percentage of injected dose (%ID). For calculation of total radioactivity in blood, bone and muscle, tissue mass was assumed to be, respectively, 7, 12 and 40% of the total body mass. High bone uptake is observed for {Al^{18}F}$^{2+}$ and its excretion pathway is mainly via the renal route. Biodistribution of [^{18}F]AlF-RESCA1 shows high in vivo stability, since no significant bone uptake, which serves as an indicator of fluorine-18 release, was observed. The major fraction of activity at 60 min p.i. is observed in the liver and intestines which indicates hepatobiliary clearance of* [^{18}F]*AlF-RESCA1.*

The major fraction of activity at 60 min p.i. was observed in the liver and intestines due to hepatobiliary clearance of [^{18}F]AlF-RESCA1. It has been postulated that due to the incorporation of the rather lipophilic *trans*-cyclohexyl building block, the radiolabelled ligand follows the enterohepatic pathway. Moreover, due to the negative charge, [^{18}F]AlF-RESCA1 is possibly a substrate for organic anion-transporting polypeptides (OATP) in hepatocytes for excretion in bile. In comparison, [^{18}F]AlF-*N*-benzyl-NODA was also rapidly cleared from the blood, showed a low bone uptake, but was mainly excreted *via* the renal route. It is difficult to predict whether the excretion pathway of the metal chelate as such will eventually influence the excretion of corresponding

biomolecule conjugates. Certainly, this effect needs to be taken into account when radiolabelling relatively small molecules, but the impact of this effect on larger biomolecules, such as HSA, is expected to be minimal and requires further evaluation.

3.5 Parameters influencing the complexation yield

The pH of the labelling buffer is critically important for the formation of {Al^{18}F}$^{2+}$-chelates. If the pH is too low, the carboxyl groups are protonated which will hinder the coordination of aluminium and moreover the dominant fluoride species in equilibrium is likely to be HF.[20] The optimal pH range for labelling RESCA1 was found to be between 4.5 and 5, but even at pH 5.5-6 high RCYs were still observed, indicating that also acid-sensitive proteins can be labelled with the proposed method (**Figure 4A**). At even higher pH values, aluminium tends to form insoluble aluminium hydroxide. This results in lower RCYs and therefore it is of great importance that the pH of the reaction mixture is carefully controlled by a suitable buffer. Noteworthy is the fact that not all buffers are compatible with radiolabelling *via* the AlF-method. Examples of non-compatible buffers are citrate (pKa_1=3.13, pKa_2=4.76, and pKa_3=6.39) and phosphate buffers (pKa_1=2.15, pKa_2=7.09, and pKa_3=12.32). Citrate also forms a complex with aluminium ions whereas phosphates precipitates aluminium ions. For this reason a 2-(*N*-morpholino)ethanesulfonic acid (MES) buffer was used for an accurate estimation of the labelling efficiency at pH 6-6.5.

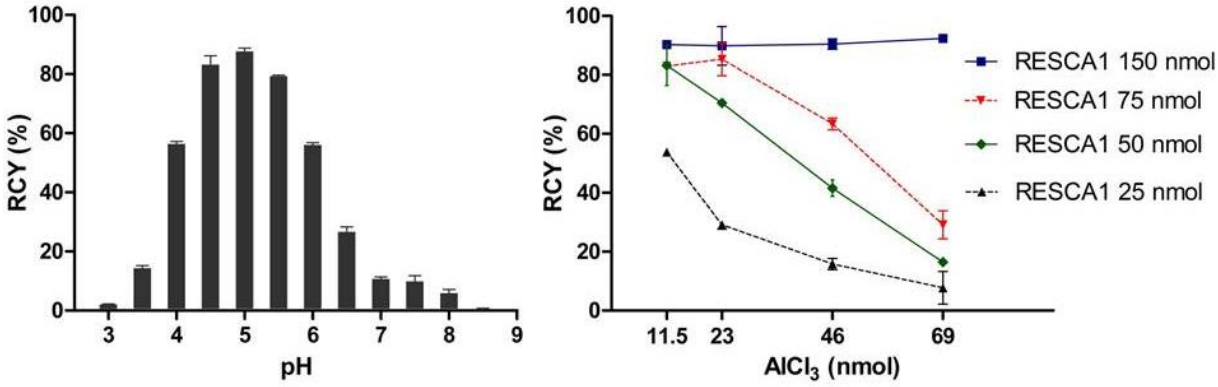

Figure 4: ***A:*** *Comparative labelling efficiencies of RESCA1 at different pH values (n=3)* ***B****: Effect of the amount of $AlCl_3$ and RESCA1 added to the reaction mixture on the RCY (%) of [^{18}F]AlF-RESCA1 (n=3)*

Another critical parameter for efficient labelling is the $^{18/19}F^-$-to-Al^{3+} ratio and the Al^{3+}-to-ligand ratio in the reaction mixture. We demonstrated previously with the chelator H_3L3 that the specific activity of fluorine-18 proves to be an important parameter for the Al^{18}F chelation yield.[10] This could be explained by the fact that not only {AlF}$^{2+}$ is formed, but with increasing amounts of fluorine-19 also other species, such as {Al$^{18/19}$F$_2$}$^+$ and Al$^{18/19}$F$_3$ can potentially be formed which are less efficiently chelated by the ligands, resulting in lower RCYs. The influence of the [Al^{3+}] to [RESCA1] ratio is shown in **Figure 4B**. The RCYs obtained when using 150 nmoles of RESCA1 were 90 ± 6%, independently of

the $AlCl_3$ concentration. When using 75 nmoles of RESCA1, the RCY was only 29 ± 5% with 69 nmoles of $AlCl_3$ and reached a maximum of 85 ± 6% at 23 nmoles of $AlCl_3$. When using 25 nmoles of RESCA1, the RCY decreased to 8 ± 6% with 69 nmoles of $AlCl_3$, whereas the lowest concentration of $AlCl_3$ resulted in the highest RCY of 53.7 ± 0.7%. With an excess of Al^{3+} relative to RESCA1, most likely AlOH-RESCA1 is formed and as a consequence there is less ligand available for chelation of $\{Al^{18}F\}^{2+}$. The optimal ligand to Al^{3+} molar ratio was found to be 3:1.

3.6 Labelling of human serum albumin (HSA)

The best method to assess the *in vivo* stability and kinetic inertness of a chelate is to attach it to a suitable vector that is slowly cleared from plasma and thus remains in circulation for a long period of time. The "naked" and negatively charged [^{18}F]AlF-RESCA1 complex is cleared relatively fast from the plasma, and does not persist *in vivo* in plasma long enough to challenge its structural integrity. To demonstrate the generic applicability of the proposed chelator for labelling of thermolabile biomolecules and to evaluate the kinetic inertness of the chelate *in vivo*, the bifunctional chelator RESCA1-TFP was conjugated via the amino group of the side-chain of lysines to the heat-sensitive protein HSA (**Figure 5**). HSA (66.5 kDa) is a globular protein with a primary sequence made up of 585 amino acid residues and is the most abundant protein in human plasma (3.5-5 g/dL).[21] It accounts for about 70% of the plasma colloid osmotic pressure. Albumin binds and carries a great variety of hydrophobic molecules such as metals, fatty acids, drugs and metabolites. Its high solubility, stability and plasma half-life of approximately 16-18 h, make HSA the ideal vector for PET blood pool imaging applications.[22]

RESCA1-TFP ester was efficiently conjugated to HSA providing RESCA1-HSA with a chelator-to-protein ratio of 3, estimated by ESI-TOF-HRMS analysis. RESCA1-HSA was labelled with $\{Al^{18}F\}^{2+}$ in good RCY at mild conditions (>70%, 12 min, 25 °C, pH 4.5). A batch of [^{18}F]AlF-RESCA-HSA (1.1 GBq) was produced and purified to a radiochemical purity higher than 95%, in less than 30 min after elution of fluorine-18 from the anion exchange QMA cartridge. [^{18}F]AlF-RESCA-HSA showed excellent stability *in vitro*. After 4 h incubation in rat plasma at 37 °C, 91% of the $Al^{18}F$-tracer was still intact as assessed by size exclusion chromotography.

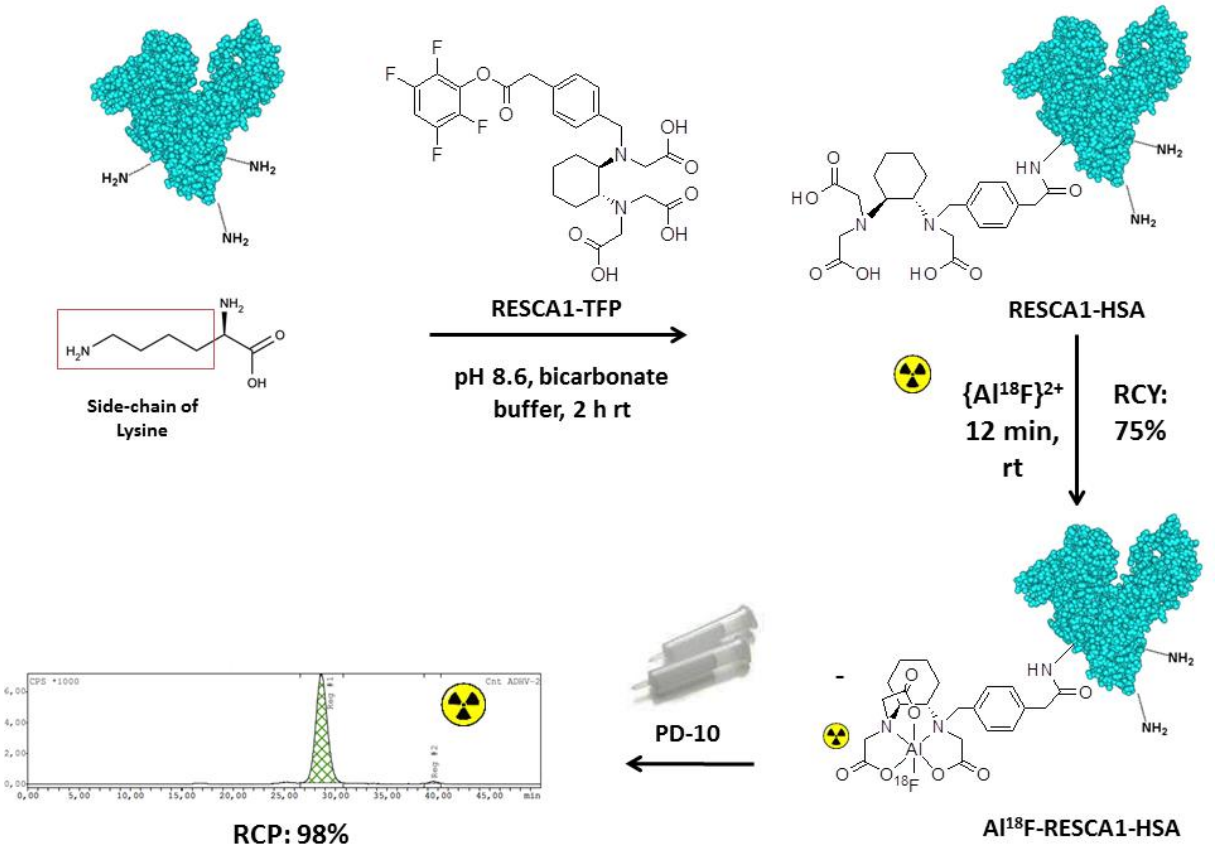

Figure 5: *Synthesis and radiolabelling of RESCA1-HSA with {Al^{18}F}$^{2+}$. RESCA1-TFP ester was conjugated to HSA providing RESCA1-HSA with a chelator-to-protein ratio of 3, estimated by ESI-TOF-HRMS analysis. Al^{18}F-RESCA-HSA was prepared in high RCY (>70%) and purity (>95%) in less than 30 min (starting after elution of fluorine-18 from the anion exchange QMA cartridge). RCP = radiochemical purity*

Biodistribution of [^{18}F]AlF-RESCA1-HSA in rats showed high retention in blood with 11.8 ± 0.6% ID/g, 10.1 ± 0.7% ID/g and 8.0 ± 0.1% ID/g at 1 h, 3 h and 6 h, respectively, from which the blood biological half-life was calculated to be 8.6 h. Bone is a highly vascular tissue, this might explain the observed bone uptake at 1h p.i. However, only minor increase in bone uptake was observed over time, indicating high *in vivo* stability of the Al^{18}F-labelled protein conjugate. Moreover, [^{18}F]AlF-RESCA-HSA showed favourable properties for PET blood pool imaging applications. A whole body PET image of a healthy rat 180 min after intravenous injection of [^{18}F]AlF-RESCA1-HSA is shown in **Figure 6.** The ventricles of the heart and the peripheral vasculature are well visualised. Other organs can be observed but retain lower concentrations of fluorine-18 than the central vasculature. The tissue concentrations in the microPET study are consistent with the biodistribution results at comparable times. We successfully labelled for the first time a heat-sensitive biomolecule via the Al^{18}F-method in one radiolabelling step. Moreover [^{18}F]AlF-RESCA1-HSA showed excellent stability and favourable properties for PET blood pool imaging applications.

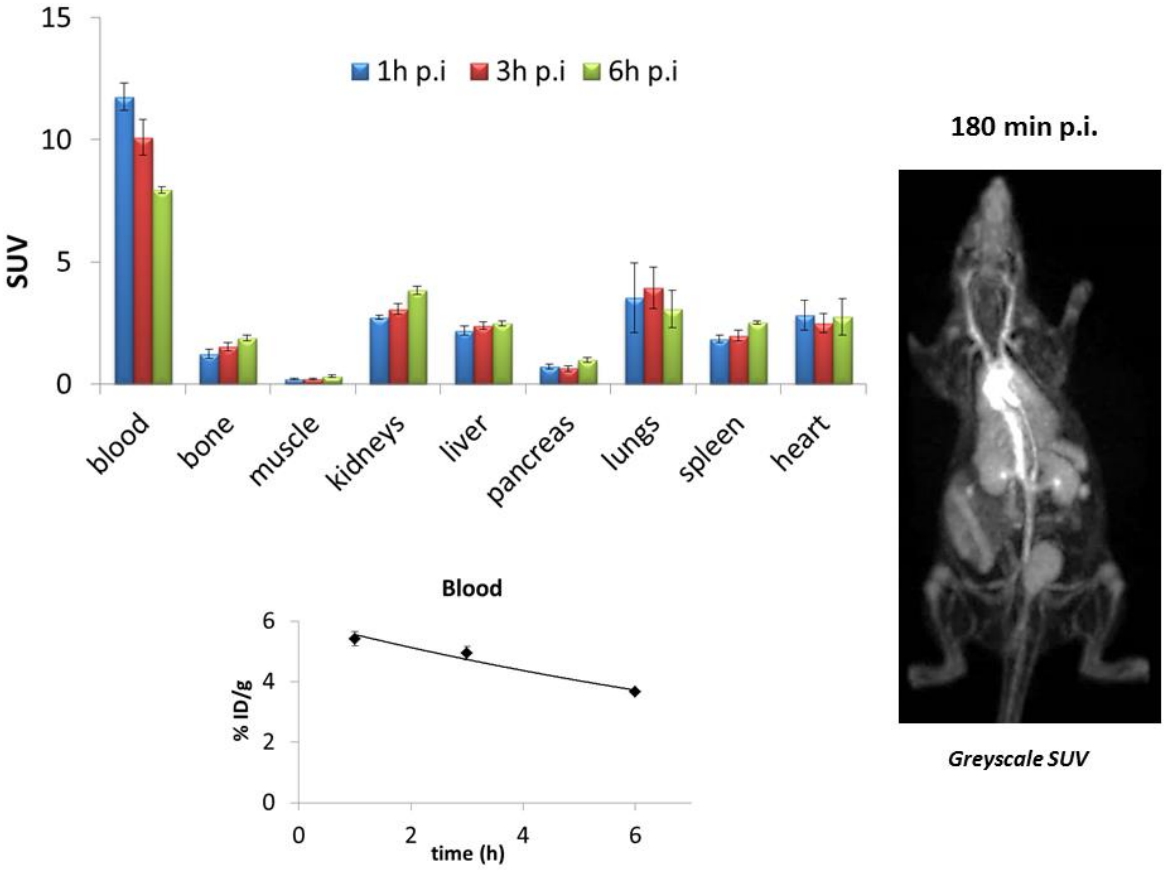

Figure 6: *Biodistribution of [^{18}F]AlF-RESCA1-HSA in rats at 1 h, 3 h and 6 h p.i. (n=4/group; 187 g-225 g) and whole-body PET image of a healthy rat 180 min after intravenous injection of [^{18}F]A^{8}F-RESCA1-HSA. Results are presented as percentage of standardised uptake values (SUV). For calculation of total radioactivity in blood, bone and muscle, tissue mass was assumed to be, respectively, 7, 12 and 40% of the total body mass. Blood data points were fitted with a one component exponential equation: y = 6,0233e-0,08x; R² = 0,9689, blood $t_{1/2}$= 8.66 h.*

4. CONCLUSIONS

Fluorine-18 is currently the radionuclide of choice for PET because of its favourable nuclear decay characteristics and ease of production. Clinicians in the molecular imaging community are not only interested in in using small organic molecules but also high molecular weight biomolecules and peptides are increasingly being considered for use as PET-radiopharmaceuticals.[23] However, the incorporation of fluorine-18 into heat-sensitive and complex biomolecules creates substantial challenges for radiochemists. In this study we identified new restrained complexing agents (RESCA1-5) that allow efficient complexation of $\{Al^{18}F\}^{2+}$ using mild labelling conditions. RESCA1 is an acyclic pentadentate ligand with an N_2O_3 coordinative set of donor atoms and was synthesised starting from commercially available chemicals. RESCA1 as such showed excellent labelling properties and its $Al^{18}F$-complex demonstrated high *in vitro* and *in vivo* stability. Small changes in the backbone of RESCA1, to

form RESCA2-5, resulted in minor to major loss of stability of the corresponding Al^{18}F complexes and thus, RESCA1 was found to be the most promising lead candidate for radiolabelling heat-sensitive biomolecules *via* the Al^{18}F-method. To demonstrate the generic applicability of the proposed method we successfully labelled the heat-sensitive biomolecule HSA at ambient temperature with $\{Al^{18}F\}^{2+}$ with high radiochemical purity in less than 30 minutes. [^{18}F]AlF-RESCA1-HSA showed excellent *in vitro* and *in vivo* stability. Moreover, [^{18}F]AlF-RESCA1-HSA showed favourable properties for PET blood pool imaging applications. This new optimised radiolabelling method may have a great impact on PET radiochemical space as it could stimulate a rapid development of new fluorine-18 labelled heat-sensitive biomolecules.

5. ACKNOWLEDGEMENTS

The authors thank Ann Van Santvoort and Tine Buelens from the Department of Nuclear Medicine and Julie Cornelis, Ivan Sannen, Pieter Haspeslagh, Michiel Nuyts and Jana Hemelaers from the Laboratory for Radiopharmacy for their assistance. Compounds RESCA1-5 and RESCA-TFP were synthesised and all NMR experiments and interpretation of spectra were performed by Dr. Joan Lecina. This research has received support within the SBO project MIRIAD, funded from the IWT Flanders.

6. REFERENCES

(1) Serdons, K., Verbruggen, A., and Bormans, G. M. (2009) Developing new molecular imaging probes for PET. *Methods 48*, 104–111.

(2) Sanchez-Crespo, A. (2013) Comparison of gallium-68 and fluorine-18 imaging characteristics in positron emission tomography. *Appl. Radiat. Isot. 76*, 55–62.

(3) Richter, S., and Wuest, F. (2014) ^{18}F-labeled peptides: The future is bright. *Molecules 19*, 20536–20556.

(4) McBride, W. J., Sharkey, R. M., Karacay, H., D'Souza, C. A., Rossi, E. A., Laverman, P., Chang, C.-H., Boerman, O. C., and Goldenberg, D. M. (2009) A novel method of ^{18}F radiolabeling for PET. *J. Nucl. Med. 50*, 991–998.

(5) McBride, W. J., D'Souza, C. A., Sharkey, R. M., Karacay, H., Rossi, E. A., Chang, C.-H., and Goldenberg, D. M. (2010) Improved ^{18}F labeling of peptides with a fluoride-aluminum-chelate complex. *Bioconjug. Chem. 21*, 1331–1340.

(6) McBride, W. J., Sharkey, R. M., and Goldenberg, D. M. (2013) Radiofluorination using aluminum-fluoride (Al^{18}F). *EJNMMI Res. 3*, 36–47.

(7) Rahmim, A., and Zaidi, H. (2008) PET versus SPECT: strengths, limitations and challenges. *Nucl. Med. Commun. 29*, 193–207.

(8) Raghavan, M., Pillai, A., and Dash, A. (2016) Sustained availability of ^{99m}Tc: possible paths forward *54*, 313–324.

(9) Awasthi, V., Watson, J., Gali, H., Matlock, G., McFarland, a., Bailey, J., and Anzellotti, a. (2014) A "dose on demand" biomarker generator for automated production of [^{18}F]F- and [^{18}F]FDG. *Appl. Radiat. Isot. 89*, 167–175.

(10) Cleeren, F., Lecina, J., Billaud, E. M., Ahamed, M., Verbruggen, A., and Bormans, G. M. (2016) New chelators for low temperature Al ^{18}F-labeling of biomolecules. *Bioconjug. Chem. 27*, 790–798.

(11) Fritzberg, A. R., Whitney, W. P., Kuni, C. C., and Klingensmith, W. (1982) Biodistribution and renal excretion of ^{99m}Tc-N,N'-bis-(mercaptoacetamido) ethylenediamine. Effect of renal tubular transport inhibitors. *Int. J. Nucl. Med. Biol. 9*, 79–82.

(12) Mitterhauser, M., Toegel, S., Wadsak, W., Lanzenberger, R. R., Mien, L.-K., Kuntner, C., Wanek, T., Eidherr, H., Ettlinger, D. E., Viernstein, H., Kluger, R., Dudczak, R., and Kletter, K. (2007) Pre vivo, ex vivo and in vivo evaluations of [^{68}Ga]-EDTMP. *Nucl. Med. Biol. 34*, 391–397.

(13) Laverman, P., McBride, W. J., Sharkey, R. M., Goldenberg, D. M., and Boerman, O. C. (2014) Al^{18}F labeling of peptides and proteins. *J. Labelled Comp. Radiopharm. 57*, 219–223.

(14) Ding, H., Xu, Y., Wang, L., Lang, L., Xie, Q., and Yang, M. (2013) First experience of ^{18}F-alfatide in lung cancer patients using a new lyophilized kit for rapid radiofluorination. *J. Nucl. Med. 54*, 691–698.

(15) Price, E. W., and Orvig, C. (2014) Matching chelators to radiometals for radiopharmaceuticals. *Chem. Soc. Rev. 43*, 260–290.

(16) Brechbiel, M. W. (1992) Synthesis of C-functionalized trans-cyclohexyldiethylenetriaminepenta-acetic Acids for Labelling of Monoclonal antibodies with the bismuth-212 a-particle emitter. *J. Chem. Soc., Perkin Trans. 1*, 1173–1178.

(17) Shetty, D., Choi, S. Y., Jeong, J. M., Lee, J. Y., Hoigebazar, L., Lee, Y.-S., Lee, D. S., Chung, J.-K., Lee, M. C., and Chung, Y. K. (2011) Stable aluminium fluoride chelates with triazacyclononane derivatives proved by X-ray crystallography and ^{18}F-labeling study. *Chem. Commun. 47*, 9732–9734.

(18) Fatemi, S. J., Kadir, F. H., and Moore, G. R. (1991) Aluminium transport in blood serum. Binding of aluminium by human transferrin in the presence of human albumin and citrate. *Biochem. J. 280*, 527–532.

(19) Ory, D., Van den Brande, J., de Groot, T., Serdons, K., Bex, M., Declercq, L., Cleeren, F., Ooms, M., Van Laere, K., Verbruggen, A., and Bormans, G. (2015) Retention of [^{18}F]fluoride on reversed phase HPLC columns. *J. Pharm. Biomed. Anal. 111*, 209–214.

(20) Martin, R. B. (1988) Ternary hydroxide complexes in neutral solutions of Al^{3+} and F^-. *Biochem. Biophys. Res. Commun. 155*, 1194–1200.

(21) Bernardi, M., Ricci, C. S., and Zaccherini, G. (2014) Role of human albumin in the management of complications of liver cirrhosis. *J. Clin. Exp. Hepatol. 4*, 302–311.

(22) Carroll, L., Evans, H. L., Aboagye, E. O., and Spivey, A. C. (2013) Biomolecular chemistry imaging – progress and prospects. *Org. Biomol. Chem*, 11, 5772–5781.

(23) Smith, G. E., Sladen, H. L., Biagini, S. C. G., and Blower, P. J. (2011) Inorganic approaches for radiolabelling biomolecules with fluorine-18 for imaging with positron emission tomography. *Dalton Trans. 40*, 6196–6205.

CHAPTER IV

AL^{18}F-LABELLED UREA-BASED PSMA INHIBITORS FOR PET IMAGING OF PROSTATE CANCER

Cleeren F.[1]; Lecina J.[1]; Ahamed M.[1];Holvoet B.[2];Deroose C.M.[2]; Goffin K.[2]; Verbruggen A.[1] and Bormans G.[1]

[1]*Laboratory for Radiopharmacy, University of Leuven, Belgium*
[2]*Department of Nuclear Medicine and Molecular Imaging, University of Leuven, Belgium*

ABSTRACT

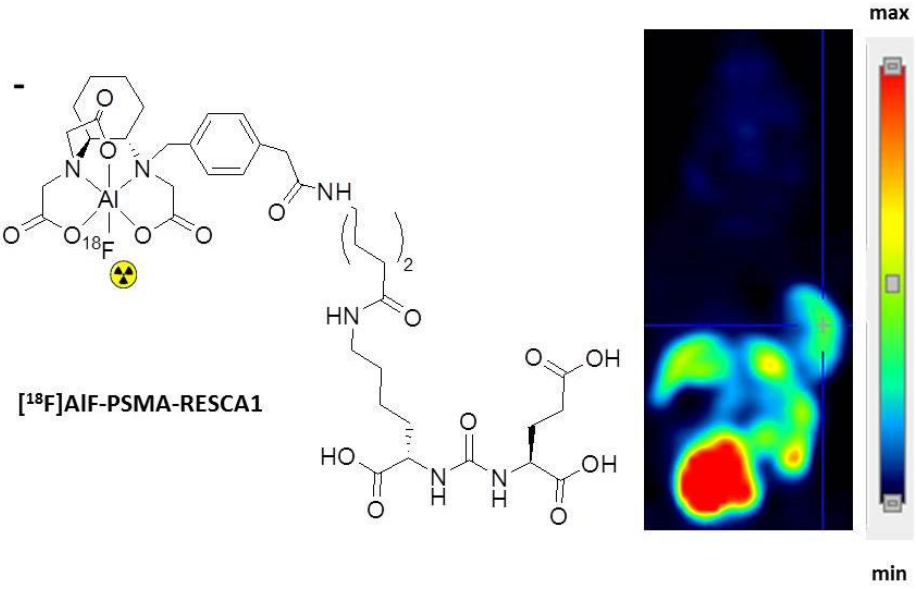

[18F]AlF-PSMA-RESCA1

Prostate-specific membrane antigen (PSMA) is overexpressed in a majority of primary and metastatic prostate cancer patients and is a promising target for specific prostate cancer imaging and therapy. We have developed two new Al^{18}F-labelled urea-based PSMA inhibitors, [^{18}F]AlF-PSMA-NODA-MPAA and [^{18}F]AlF-PSMA-RESCA1. Here we describe the preclinical evaluation of these tracers and the results with the new radioligands were compared with those of [^{18}F]AlF-PSMA-L3 and [^{68}Ga]Ga-HBEDD-CC-PSMA, currently the most widely used PSMA-ligand. [^{18}F]AlF-PSMA-NODA-MPAA and [^{18}F]AlF-PSMA-RESCA1 were successfully produced with high yields and radiochemical purity in less than 30 min. Both compounds showed improved stability compared to [^{18}F]AlF-PSMA-L3. Cell uptake and internalisation experiments with LNCaP (PSMA^{+}) and PC-3 (PSMA^{-}) cells revealed similar specific internalisation and cell accumulation for [^{18}F]AlF-PSMA-RESCA1 and [^{68}Ga]Ga-PSMA-HBED-CC. In contrast, [^{18}F]AlF-PSMA-NODA-MPAA and [^{18}F]AlF-PSMA-L3 showed considerable lower uptake in LNCaP cells. All tracers were cleared fast from plasma and PSMA-negative tissue mainly by the kidneys but also hepatobiliary excretion was observed for [^{18}F]AlF-PSMA-RESCA1. High specific accumulation of all tracers was observed in PSMA-expressing organs and PSMA^{+} LNCaP tumours. Autoradiography on human prostate tumour tissue demonstrated specific binding of all tested tracers to the human PSMA receptor.

1. INTRODUCTION

Prostate cancer is the second most commonly diagnosed cancer among men worldwide. Despite advances in surgical technique (radical prostatectomy), radiotherapy and brachytherapy, initial curative therapy fails in a significant proportion of men with prostate cancer.[1] In men with biochemical failure, elevated prostate specific antigen (PSA) levels are observed after initial therapy indicating local recurrence of the disease and/or metastasis. In this context imaging techniques such as PET/CT or PET/MRI can play an important role in (re)staging and monitoring of patients with prostate cancer, especially where the disease has spread beyond the prostate gland.[2] [^{18}F]Fluorocholine and [^{11}C]choline are still considered the most validated tracers for detection of recurrent prostate cancer, however both suffer from poor sensitivity at low PSA levels.[3] Prostate-specific membrane antigen (PSMA), a transmembrane folate hydrolase, is overexpressed in a majority of primary and metastatic prostate cancer patients and is a promising target for specific prostate cancer imaging and therapy. The first widely used radiotracer to image the disease was the ^{111}In-labelled monoclonal antibody 7E11 (ProstaScint™) that targets PSMA.[4] However, ProstaScint™ is a technically demanding agent to administer because imaging can only be performed four to six days after administration of the agent, necessitating a second visit by the patient. More recently radiolabelled inhibitors of PSMA, bearing Glu-NH-CO-NH-Lys as a pharmacophore, showed the ability to image PSMA expressing tumors.[5] Currently, [^{68}Ga]Glu-NH-CO-NH-Lys-(Ahx)-[Ga-N,N'-bis[2-hydroxy-5-(carboxyethyl)benzyl]ethylenediamine-N,N'-diacetic acid] ([^{68}Ga]Ga-PSMA-HBEDD-CC), is the most widely used PSMA-ligand (**Figure 1**).[6] This urea based PSMA inhibitor demonstrates excellent pharmacokinetics as well as stability *in vivo*, leading to its clinical applications worldwide for imaging of prostate cancer.[7] Moreover, in patients with a low, rising PSA level, [^{68}Ga]Ga-PSMA-HBEDD-CC demonstrated a significantly higher detection rate for recurrent prostate cancer than [^{18}F]fluorocholine and [^{11}C]-choline.[3] In conclusion, [^{68}Ga]Ga-PSMA-HBEDD-CC PET/CT can be considered as an effective imaging tool for early detection of prostate cancer recurrence.

However, for PET imaging, fluorine-18 ($t_{1/2}$: 109.8 min) is the radionuclide of choice because of its favourable decay properties (~ 97% ß$^+$-emission, 635-keV maximum positron energy), low β$^+$-trajectory (< 2 mm in water), small atom size and moreover, it is readily produced in large quantities (>400 GBq/batch) with a cyclotron. In contrast, gallium-68 ($t_{1/2}$: 68 min) is a generator-based radionuclide that does not require an on-site cyclotron. Only limited amounts of radiotracer can be produced during one production (typically up to 1500 MBq). For PET tracers that are to be administered in a large number of patients, the relative small batch size can cause extended waiting lists for patients or require repeated productions with increased production costs. In contrast, the

half-life and multi-curie production of fluorine-18 allows multi-dose production and transportation of ^{18}F-based radiotracers to remote hospitals which is more challenging with ^{68}Ga-based radiotracers.

Chen and colleagues reported 2-(3-{1-carboxy-5-[(6-[^{18}F]fluoro-pyridine-3-carbonyl)-amino]-pentyl}-ureido)-pentanedioic acid ([^{18}F]DCFPyL) as a promising ^{18}F-labelled urea-based PSMA inhibitor for imaging of prostate cancer (**Figure 1**). The first clinical trials indicate that [^{18}F]DCFPyL PET/CT provides high image quality and visualises small prostate lesions with excellent sensitivity.[8] However, more clinical trials are needed to prove its superiority above [^{68}Ga]Ga-PSMA-HBEDD-CC and the multi-step radiosynthesis is rather complex, which might limit its worldwide application.

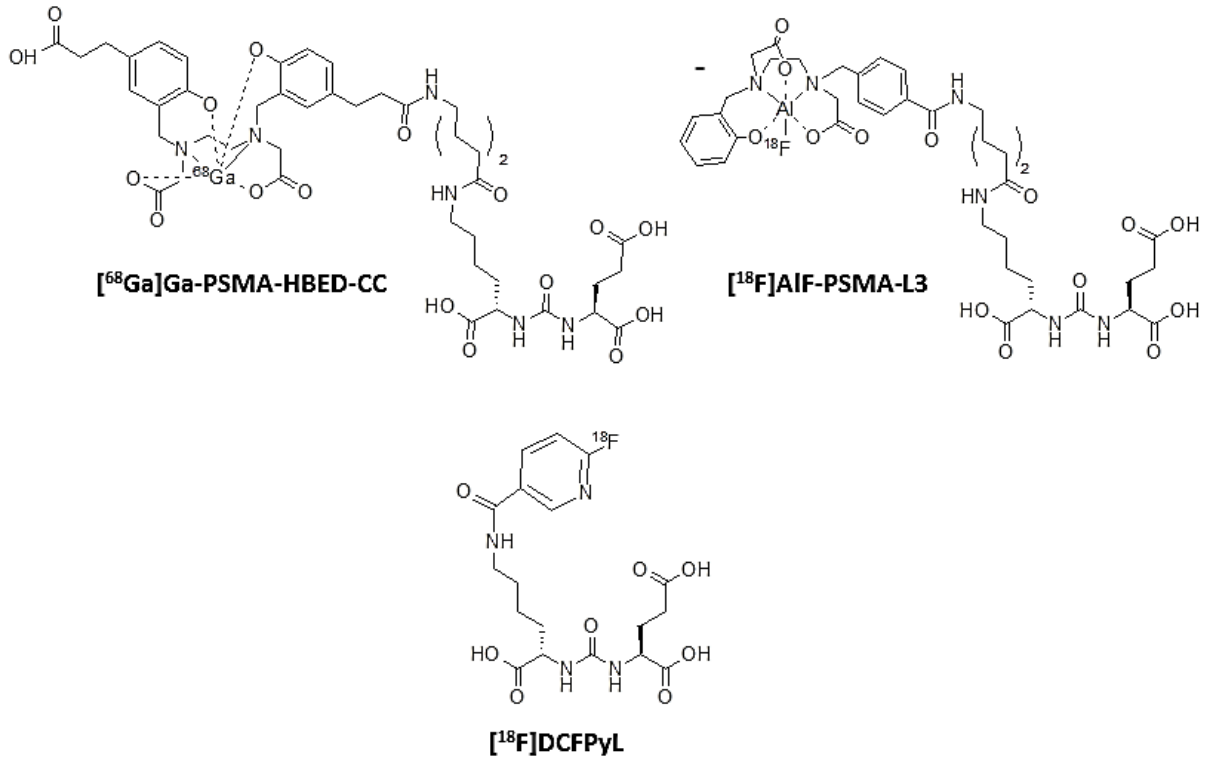

Figure 1: *Chemical structures of* [^{68}Ga]*Ga-PSMA-HBEDD-CC,* [^{18}F]*AlF-PSMA-L3 and [^{18}F]DCFPyL*

A promising approach for ^{18}F-labelling of biomolecules consists of chelation of $\{Al^{18}F\}^{2+}$ by biomolecules conjugated to a chelator in aqueous environment. This methodology is promising in view of its potential to evolve to a simple "kit" type preparation. Recently, restrained complexing agent 1 (RESCA1), an acyclic pentadentate ligand able to complex $\{Al^{18}F\}^{2+}$ efficiently at 25 °C, was developed in the Laboratory of Radiopharmacy (**Chapter III**). Here we describe the preclinical evaluation of two new Al^{18}F-labelled urea-based PSMA inhibitors, [^{18}F]AlF-PSMA-NODA-MPAA and [^{18}F]AlF-PSMA-RESCA1, to assess the influence of the used chelator on the prostate cancer PET-imaging properties. Moreover, the results were compared with those of the established radiotracer [^{68}Ga]Ga-PSMA-HBEDD-CC and the reported tracer [^{18}F]AlF-Glu-NH-CO-NH-Lys(Ahx)L3 ([^{18}F]AlF-

PSMA-L3, **Figure 1**), which was previously developed in the Laboratory of Radiopharmacy (**Chapter II**).[9]

2. MATERIALS AND METHODS

2.1 General

All reagents and solvents were purchased from Sigma-Aldrich (Bornem, Belgium), Fluka (Bornem, Belgium), Fisher (Doornik, Belgium) or Acros Organics (Geel, Belgium). Fluorine-18 was produced on site using a cyclotron (IBA Cyclone 18/9, IBA, Louvain-la-Neuve, Belgium) by irradiation of $H_2{}^{18}O$ with 18-MeV protons. Radioactivity was measured using an ionisation chamber based activity meter (Capintec Radioisotope Calibrator CRC-721, Ramsey, NJ, USA).

Determination of the molecular ion mass of various compounds was achieved using a Dionex Ultimate 3000 LC System (Thermo Fisher Scientific, Sunnyvale, USA) coupled in series to an ultra-high resolution time-of-flight mass spectrometer (TOF-HRMS) (MaXis impact, Bruker, Bremen, Germany), equipped with orthogonal electrospray ionisation (ESI) interface. Acquisition and processing of data were conducted using HyStar and Compass DataAnalysis (version 3.2, Bruker), respectively. Calculated monoisotopic mass values were obtained using Compas IsotopePattern (version 3.2, Bruker). Prostate tumour slices (LNCaP and PC-3), and slices from human prostate tissue were obtained using a cryotome (Shandon Cryotome FSE, Thermo Fisher Scientific). Slices (20 µm) were cut at a temperature between -15 °C and -18 °C and stored at -20 °C. The use of human tissue was approved by the ethical committee from UZ Leuven. (*Study S54424: collection of human prostate tissue*). Preparative high performance liquid chromatography (prep-HPLC) was carried out with a system consisting of a Merck-Hitachi L-6200 pump and an XTerra preparative C18 10 µm 10 mm x 250 mm column (Waters, Milford, USA). The mobile phase consisted of a gradient of water and acetonitrile, eluted at a flow rate of 5 mL/min. The eluate was analysed for its UV absorbance (Merck Hitachi L-4200 UV-VIS detector) at 254 nm.

ITLC-SG papers (Varian, Diegem, Belgium) were developed in an elution chamber using a mixture of acetonitrile and water (75:25, v/v). Autoradiography was performed using phosphor storage screens (super-resolution screen, Perkin Elmer, Waltham, USA). Screens were read in a Cyclone Plus system (Perkin Elmer) and analysed using Optiquant software (Perkin Elmer).

Analytical radio-HPLC (XBridge C18 column, 3.5 µm, 3.0 mm x 100 mm, Waters, Milford, USA) was performed using gradient elution at a flow rate of 0.8 ml/min. Method pH 2: Solvent A (H_2O, 0.1% TFA) and solvent B (acetonitrile, 0.1% TFA). The elution gradient was 95% A to 5% A over 0-30 min.

Method pH 7.4. Solvent A (phosphate buffered saline (PBS) 0.1M, pH 7.4) and solvent B (acetonitrile). The elution gradient was 100% A to 50% A over 0-30 min.

2.2 Synthesis of PSMA-NODA-MPAA and PSMA-RESCA1

2.2.1 Synthesis of NO_2AtBu-MPAA

A solution of di-tert-butyl 2,2'-(1,4,7-triazacyclononane-1,4-diyl)diacetate (0.100 g, 0.28 mmoles, NO_2AtBu, Chematech, Dijon, France) in anhydrous acetonitrile (5 ml) was slowly added to a solution of 4-(bromomethyl)phenylacetic acid (0.25 mmoles) in anhydrous acetonitrile (3 ml). The mixture was allowed to stir at 0 °C and after two hours K_2CO_3 (0.20 mmoles) was added. Afterwards, the mixture was allowed to stir at room temperature overnight. The solution was filtered and the solvent removed under vacuum. The obtained oil was purified, using flash chromatography (Reveleris® X2 Flash Chromatography System, Reveleris 40 g, C_{18} column (Grace, Deerfield, US)) equipped with an evaporative light scattering detector and UV detector (254 nm), and the following method. Solvent A (water) and solvent B (acetonitrile), flow rate 28 ml/min. The elution gradient was 100% A to 20% A over 0-12 min. Afterwards, the solvent was evaporated under reduced pressure affording NO_2AtBu-NODA-MPAA (56 mg, 40% yield). **HRMS (ESI)**: Calcd. for $C_{27}H_{43}N_3O_6$ $[M+H^+]$ 506.3225 ; found 506.3261.

2.2.2 Synthesis of PSMA-NODA-MPAA

To a solution of Glu-NH-CO-NH-Lys(Ahx)tBu (72.6 mg; 0.12 mmoles, synthesis is decribed in supplemental information **Chapter II**) in dichloromethane (23 ml) were successively added *N*,*N*-diisopropylethylamine (63.2 µL; 0.36 mmoles), *O*-(*N*-Succinimidyl)-*N*,*N*,*N*',*N*'-tetramethyluronium tetrafluoroborate (TSTU) (91 mg; 0.30 mmoles) and NO_2AtBu-NODA-MPAA (73.5 mg; 0.15 mmoles). The mixture was stirred at rt overnight. The solvent was then evaporated under reduced pressure and the concentrate was diluted with a mixture of water/acetonitrile (50:50, 1 ml) and purified by preparative RP-HPLC using the following method. Solvent A (water) and solvent B (acetonitrile), flow rate 5 ml/min. The elution gradient was 80% A to 20% A over 0-30 min After HPLC purification, the compound was stirred in trifluoroacetic acid (2 mL) at rt for 12 h and the deprotection was monitored using LC-MS. Afterwards the solvent was evaporated under reduced pressure affording PSMA-NODA-MPAA (35.2 mg, 36% yield). **HRMS (ESI)**: Calcd. for $C_{37}H_{57}N_7O_{13}$ $[M+H^+]$ 808.4087; found 808.4093

2.2.3 Synthesis of PSMA-RESCA1

To a solution of Glu-NH-CO-NH-Lys(Ahx)tBu (72.3 mg; 0.12 mmoles) in dichloromethane (3 ml) were successively added *N*,*N*-diisopropylethylamine (41.5 µL; 0.238 mmoles), *O*-(*N*-Succinimidyl)-*N*,*N*,*N*',*N*'-tetramethyluronium tetrafluoroborate (TSTU) (90 mg; 0.299 mmoles) and di-tert-butyl 2,2'-(((1R,2R)-2-((2-(tert-butoxy)-2-oxoethyl)(4-(2-oxo-2-(2,3,5,6-25 tetrafluorophenoxy)ethyl)benzyl)amino)cyclohexyl)azanediyl)diacetate (64 mg; 0.12 mmoles, RESCA1tBu-AA, synthesis is described in patent WO/2016/065435). The mixture was stirred at rt overnight. The solvent was then evaporated under reduced pressure and the concentrate was diluted with a mixture of water/acetonitrile (50:50, 1 ml) and purified by preparative RP-HPLC using the following method. Solvent A (water) and solvent B (acetonitrile), flow rate 5 ml/min. The elution gradient was 80% A to 20% A over 0-30 min. After HPLC purification, the compound was stirred in trifluoroacetic acid (2 mL) at rt for 12 h. The deprotection was monitored using LC-MS. Afterwards the solvent was evaporated under reduced pressure affording PSMA-RESCA1 (10.5 mg, 10% yield). **HRMS (ESI)**: Calcd. for $C_{39}H_{58}N_6O_{15}$ [M+H$^+$] 851.4033; found 851.4062

2.3 Remotely controlled radiosynthesis and purification of [^{18}F]AlF-PSMA-RESCA1 and [^{18}F]AlF-PSMA-NODA-MPAA

[^{18}F]F$^-$ was separated from [^{18}O]H_2O by trapping on a SepPak Light Accel plus QMA anion exchange cartridge (Cl$^-$ form; Waters). The cartridge was washed with water (3 mL) and [^{18}F]F$^-$ was eluted from the cartridge with an aqueous solution of sodium chloride 0.9% (0.3 mL). [^{18}F]F$^-$ was added to 5 µl of 20 mM (100 nmoles) aluminium chloride ($AlCl_3$) in sodium acetate buffer (0.1 M, pH 4.5). The solution was incubated at rt for 5 min to form {Al^{18}F}$^{2+}$. A solution of PSMA-RESCA1 or PSMA-NODA-MPAA (115 µl, 2.58 mM) in sodium acetate buffer (0.1 M, pH 4.5) was added and the reactor was heated at rt (20-25°C) or 110°C respectively for 12 min. After dilution with water (0.5 mL), the crude reaction mixture was purified with HPLC (XBridge C_{18} column, 5 µm, 4.6 mm x 150 mm, Waters) using the following method. Solvent A (ammonium acetate 0.05M pH 5.5) and solvent B (EtOH), flow rate 1 ml/min. The elution gradient was 100% A to 80% A over 0-25 min. UV detection of the eluate was performed at 254 nm. Identification of the [Al^{18}F]-complexes was done by radio-LC-HRMS (Acquity UPLC BEH C_{18} column, 1.7 µm, 2.1 mm x 150 mm, Waters. 0.6 mL/min A: H_2O B: ACN, 0-2 min 5% B, 2 to 8 min 5% B to 95% B, 8-10 min 95% B, 10 to 12 min 95% B to 5% B).

2.4 Stability tests of [^{18}F]AlF-PSMA-NODA-MPAA and [^{18}F]AlF-PSMA-RESCA1 in rat plasma

A volume of 200 µL of radiotracer solution was added to freshly prepared rat plasma (1 mL). The mixtures were incubated at 37 °C and analysed by iTLC-SG at 10, 30, 60 and 180 min after the start of

the incubation. Plasma samples were denatured by addition of the plasma solution (50 µL) to acetonitrile (50 µL). The mixture was stirred and centrifuged (1300 g, 3 min). Finally the supernatant was analysed using iTLC-SG.

2.5 Internalisation experiments

Internalisation experiments were performed using a protocol described by Eder *et al*. with some minor modifications.[6] LNCaP or PC-3 cells (200.000/well) were seeded in 24-well cell culture plates and incubated at 37 °C for 24 h. After washing with PBS, the cells were incubated with radiolabelled compounds [^{68}Ga]Ga-PSMA-HBEDD-CC, [^{18}F]AlF-PSMA-NODA-MPAA, [^{18}F]AlF-PSMA-RESCA1 or [^{18}F]AlF-PSMA-L3 for 45 min at 37 °C or at 4 °C. To determine specific cell accumulation, cells were blocked using the PSMA inhibitor 2-(phosphonomethyl)pentane-1,5-dioic acid (2-PMPA, Tocris Bioscience, Avonmouth, UK) to a final concentration of 100 µM. After 45 min, cells were washed three times with 0.250 mL of ice-cold PBS. Cells were incubated twice with 0.5 mL glycine-HCl in PBS (50 mM, pH 2.8) for 5 min at rt to remove radioactivity bound on the surface of the cells. The cells were washed again three times with ice-cold PBS and lysed using 0.250 mL lysis buffer (reagent A100, Chemometic, Allerod, Denmark). After 5 min incubation, 0.250 mL neutralisation buffer (reagent B, Chemometic) was added to raise the pH and avoid DNA degradation. The surface-bound and internalised fractions were counted using an automated gamma counter equipped with a 3-inch NaI(Tl) well crystal coupled to a multichannel analyser, mounted in a sample changer (Perkin Elmer 1480 Wizard 3q). Counts were corrected for background radiation, physical decay and counter dead time. The amounts of cells per well were counted using an automated counting device (NucleoCounter® NC-200™, Chemometic) and results were expressed as percentage of applied radioactivity bound to 10^6 cells. Data are expressed as mean ± SD (n=3).

2.6 Biodistribution and µPET studies

Animals were housed in individually ventilated cages in a thermo-regulated (~22 °C), humidity-controlled facility under a 12h-12h light-dark cycle, with access to food and water *ad libitum*. All animal experiments were conducted according to the Belgian code of practice for the care and the use of animals, after approval from the university animal ethics committee.

The biodistribution studies of [^{68}Ga]Ga-PSMA-HBEDD-CC, [^{18}F]AlF-PSMA-NODA-MPAA and [^{18}F]AlF-PSMA-RESCA1 were carried out in healthy male Naval Medical Research Institute (NMRI) mice (body weight: 30-40 g) at 10 and 60 min post injection (p.i.) (*n* = 4/time point). Mice were injected with 2 MBq [^{68}Ga]Ga-PSMA-HBEDD-CC, Al^{18}F-PSMA-NODA-MPAA or Al^{18}F-PSMA-RESCA1 with or without co-administration of 2 mg/kg 2-(phosphonomethyl)pentane-1,5-dioic acid (2-PMPA) *via* a tail vein under

anesthesia (2.5% isoflurane in O_2 at 1 L/min flow rate) and sacrificed by decapitation at above specified time points. Blood and major organs were collected in tared tubes and weighed. Quantification of radioactivity in blood, organs and other body parts was performed using an automated gamma-counter equipped with a 3-inch NaI(Tl) well crystal coupled to a multichannel analyser, mounted in a sample changer (Perkin Elmer 1480 Wizard 3q). Counts were corrected for background radiation, physical decay and counter dead time. For calculation of total radioactivity in blood, bone and muscle, tissue mass was assumed to be, respectively, 7, 12 and 40% of the total body mass.[10,11] Results are presented as percentage of injected dose (%ID) or %ID/g.

10 X 10^6 cells of either LNCaP or PC-3 in 50% Matrigel (VWR, Radnor, US) were subcutaneously inoculated into the right shoulder of 7- to 8-week-old BALB/c nu/nu mice (body mass: 20-25 g) obtained from Janvier (Le Genest-Saint-Isle, France). The tumors were allowed to grow for 4 to 5 weeks until approximately 0.5 to 0.75 cm^3 in size. Small animal whole-body PET imaging on mice was performed using a FOCUS^{TM} 220 microPET scanner (Concorde Microsystems, Knoxville, US). Prior to PET imaging, mice were anesthetised and kept under anesthesia throughout the whole procedure using 2.5% isoflurane in oxygen (2 L/min). Animals were injected intravenously with [^{68}Ga]Ga-PSMA-HBEDD-CC (6 MBq), [^{18}F]AlF-PSMA-NODA-MPAA (11 MBq), [^{18}F]AlF-PSMA-RESCA1 (11 MBq) or [^{18}F]AlF-PSMA-L3 (11 MBq) and scanned dynamically for 60 min. Time activity curves (TACs) were generated for liver, tumor and kidneys with PMOD software (v 3.2, PMOD Technologies, Zürich, Switzerland).

3 RESULTS AND DISCUSSION

The prostate is located just below the urinary bladder, surrounding the urethra. Prostate enlargement happens to almost all men as they get older and can be benign or malignant. Prostate cancer is one of the most diagnosed cancers among men and PET is playing an important role in the staging and restaging of the disease. In the first stage it is important to know if the cancer has spread to any lymph nodes (N-staging). This initial staging will determine the further treatment strategy. After radical prostatectomy, external radiotherapy or brachytherapy the levels of prostate specific membrane antigen (PSA) in blood are monitored. Rise of PSA levels indicates local recurrence and or metastasis. An accurate restaging of the disease is of major importance because local recurrence or an oligometastatic disease can be treated with surgery or local radiotherapy and thus systemic hormonal therapy can be avoided. Therefore there is a high medical need for a highly sensitive and specific molecular imaging agent for (re)staging and monitoring of prostate cancer patients. PSMA is overexpressed in a majority of primary and metastatic prostate cancer patients and is a very promising target for specific prostate cancer imaging and therapy. Urea-based PSMA inhibitors are

low-molecular-weight peptidomimetics that -when appropriately labelled- can be used to image PSMA-expressing tumours.[12] [^{68}Ga]Ga-PSMA-HBEDD-CC is the most frequently used PSMA-radioligand and has already demonstrated high potential for detection of recurrent prostate cancer.[7] However, labelling with fluorine-18 would offer advantages with respect to availability, production amount, and image resolution compared to labelling with gallium-68. [^{18}F]DCFPyL is a promising ^{18}F-labelled urea-based PSMA inhibitor for imaging of prostate cancer. However, its radiosynthesis is rather complex starting from 6-[^{18}F]fluoronicotinic acid-2,3,5,6-tetrafluoro-phenyl ester ([^{18}F]-Py-TFP).[13] Though, Bouvet et al. described recently a synthesis method for [^{18}F]DCFPyL via direct nucleophilic heteroaromatic substitution in a single reactor automated synthesis unit.[14] As an alternative we describe here the use of new Al^{18}F-labelled urea-based PSMA inhibitors. The advantage of using the Al^{18}F-strategy is that the one-step radiolabelling is simple and might evolve into a "kit" type preparation. Recently, new acyclic pentadentate ligands were developed in Laboratory of Radiopharmacy of KU Leuven that are able to complex {Al^{18}F}$^{2+}$ efficiently at low temperatures (< 40 °C). The ligand H_3L3 was derivatised and successfully conjugated with an urea-based inhibitor of PSMA. [^{18}F]AlF-PSMA-L3 was produced with high radiochemical purity and the first preclinical results in healthy mice appeared promising (**Chapter II**)**,** however further preclinical evaluation is needed to assess the *in vivo* stability and tumour-targeting properties. Recently, we developed RESCA1, an acyclic pentadentate chelator that is able to complex {Al^{18}F}$^{2+}$ efficiently at 25°C (**Chapter III**). [^{18}F]AlF-RESCA1 shows superior stability in comparison with [^{18}F]AlF-L3, comparable with the stability of [^{18}F]AlF-N-benzyl-NODA. Here we report the radiosynthesis and preclinical evaluation of [^{18}F]AlF-PSMA-RESCA1 and [^{18}F]AlF-PSMA-NODA-MPAA**.** The results are compared with those of the established ligand [^{68}Ga]Ga-PSMA-HBEDD-CC and the previously reported ligand [^{18}F]AlF-PSMA-L3 (**Chapter II**).

The *tert*-butyl protected bifunctional chelators RESCA1tBu-AA and NO_2AtBu-MPAA were conjugated with a hydrophilic urea-based inhibitor of PSMA, Glu-NH-CO-NH-Lys, to form PSMA-RESCA1 and PSMA-NODA-MPAA, respectively (**Figure 2**). The process of radiosynthesis and purification with preparative radio-HPLC was performed using a home-built remotely controlled system. [^{18}F]AlF-PSMA-RESCA1 and [^{18}F]AlF-PSMA-NODA-MPAA were prepared in high radiochemical yields (50-60%) and purity (>95%) in less than 35 minutes (starting after elution of fluorine-18 from the anion exchange QMA cartridge). In view of developing the radiochemistry into a kit preparation, RESCA1 has the advantage that chelation of {Al^{18}F}$^{2+}$ can occur at room temperature whereas for NODA high temperatures (>100 °C) are required. The specific activity for both tracers was between 25 and 30 GBq/µmol, calculated on the starting amount of PSMA-RESCA1 and PSMA-NODA-MPAA. Both tracers

were stable (>95%) in saline at room temperature for at least three hours and identification of the [Al^{19}F]-complexes was done by radio-LC-HRMS (**Table 1**).

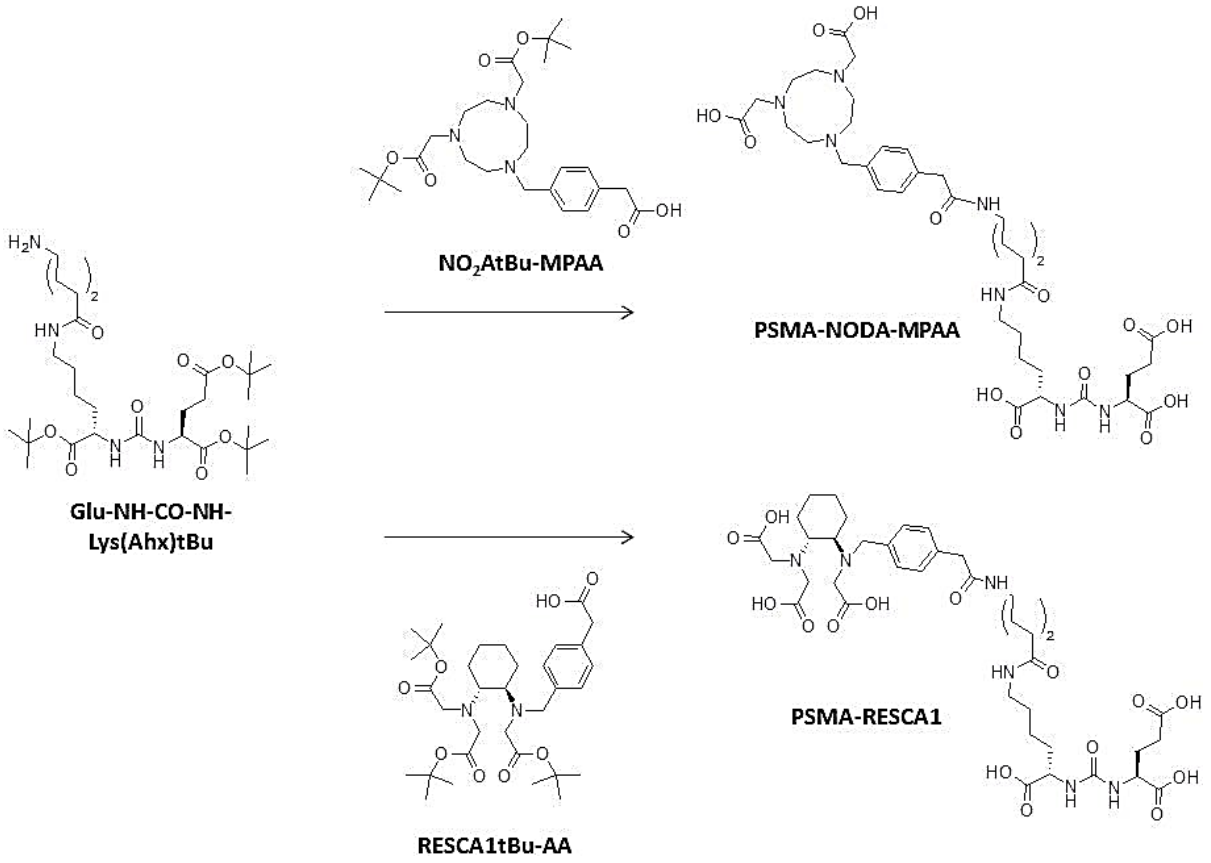

Figure 2: *Synthesis of PSMA-NODA-MPAA and PSMA-RESCA1*

Table 1: *Analytical data of Ga-PSMA-HBED-CC, AlF-PSMA-L3, AlF-PSMA-NODA-MPAA and AlF-PSMA-RESCA1*

Ligand	HRMS (ESI) calculated	HRMS (ESI) found	Analytical HPLC retention at pH 2 (min)[a]	Analytical HPLC retention at pH 7.4 (min)[a]
Ga-PSMA-HBED-CC	$[M+H]^+$:1012.3187	/	8.23	7.25
AlF-PSMA-L3	$[M]^-$: 873.3268	$[M]^-$: 873.3265	7.88	9.53
AlF-PSMA-NODA-MPAA	$[M+H]^+$: 852.3730	$[M+H]^+$: 852.3739	6.97	8.82
AlF-PSMA-RESCA1	$[M]^-$: 893.3530	$[M]^-$: 893.3522	7.72	9.68

[a] *compounds were labelled with ^{68}Ga or {Al^{18}F}$^{2+}$, retention radiometric signal.*

As derived from the molecular ion mass, [^{18}F]AlF-PSMA-RESCA1 and [^{18}F]AlF-PSMA-L3 have a negative charge, located at the Al^{18}F-complexes. In contrast, PSMA-NODA-MPAA and PSMA-HBED-CC

form neutral complexes with $\{Al^{18}F\}^{2+}$ and $^{68}Ga^{3+}$ respectively. To compare the lipophilicity of all tracers at pH 2 and physiological pH (pH 7.4) we performed analytical HPLC analysis (**Table 1**). At pH 2, [^{68}Ga]Ga-PSMA-HBEDD-CC has the longest retention time (8.23 min), indicating high lipophilicity. However, in physiological conditions, the shortest retention time was observed for [^{68}Ga]Ga-PSMA-HBEDD-CC, indicating lower liphopilicity compared to the other ligands. This shift in retention time might be explained by deprotonation at pH 7.4 of the free carboxylic group present on the HBED-CC moiety that is not part of the gallium-complex. At pH 7.4, [^{18}F]AlF-PSMA-RESCA1 has the longest retention time, indicating higher lipophilicity compared to the other ligands. This might be explained by the presence of the lipophilic *trans*-cyclohexyl moiety of RESCA1.

After 3 h incubation in rat plasma at 37 °C, 93% of [^{18}F]AlF-PSMA-RESCA1 and 96% of [^{18}F]AlF-PSMA-NODA-MPAA was still intact as assessed by instant thin layer chromatography (iTLC), indicating excellent stability of both compounds. In comparison, [^{18}F]AlF-PSMA-L3 shows lower stability *in vitro*. Only 62% of tracer was still intact after 3 h incubation in rat plasma at 37 °C, indicating demetallation and/or defluorination over time. Cell uptake and internalisation experiments with LNCaP ($PSMA^+$) cells revealed similar internalisation and cell accumulation for [^{68}Ga]Ga-PSMA-HBED-CC and [^{18}F]AlF-PSMA-RESCA1 which could be blocked almost completely with the non-structural related PSMA inhibitor 2-PMPA, indicating that both processes were mediated by specific binding to PSMA (**Figure 3**).

Moreover, no significant accumulation was observed with PC-3 cells ($PSMA^-$), confirming the specific interaction. For both compounds about 45% of the receptor bound fraction was internalised after 45 min at 37 °C, whereas at 4 °C no significant internalisation was observed, as expected. In contrast, [^{18}F]AlF-PSMA-NODA-MPAA and [^{18}F]AlF-PSMA-L3 showed considerable lower uptake in LNCaP cells than [^{68}Ga]Ga-PSMA-HBED-CC and for both tracers minor non-specific uptake in PC-3 cells was observed, which was not observed for [^{18}F]AlF-PSMA-RESCA1 or [^{68}Ga]Ga-PSMA-HBED-CC.

The results of the biodistribution study of [^{68}Ga]Ga-PSMA-HBED-CC-, [^{18}F]AlF-PSMA-RESCA1 and [^{18}F]AlF-PSMA-NODA-MPAA in healthy mice are shown in **Figure 4,** the biodistribution of [^{18}F]AlF-PSMA-L3 in healthy mice was reported previously (**Chapter II**). The graphs show the uptake, presented as %ID, in different organs at 10 min and 60 min p.i. of the tracer. [^{18}F]AlF-PSMA-RESCA1 and [^{18}F]AlF-PSMA-NODA-MPAA both showed high *in vivo* stability, since no significant bone uptake, which would be an indication of release of fluorine-18, was observed (0.80 ± 0.22% ID/g and 0.13 ± 0.02% ID/g). [^{18}F]AlF-PSMA-RESCA1 was cleared fast from PSMA-negative tissue and plasma mainly by the kidneys but also hepatobiliary excretion was observed, which might be explained by the more lipophilic properties of [^{18}F]AlF-PSMA-RESCA1 at physiological conditions (HPLC retention in **Table 1**).

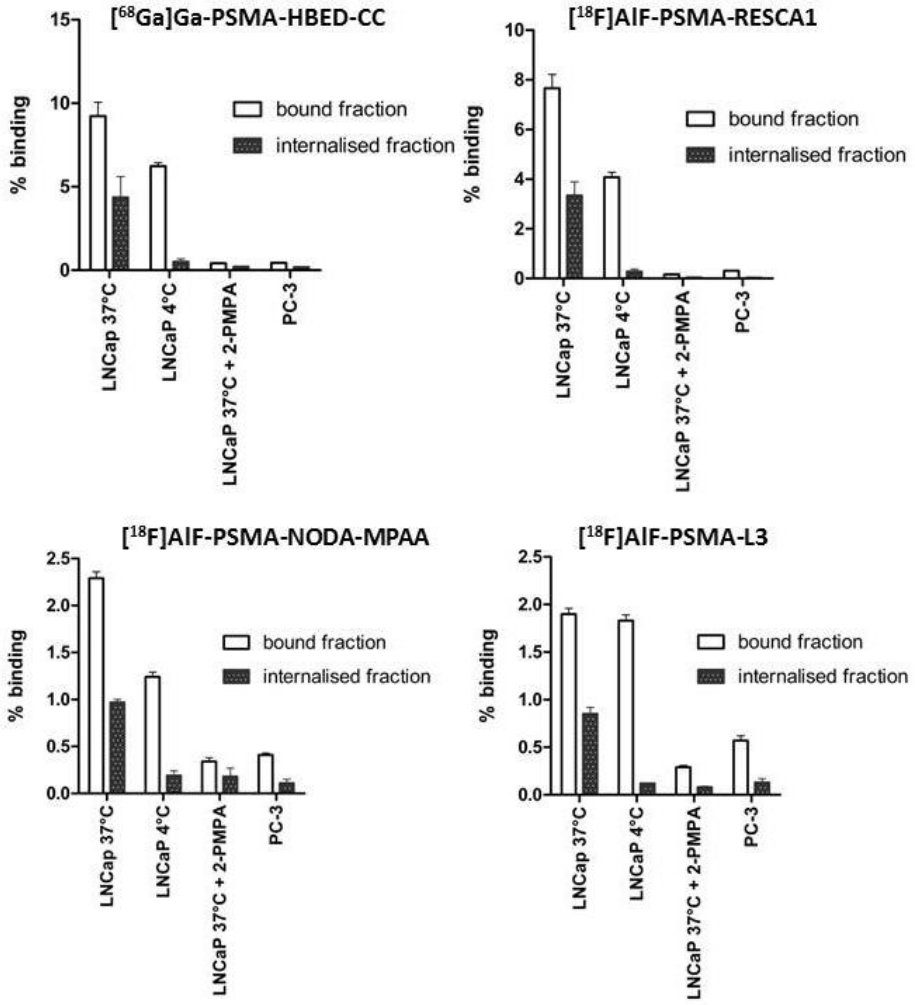

Figure 3: *Cell binding and internalisation of [^{68}Ga]Ga-PSMA-HBED-CC, [^{18}F]AlF-PSMA-L3, [^{18}F]AlF-PSMA-RESCA1 and [^{18}F]AlF-PSMA-NODA-MPAA. Specific cell uptake was evaluated by blockade with 100 µM 2-PMPA. Values are expressed as percentage of applied radioactivity bound to 10^{6} cells. Data are expressed as mean ± SD (n=3). Bound fraction is the sum of receptor-bound fraction and internalised fraction.*

In contrast, [^{68}Ga]Ga-HBEDD-CC-PSMA, [^{18}F]AlF-PSMA-NODA-MPAA and [^{18}F]AlF-PSMA-L3 were cleared mainly by the kidneys and almost no liver uptake was observed. The retention at 60 min p.i. of all tracers in organs with reported high expression of PSMA such as kidney and spleen was nearly completely blocked when the non-structural related inhibitor 2-PMPA was co-injected to block PSMA specific binding. Since 2-PMPA is a non-structurally related PSMA inhibitor, this indicates *in vivo* PSMA-specific retention of all tested tracers. The same effect was shown with *in vitro* autoradiography on kidney slices of healthy mice with or without blocking with 2-PMPA. Pronounced specific uptake was observed for all tracers in the renal cortex, which corresponds to the reported PSMA receptor distribution in the kidneys of mice.[15] With reference to clinical application, PSMA expression is considerably lower in human kidneys compared to mouse kidneys.[16] For [^{18}F]AlF-PSMA-RESCA1 and [^{18}F]AlF-PSMA-NODA-MPAA no increased bone uptake was observed with co-injection of

2-PMPA (0.66 ± 0.48% ID/g and 0.15 ± 0.02% ID/g). In contrast [^{18}F]AlF-PSMA-L3 showed pronounced bone uptake with co-injection of 2-PMPA (4.55 ± 1.39% ID/g) which indicates lower *in vivo* stability.

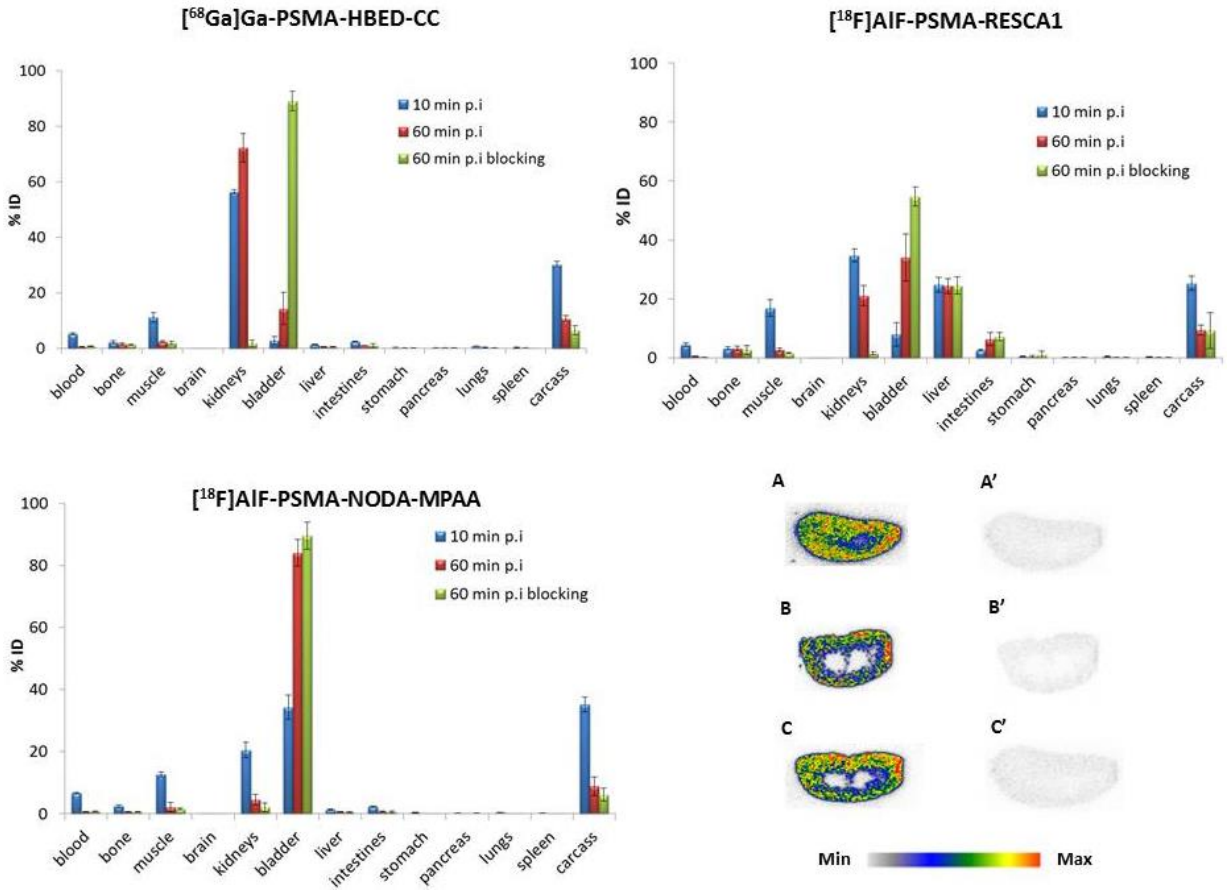

Figure 4: *Biodistribution (%ID) of [^{68}Ga]Ga-HBED-CC-PSMA, [^{18}F]AlF-PSMA-RESCA1 and [^{18}F]AlF-PSMA-NODA-MPAA with or without co-administration of 2 mg/kg 2-PMPA at 10 min and 60 min p.i. and autoradiography on kidney slices of healthy mice with (A',B' and C') or without (A,B and C) blocking with 2-PMPA (100 µM).A: [^{68}Ga]Ga-HBED-CC-PSMA, B: [^{18}F]AlF-PSMA-RESCA1 and C: [^{18}F]AlF-PSMA-NODA-MPAA. For calculation of total radioactivity in blood, bone and muscle, tissue mass was assumed to be, respectively, 7, 12 and 40% of the total body mass.*

High accumulation of all tracers was observed on PSMA^{+} LNCaP tumour slices, visualised with digital autoradiography (**Figure 5**). The retention of all tracers was nearly completely blocked when 2-PMPA (100 µM) was added to the tracer solution, indicating PSMA-specific binding. No significant binding was observed on PSMA^{-} PC-3 tumour slices, which again confirms the high specificity of all tested tracers. Autoradiography on human prostate tumour tissue showed specific affinity for the human PSMA receptor for all Al^{18}F-labelled tracers. Pathological validation confirmed presence of tumour in the biopt, but only limited amount of tumour burden was observed. Nevertheless, significant uptake of all Al^{18}F-tracers was observed, indicating high affinity and sensitivity for the human PSMA receptor. The observed heterogeneous focal uptake was comparable with the uptake of the established clinical tracer [^{68}Ga]Ga-PSMA-HBED-CC and was nearly completely blocked when 2-PMPA

(100 µM) was added to the tracer solution. Normal human prostate tissue showed considerably lower uptake of all tracers which corresponds to the lower expression level of PSMA receptors in healthy prostate tissue.

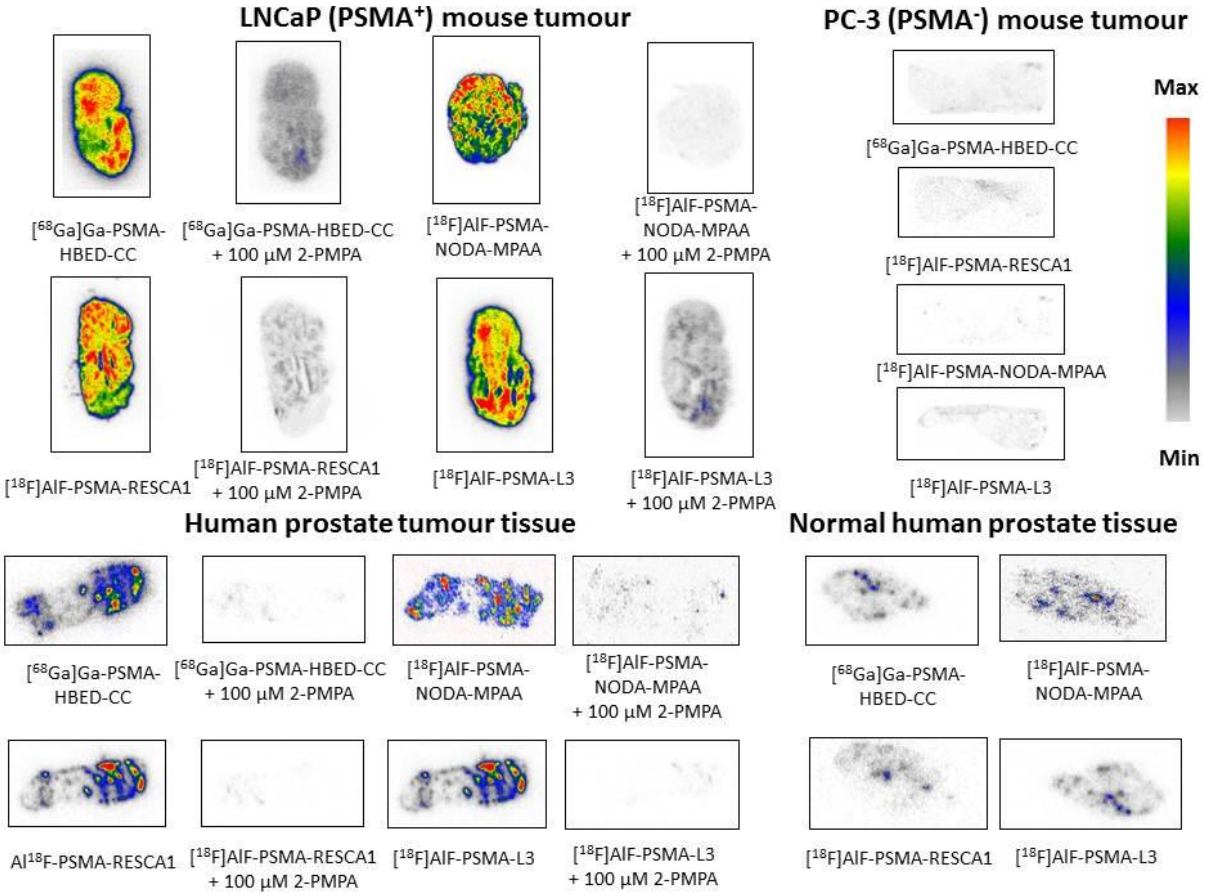

Figure 5: *In vitro digital autoradiography on LNCaP (PSMA$^+$) tumor slices, PC-3 (PSMA$^-$) tumor slices , human prostate tumor tissue and healthy human prostate tissue with [^{68}Ga]Ga-PSMA-HBED-CC, [^{18}F]AlF-PSMA-L3, [^{18}F]AlF-PSMA-RESCA1 and [^{18}F]AlF-PSMA-NODA-MPAA with or without blocking with 2-PMPA (100 µM). Pathological validation of tumor burden on human prostate tissue: Biopt human prostate tumour tissue: very limited amount of tumour, Biopt normal human prostate tissue: no tumour*

Dynamic PET analysis of tumour inoculated mice revealed for all tracers rapid and high uptake of radioactivity in LNCaP (PSMA$^+$) tumours (**Figure 6**) and high tumour-to-background ratios. [^{68}Ga]Ga-HBEDD-CC-PSMA, [^{18}F]AlF-PSMA-NODA-MPAA and [^{18}F]AlF-PSMA-L3 were cleared fast by the kidneys and almost no liver uptake was observed. In contrast, [^{18}F]AlF-PSMA-RESCA1 was cleared fast from PSMA-negative tissue and plasma by the kidneys but also hepatobiliary excretion was observed, which is consistent with the *ex vivo* biodistribution data. [^{68}Ga]Ga-HBEDD-CC-PSMA and [^{18}F]AlF-PSMA-RESCA1 showed no significant uptake in PC-3 (PSMA$^-$) tumors, confirming the specificity of both tracers. No microPET scans were performed with [^{18}F]AlF-PSMA-NODA-MPAA and [^{18}F]AlF-PSMA-L3 in PC-3 (PSMA$^-$) tumour bearing mice. [^{18}F]AlF-PSMA-L3 showed high LNCaP tumour uptake but also increased bone uptake was observed over time. Non-specific bone accumulation might

compromise the utility of this tracer for non-invasive imaging of prostate cancer metastasis, because most metastatic lesions occur in lymph nodes and in bone.[4] Despite the lower stability and low *in vitro* cell accumulation, [^{18}F]AlF-PSMA-L3 demonstrated high LNCaP tumour uptake *in vivo* with average SUVs of around 1.2. However, these results have to be interpreted carefully because of the limited number of scanned tumour mice and the lack of a direct head-to-head comparison with *[^{68}Ga]Ga-HBEDD-CC-PSMA*.

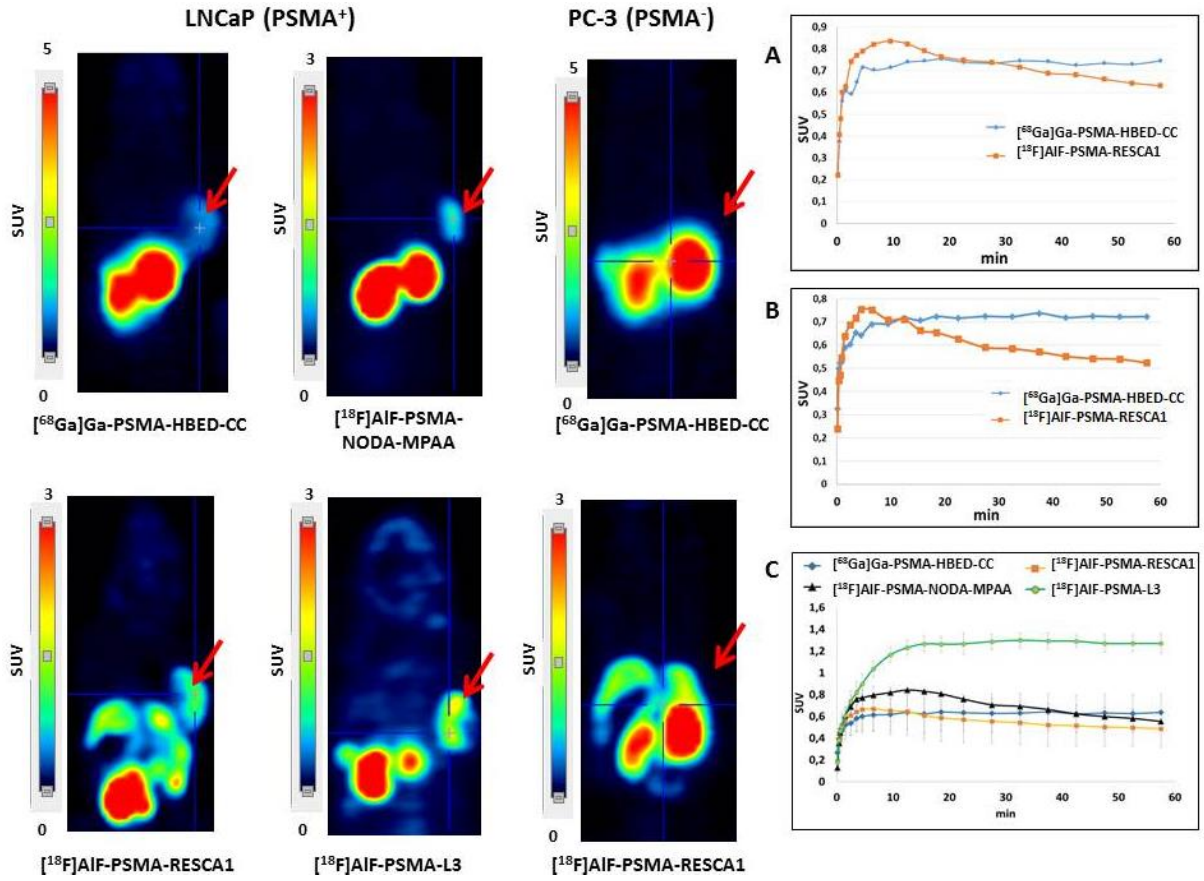

Figure 6: *Whole-body coronal microPET image of BALB/c nu/nu mice bearing (PSMA^{+}) LNCaP or (PSMA^{-}) PC-3 xenografts. Summed images (30-60 min p.i., average volume time weighted), red arrows indicate position of LNCaP or PC-3 tumours. Graph A and B show the time-activity curves (SUV) in tumour for [^{68}Ga]Ga-HBEDD-CC-PSMA and [^{18}F]AlF-PSMA-RESCA1, microPET scans were performed in the same mice at the same day. Graph C shows the time-activity curves in tumour for [^{68}Ga]Ga-HBEDD-CC-PSMA (n=3), [^{18}F]AlF-PSMA-RESCA1 (n=3), [^{18}F]AlF-PSMA-NODA-MPAA (n=1) and [^{18}F]AlF-PSMA-L3 (n=3).*

In order to allow a head-to-head comparison of tumour uptake between [^{18}F]AlF-PSMA-RESCA1 and [^{68}Ga]Ga-HBEDD-CC-PSMA, we performed two microPET scans on the same day in the same LNCaP tumour bearing mice. In the morning we performed a microPET scan with [^{68}Ga]Ga-HBEDD-CC-PSMA and 6 hours later, we repeated the experiment with [^{18}F]AlF-PSMA-RESCA1 in the same mice (**Figure 6**). [^{18}F]AlF-PSMA-RESCA1 showed rapid and high uptake of radioactivity in LNCaP tumours (SUV_{5min} 0.7 ± 0.2) which slightly decreased over time (SUV_{60min} 0.5 ± 0.2). [^{68}Ga]Ga-HBEDD-CC-PSMA showed

comparable but somewhat lower initial tumour uptake (SUV_{5min} 0. 6 ± 0.1) than [^{18}F]AlF-PSMA-RESCA1 but the LNCaP (PSMA$^+$) tumour uptake was constant or even slightly increased over time (SUV_{60min} 0.6 ± 0.2). To conclude, all tracers showed rapid and high uptake of radioactivity in LNCaP (PSMA$^+$) tumours with high tumour-to-background ratios.

4 CONCLUSIONS

Two new Al^{18}F-labelled urea-based PSMA inhibitors were successfully produced with high yields and radiochemical purity in less than 30 min. The results of preclinical studies were compared with those of the established ligand [^{68}Ga]Ga-PSMA-HBEDD-CC and the previously reported ligand [^{18}F]AlF-PSMA-L3. Cell uptake and internalisation experiments with LNCaP (PSMA$^+$) and PC-3 (PSMA$^-$) cells revealed similar specific internalisation and cell accumulation for [^{18}F]AlF-PSMA-RESCA1 and [^{68}Ga]Ga-PSMA-HBED-CC. In contrast, [^{18}F]AlF-PSMA-NODA-MPAA and [^{18}F]AlF-PSMA-L3 showed considerable lower uptake in LNCaP cells. Moreover, [^{18}F]AlF-PSMA-L3 suffers from instability over time which compromises the utility of this tracer. All tracers were cleared fast from plasma and PSMA-negative tissue mainly by the kidneys but also hepatobiliary excretion was observed in the case of [^{18}F]AlF-RESCA1-PSMA. High specific accumulation of all tracers was observed on PSMA$^+$ LNCaP tumour slices and autoradiography on human prostate tumour tissue showed specific affinity for the human PSMA receptor. Dynamic PET analysis revealed rapid and high uptake of radioactivity in LNCaP (PSMA$^+$) tumours and high tumour-to-background ratios for all examined tracers.

ACKNOWLEDGMENTS

The authors thank Ann Van Santvoort and Tine Buelens from the Department of Nuclear Medicine and Julie Cornelis, Ivan Sannen, Pieter Haspeslagh and Jana Hemelaers from the Laboratory for Radiopharmacy for their assistance. Compound Glu-NH-CO-NH-Lys(Ahx) was synthesised by Dr. Muneer Ahamed. RESCA-TFP was synthesised by Dr. Joan Lecina and cell culture was performed by Bryan Holvoet. This research has received support within the SBO project MIRIAD, funded from the IWT Flanders.

5 REFERENCES

(1) Morigi, J. J., Stricker, P. D., Leeuwen, P. J. Van, Tang, R., Ho, B., Nguyen, Q., Hruby, G., Fogarty, G., Jagavkar, R.et al. (2015) Prospective Comparison of ^{18}F-Fluoromethylcholine Versus ^{68}Ga-PSMA PET/CT in Prostate Cancer Patients Who Have Rising PSA After Curative Treatment and Are Being Considered for Targeted Therapy. *J. Nucl. Med. 56*, 1185–1190.

(2) Chatalic, K. L. S., Franssen, G. M., Weerden, W. M. Van, Mcbride, W. J., Laverman, P., De, E., Hajjaj, B., Brunel, L., Goldenberg, D. M., Fehrentz, J.et al. (2016) Preclinical Comparison of Al^{18}F- and ^{68}Ga-Labeled Gastrin-Releasing Peptide Receptor Antagonists for PET Imaging of Prostate Cancer. *J. Nucl. Med. 55*, 2050–2057.

(3) Afshar-oromieh, A., Zechmann, C. M., Malcher, A., Eder, M., Eisenhut, M., Linhart, H. G., Holland-letz, T., Hadaschik, B. A., Giesel, F. L., Debus, J.et al (2014) Comparison of PET imaging with a ^{68}Ga-labelled PSMA ligand and ^{18}F-choline-based PET / CT for the diagnosis of recurrent prostate cancer. *Eur J Nucl Med Mol Imaging 41*, 11–20.

(4) Mease, R. C., Foss, C. a, and Pomper, M. G. (2013) PET imaging in prostate cancer: focus on prostate-specific membrane antigen. *Curr. Top. Med. Chem.41, 11-20*

(5) Bar, J., Pachl, P., Poštová-slave, L., Tykvart, J., Majer, P., Konvalinka, J., and Šácha, P. (2014) Rational design of urea-based glutamate carboxypeptidase II (GCPII) inhibitors as versatile tools for specific drug targeting and delivery. *Bioorg. Med. Chem. 22*, 4099–4108.

(6) Eder, M., Schäfer, M., Bauder-Wüst, U., Hull, W. E., Wängler, C., Mier, W., Haberkorn, U., and Eisenhut, M. (2012) ^{68}Ga-complex lipophilicity and the targeting property of a urea-based PSMA inhibitor for PET imaging. *Bioconjug. Chem. 23*, 688–697.

(7) Afshar-Oromieh, A., Malcher, A., Eder, M., Eisenhut, M., Linhart, H. G., Hadaschik, B. A., Holland-Letz, T., Giesel, F. L., Kratochwil, C.et al. (2013) PET imaging with a [^{68}Ga]gallium-labelled PSMA ligand for the diagnosis of prostate cancer: biodistribution in humans and first evaluation of tumour lesions. *Eur. J. Nucl. Med. Mol. Imaging 40*, 486–495.

(8) Dietlein, M., Kobe, C., Kuhnert, G., Stockter, S., Fischer, T., Schomäcker, K., Schmidt, M., Dietlein, F., Zlatopolskiy, B. D., Krapf, P.et al. (2015) Comparison of [^{18}F] DCFPyL and [^{68}Ga] Ga-PSMA-HBED-CC for PSMA-PET Imaging in Patients with Relapsed Prostate Cancer *Eur J Nucl Med Mol Imaging* 41, 575–584.

(9) Cleeren, F., Lecina, J., Billaud, E. M., Ahamed, M., Verbruggen, A., and Bormans, G. M. (2016) New chelators for low temperature Al^{18}F-labeling of biomolecules. *Bioconjug. Chem. 27*, 790–798.

(10) Fritzberg, A. R., Whitney, W. P., Kuni, C. C., and Klingensmith, W. (1982) Biodistribution and renal excretion of ^{99m}Tc-N,N'-bis-(Mercaptoacetamido) ethylenediamine. Effect of renal tubular transport inhibitors. *Int. J. Nucl. Med. Biol. 9*, 79–82.

(11) Mitterhauser, M., Toegel, S., Wadsak, W., Lanzenberger, R. R., Mien, L.-K., Kuntner, C., Wanek, T., Eidherr, H., Ettlinger, D. E., Viernstein, H., Kluger, R., Dudczak, R., and Kletter, K. (2007) Pre vivo, ex vivo and in vivo evaluations of [^{68}Ga]-EDTMP. *Nucl. Med. Biol. 34*, 391–407.

(12) Eder, M., Schäfer, M., Bauder-Wüst, U., Haberkorn, U., Eisenhut, M., and Kopka, K. (2014) Preclinical evaluation of a bispecific low-molecular heterodimer targeting both PSMA and GRPR for improved PET imaging and therapy of prostate cancer. *Prostate 74*, 659–668.

(13) Szabo, Z., Mena, E., Rowe, S. P., Plyku, D., Nidal, R., Mario, A., Antonarakis, E. S., Fan, H., Dannals, R. F., Chen, Y.et al. (2015) Initial Evaluation of [^{18}F]DCFPyL for Prostate-Specific Membrane Antigen (PSMA)-Targeted PET Imaging of Prostate Cancer. *Mol. Imaging Biol. 17*, 565–574.

(14) Bouvet, V., Wuest, M., Jans, H., Janzen, N., Genady, A. R., Valliant, J. F., Benard, F., and Wuest, F. (2016) Automated synthesis of [^{18}F] DCFPyL via direct radiofluorination and validation in preclinical prostate cancer models. *EJNMMI Res. 6*, 1–15.

(15) Chatalic, K. L. S., Heskamp, S., Konijnenberg, M., Molkenboer-kuenen, J. D. M., Weerden, W. M. Van, Boerman, O. C., and Jong, M. De. (2016) Towards Personalized Treatment of Prostate Cancer : PSMA I & T , a Promising Prostate-Specific Membrane Antigen-Targeted Theranostic Agent *Theranostics 6*, 849–861.

(16) Ghosh, A., and Heston, W. D. W. (2004) Tumor Target Prostate Specific Membrane Antigen (PSMA) and its Regulation in Prostate Cancer *J Cell Biochem 91*, 528–539.

CHAPTER V

ONE STEP Al^{18}F-LABELLING OF CRIg-TARGETING NANOBODIES

Cleeren F[1], Lecina J[1], Raes G[2,3], Devoogdt N[4], Xavier C[4], Caveliers V[4], Verbruggen A[1] and Bormans G[1]

[1]*Laboratory for Radiopharmacy, University of Leuven, Belgium*

[2] *Laboratory of Cellular and Molecular Immunology, Vrije Universiteit Brussel, Brussels, Belgium*

[3]*VIB Laboratory of Myeloid Cell Immunology, Vrije Universiteit Brussel, Brussels, Belgium*

[4]*In Vivo Cellular and Molecular Imaging Center, Vrije Universiteit Brussel, Brussels, Belgium*

ABSTRACT

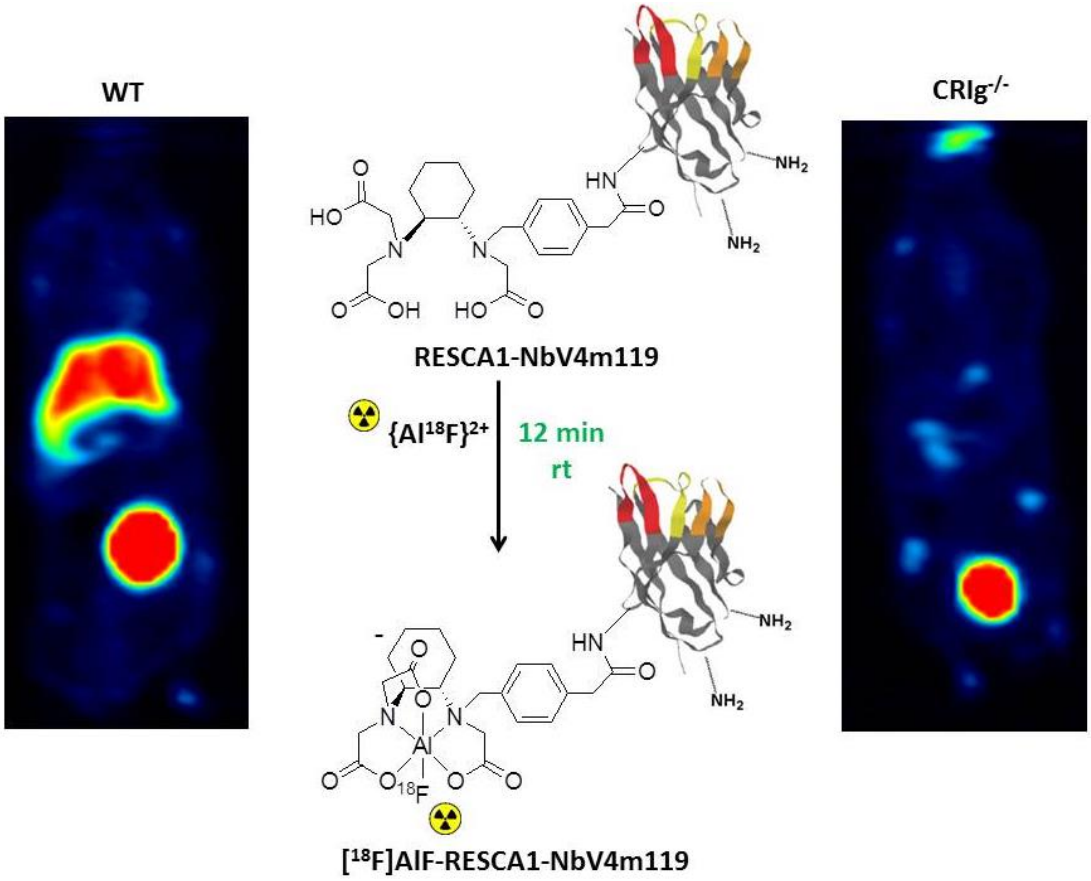

Nanobodies are the smallest antigen-binding antibody fragments available and interact fast and with nanomolar affinity with their target. Unbound nanobodies are cleared rapidly from the blood and if radiolabelled with a positron emitting radionuclide, this results in high contrast PET images as early as 1 hour after administration. Here we describe a generic approach for a one-step radiolabelling of nanobodies via the $Al^{18}F$-method at ambient temperature using the recently developed chelator "restrained complexing agent 1 (RESCA1)". We derivatised the nanobody, NbV4m119, targeting the CRIg receptor, with RESCA1 and successfully labelled the construct with $\{Al^{18}F\}^{2+}$ in good radiochemical yields in less than 35 minutes. [^{18}F]AlF-RESCA1-NbV4m119 showed excellent *in vitro* stability. Biodistribution and microPET studies in mice demonstrated that [^{18}F]AlF-RESCA1-NbV4m119 is excreted mainly *via* the renal pathway. However, in accordance with the high CRIg expression on Kupffer cells, also high liver uptake was observed in WT mice. In contrast, no significant liver uptake was observed in $CRIg^{-/-}$ mice indicating excellent specificity of the $Al^{18}F$-labelled tracer. In addition, we optimised a generic radio-HPLC-HRMS system for analysis and quality control of radiolabelled nanobodies. Fluorine-18 labelled nanobodies can be considered as "magic bullets" for immuno-imaging and this generic radiolabelling method may stimulate the development of other nanobody-based radiotracers.

1. INTRODUCTION

The molecular imaging technique immuno-positron emission tomography (immuno-PET) combines the selective localisation of monoclonal antibodies (mAbs) or antibody fragments at their target *in vivo* and the high resolution and sensitivity of PET. The immuno-PET tracer should exhibit a high target-to-background ratio, high target specificity, high stability, good solubility and low immunogenicity.[1] The advantage of using mAbs as vector molecules in immuno-PET is their nanomolar affinity and high accumulation at the target site.[2] Moreover, the availability of a large number of FDA-approved mAbs for imaging purposes can stimulate clinical translation.[1] However, as a result of the long residence time in blood of full-length antibodies, imaging with sufficient contrast between target and non-target tissues can only be performed several days post injection with peak contrast mostly after 2-4 days. Hence, due to the slow kinetics, radiolabelling with long-lived radionuclides such as zirconium-89 (^{89}Zr, $t_{1/2}$: 3.3 days) or iodine-124 (^{124}I, $t_{1/2}$: 4.2 days) is required which causes a high radiation burden for the patient (20-40 mSv per scan). The use of long-lived radionuclides is unpractical for routine clinical use and moreover, has a severe social impact on patients. For example, only limited visiting time of family is allowed for radioprotection reasons.

Nanobodies (V_{HH}) are the antigen-binding fragments (13-15 kDa) derived from heavy-chain-only antibodies occurring naturally in Camelid species.[3] Nanobodies bind their antigens very fast and specifically with high affinity *in vivo*, whereas unbound nanobody is rapidly cleared from the blood by the kidneys.[4] Using nanobodies labelled with a positron emitting radionuclide, high contrast PET images can be acquired as early as 1 hour after tracer administration.[5] This early imaging allows the use of short-lived PET radionuclides such as gallium-68 (^{68}Ga, $t_{1/2}$: 68 min), fluorine-18 (^{18}F, $t_{1/2}$: 109.8 min) or copper-64 (^{64}Cu, $t_{1/2}$: 12.7 hours), resulting in more patient-friendly imaging procedures and lower radiation burden. Nanobodies are single-domain binders, therefore they have good solubility compared to other antibody fragments and can be easily generated against any antigen of interest with excellent expression yield in both *Eschericia coli* and yeast.[1] Nanobodies could be considered as "magic bullets" for imaging, however, the high accumulation of unbound V_{HH}s in kidneys, resulting in high renal radiation dose from radiolabelled nanobodies and more complicating analysis of nearby tissue should be taken into account.[6] Nevertheless, the preclinical data reported to date with nanobody-derived probes is promising and nanobody-based molecular imaging might play an important role in the diagnosis and management of various diseases.[7]

In the past, most nanobody-derived probes were labelled with technetium-99m (^{99m}Tc, $t_{1/2}$: 6 hours) for SPECT imaging. When derivatised with a terminal hexahistidine tag, nanobodies can easily be radiolabelled based on ^{99m}Tc(I)-tricarbonyl chemistry, without any additional modification of the protein.[8] ^{99m}Tc-V_{HH}s have been proposed as potential molecular imaging agents in several contexts,

such as oncology and inflammatory diseases. However, compared to SPECT, PET imaging offers indisputably superior images that are characterised by (1) higher spatial resolution, (2) superior imaging contrast, (3) less scatter, and (4) better attenuation correction.[9] Therefore, PET has gained more clinical popularity over the last decade and also PET radionuclides have been applied for labelling of nanobodies. In accordance with the short biological half-life of the nanobody, both ^{68}Ga and ^{18}F are ideal radioisotopes for their labelling. Radiolabelling of anti-EGFR and anti-HER2 nanobodies with ^{68}Ga has been reported and is attractive because the radioisotope is available as a bench-top generator product and does not require a cyclotron as it is the case for fluorine-18.[5,10] However, fluorine-18 has several advantages such as favourable decay properties (~ 97% ß$^+$-emission, 635-keV maximum positron energy), low β$^+$-trajectory (< 2 mm in water), small atom size and moreover, it is readily produced in large quantities (>400 GBq/batch) with a cyclotron. The half-life is long enough to allow transportation to remote hospitals without an on-site cyclotron and it is short enough to avoid extended irradiation of patients. The success and medical importance of 2-[^{18}F]fluoro-2-deoxyglucose ([^{18}F]FDG), have led to the installation of many of these expensive cyclotron infrastructures all over the world. Consequently, fluorine-18 is now readily available in an expanding number of hospitals and research centres and the infrastructure is in place to expand its application far beyond [^{18}F]FDG.[11]

The Al^{18}F labelling method is a relatively new approach that allows radiofluorination of biomolecules such as peptides and proteins in a one-step procedure.[12] This method avoids laborious multistep procedures often required when secondary labelling agents, such as N-succinimidyl 4-[^{18}F]fluorobenzoate ([^{18}F]SFB), are used to radiolabel biomolecules with fluorine-18.[13] Conventional radiofluorination strategies involve carbon-fluorine bond formation in anhydrous aprotic solvents. In contrast, the Al^{18}F-strategy involves the formation of aluminium monofluoride ({Al^{18}F}$^{2+}$) which is trapped by a suitable chelator –mostly conjugated to a biomolecule- in aqueous medium. Recently, we reported a new restrained complexing agent (RESCA1), which displays a less rigid structure than the established macrocyclic AlF-chelator 1,4,7-triazacyclononane-1,4-diacetate (NODA) in order to reduce the activation energy of the complexation reaction. The area of improvement includes radiolabelling at ambient temperatures (≤40 °C), whilst maintaining *in vivo* stability. The generic applicability of the proposed method was demonstrated by labelling the heat-sensitive biomolecule human serum albumin (HSA) at ambient temperature with {Al^{18}F}$^{2+}$ with high radiochemical purity in less than 30 minutes. [^{18}F]AlF-RESCA1-HSA showed excellent *in vitro* and *in vivo* stability and moreover, Al^{18}F-RESCA1-HSA showed favourable properties for PET blood pool imaging applications (**Chapter III**).

The objective of current study was to efficiently radiolabel macrophage CRIg-targeting nanobodies *via* the Al^{18}F-method for PET imaging of joint inflammation. The complement receptor of the Ig superfamily (CRIg) has a pronounced expression on Kupffer cells, which are resident liver macrophages, and CRIg is found to a certain extent on resident tissue macrophages subsets in various tissues, including normal synovium.[14] However, it has been shown that CRIg is more abundant in rheumatoid arthritis (RA) synovial tissue and consequently, CRIg is a promising marker for specific molecular imaging of RA, allowing non-invasive quantification of joint inflammation.[15] Here, we describe a generic approach for Al^{18}F-labelling, automated purification, characterisation and preclinical evaluation in mice of nanobodies (NbV4m119) targeting CRIg.

2. MATERIALS AND METHODS

2.1 General

All reagents and solvents were purchased from Sigma-Aldrich (Bornem, Belgium), Fluka (Bornem, Belgium), Fisher (Doornik, Belgium) or Acros Organics (Geel, Belgium). Fluorine-18 was produced on site using a cyclotron (IBA Cyclone 18/9, IBA, Louvain-la-Neuve, Belgium) by irradiation of $H_2{}^{18}O$ with 18-MeV protons. Radioactivity was measured using an ionisation chamber based activity meter (Capintec Radioisotope Calibrator CRC-721, Ramsey, NJ, USA). NbV4m119 and the CRIg$^{-/-}$ mice were generously provided by Geert Raes from the VIB laboratory of myeloid cell immunology. The synthesis and characterisation of compound RESCA-TFP is described in patent WO/2016/065435.

2.2 Radio-LC-HRMS

A Dionex Ultimate 3000 UPLC System (Thermo Fisher Scientific, Sunnyvale, USA) coupled in series to a 3- inch NaI(Tl) radioactivity detector and an ultra-high resolution time-of-flight mass spectrometer with electron spray ionisation (ESI) (MaXis impact, Bruker, Bremen, Germany) was used for analysis of the nanobody constructs. For deconvolution analysis of the raw mass spectral data the software program DataAnalysis (Bruker Daltonik, Bremen, Germany) was used. Calculated average neutral molecular ion mass values were obtained using Compas Isotope Pattern (version 3.2, Bruker). Both an Acquity UPLC BEH C18 column (1.7 µm, 2.1 mm x 150 mm, Waters) and a Zorbax SB-C3 column (1.8 µm, 3.0 mm x 100 mm, Agilent) were tested using following method. Solvent A (H_2O, 0.1% HCOOH) and solvent B (acetonitrile; 0.1% HCOOH), flow rate 0.3 ml/min. The elution gradient was: 0-1 min: 99% A; 1-7 min: from 99% A to 1% A; 7-10 min: 1% A; 10.1-12 min: 99% A. UV detection of the eluate was performed at 280 nm.

2.3 Synthesis of RESCA1-V4m119 Nb

A solution of RESCA1-TFP (23 µl, 1.4294 x 10^{-6} moles) in DMSO was added in 12 molar excess to a solution of NbV4m119 (2.5 ml, 1.1912 x 10^{-7} moles,) in 0.05 M sodium bicarbonate pH 8.6 and the mixture was incubated for 3 h at room temperature. The conjugate was successfully purified by gel filtration (PD-10 desalting column, GE Healthcare Bio-Science AB, Uppsala, Sweden) and the concentration of RESCA1-NbV4m119 was determined spectrophotometrically at 280 nm (Nanodrop 2000, Thermo Fisher scientific). Analysis of the purified compound was performed by size-exclusion chromatography on a Superdex 75 10/300 GL column (GE Healthcare) using sodium phosphate buffer (0.01 M, pH 7.4, 0.14 M NaCl), as eluent at a flow rate of 0.5 ml/min and with the LC-HRMS method described above. UV detection of the eluate was performed at 280 nm.

2.4 Radiosynthesis and semi-automated purification of [^{18}F]AlF-RESCA1-NbV4m119

[^{18}F]F^- was separated from [^{18}O]H_2O by trapping on a SepPak Light Accel plus QMA anion exchange cartridge (Cl^- form; Waters). The cartridge was washed with water (3 mL), [^{18}F]F^- was eluted from the cartridge with an aqueous solution of sodium chloride 0.9% (0.3 mL) and the eluate was diluted with water (2.7 ml). This [^{18}F]F^- solution (0.5 ml) was added to 12.5 µL of 2 mM aluminum chloride ($AlCl_3$) in sodium acetate buffer (0.1 M, pH 4.5). The solution was incubated at room temperature (rt) for 5 min to form $\{Al^{18}F\}^{2+}$. A solution of RESCA1-NbV4m119 (1.5 mL, 0.55 mg/ml) in sodium acetate buffer (0.1 M, pH 4.5) was added to the freshly prepared $\{Al^{18}F\}^{2+}$ solution and the mixture was incubated at ambient temperature (20-22°C) for 12 min. After incubation, the mixture was purified by preparative HPLC using three or four Hitrap desalting columns (GE Healthcare) in series. Radiochemical identity and purity were assessed by size-exclusion chromatography on a Superdex 75 10/300 GL column (GE Healthcare) using sodium phosphate buffer (0.01M, pH 7.4, 0.14 M NaCl), as eluent at a flow rate of 0.5 ml/min. UV detection of the eluate was performed at 280 nm and a 3 inch NaI(Tl) radioactivity detector was coupled in series. The identity of the main compound was confirmed using unlabelled NbV4m119 as reference material.

2.5 Stability studies of [^{18}F]AlF-RESCA1-NbV4m119 in rat plasma

A volume of 200 µL of [^{18}F]AlF-RESCA1-NbV4m119 solution was added to rat plasma (1 mL). The mixture was incubated at 37 °C for 4 hours and analysed (10 µl) at 0, 1, 2, 3 and 4 h with size-exclusion chromatography on a Superdex 75 10/300 GL column using sodium phosphate buffer (0.01M, pH 7.4, 0.14 M NaCl) as eluent at a flow rate of 0.5 ml/min.

2.6 Biodistribution and microPET studies

Quantification of radioactivity for biodistribution studies was performed using an automated gamma-counter equipped with a 3-inch NaI(Tl) well crystal coupled to a multichannel analyser, mounted in a sample changer (Perkin Elmer 1480 Wizard 3q, Waltham, USA). Counts were corrected for background radiation, physical decay and counter dead time. Animals were housed in individually ventilated cages in a thermo-regulated (~22 °C), humidity-controlled facility under a 12h-12h light-dark cycle, with access to food and water *ad libitum*. All animal experiments were conducted according to the Belgian code of practice for the care and the use of animals, after approval from the university animal ethics committee. The biodistribution study of [^{18}F]AlF-RESCA1-NbV4m119 was carried out in healthy male C57BL/6 mice (body weight: 22-26 g) at 1 h and 3 h post injection (p.i.) (*n* = 3/time point) or in CRIg-deficient mice (CRIg$^{-/-}$, C57BL/6 background, body weight: 20-23 g) at 3 h p.i. (*n* = 3/time point). Mice were injected with the Al^{18}F-tracer (7-8 MBq) *via* a tail vein under anesthesia (2.5% isoflurane in O_2 at 1 L/min flow rate) and sacrificed by decapitation at above specified time points. Blood and major organs were collected in tared tubes and weighed. The radioactivity in blood, organs and other body parts was counted using an automated γ-counter. For calculation of total radioactivity in blood, bone and muscle tissue mass was assumed to be, respectively, 7, 12 and 40% of the total body mass.[16,17] Results are presented as percentage of injected dose (%ID) or in standardised uptake values (SUV). Small animal whole-body PET imaging on mice was performed using a FOCUS^{TM} 220 microPET scanner (Concorde Microsystems, Knoxville, US) and PMOD software (v 3.2, PMOD Technologies, Zürich, Switzerland).

2.7 Statistical analysis

Quantitative data are expressed as mean ± standard deviation. Means were compared using the unpaired two-tailed Student t-test. Values were considered statistically significant for $P < 0.05$.

3. RESULTS AND DISCUSSION

Nanobodies can be considered as “magic bullets” for imaging and might play an important role in the diagnosis and management of various diseases.[6] The objective of this study was to efficiently radiolabel macrophage CRIg-targeting nanobodies *via* the Al^{18}F-method for PET imaging of joint inflammation. Zheng et al. generated successfully nanobody NbV4m119, that targets specifically CRIg.[15] Moreover they radiolabelled NbV4m119 with the SPECT radionuclide ^{99m}Tc *via* standard ^{99m}Tc(I)-tricarbonyl chemistry and could efficiently visualise joint inflammation in mice with collagen-induced arthritis (CIA). Furthermore SPECT/CT with ^{99m}Tc-NbV4m119 could detect early signs of inflammation even before manifestation of anatomically visible signs of the disease. Compared to SPECT, PET imaging offers superior images. Among β^+-emitting radioisotopes, the halogen fluorine-18

is the most commonly used due to its optimal chemical properties and almost ideal nuclear decay characteristics.[18] Blykers et al. reported the ^{18}F-labelling of nanobodies targeting the macrophage mannose receptor (MMR) for imaging of MMR-expressing tumor-associated macrophages (TAMs), providing prognostic information about the tumor stroma.[19] The anti-MMR 3.49 Nb was labelled using the prosthetic group [^{18}F]SFB with a 5-10% radiochemical yield using an optimised protocol yielding [^{18}F]FB-anti MMR-3.49 Nb. However, the multistep synthesis is laborious (180 minutes, starting from [^{18}F]F$^-$ and the final product was purified manually with a disposable PD-10 desalting column, resulting in suboptimal conditions regarding radioprotection for the radiochemist. Moreover, only limited amounts of purified product (200-500 MBq) were obtained with moderate specific activity (10 to 30 GBq/µmol). We now tested the Al^{18}F-method using RESCA1 as chelator as a potential superior alternative for an efficient one-step radiolabelling of nanobodies at ambient temperature.

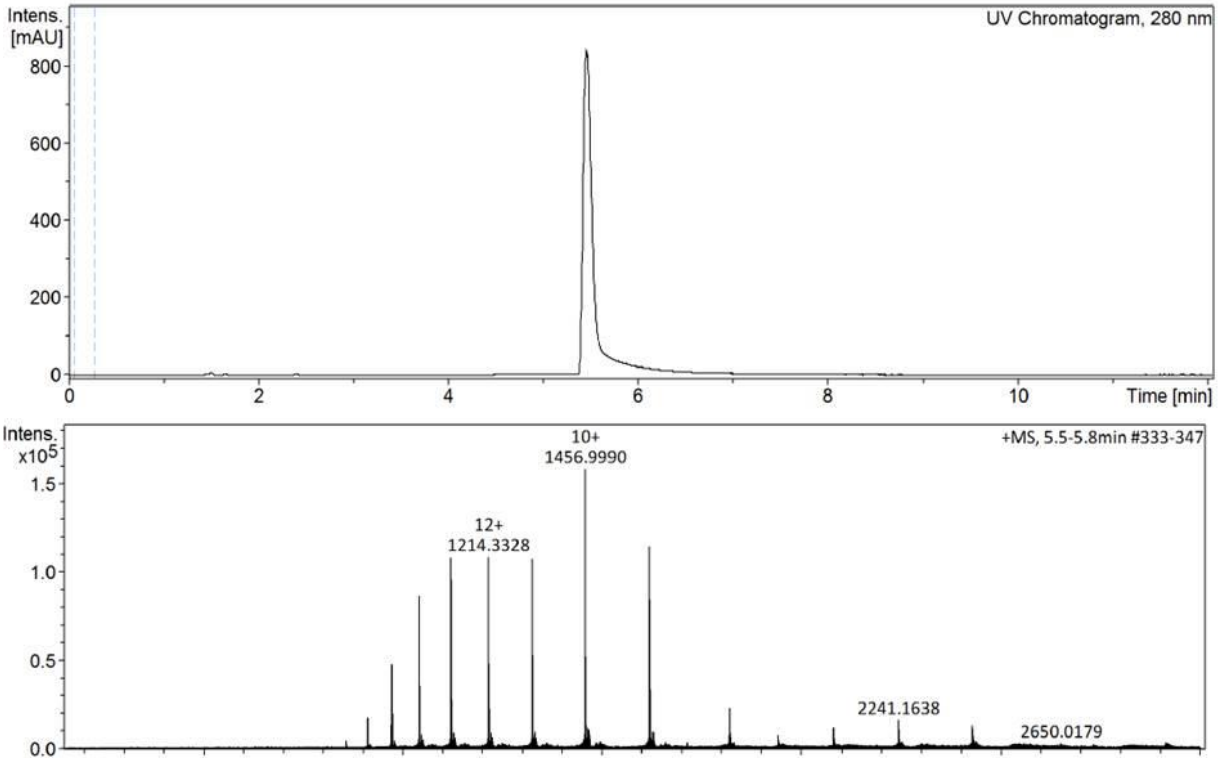

Figure 1: ***A:*** *LC-UV280 nm chromatogram of unlabelled NbV4m119 (Retention time (Rt): 5.5 min).* ***B:*** *MS spectrum of unlabelled NbV4m119. The theoretical average neutral molecular mass of the unlabelled NbV4m119 was 14577.85 Da [M] (Calculated for $C_{643}H_{950}N_{188}O_{196}S_4$) and the observed mass after deconvolution was 14577.61 ± 0.02 Da [M].*

Characterisation of a radiolabelled nanobody is important in order to assure that the radiolabelling procedure does not affect the nanobody integrity. We have therefore explored radio-liquid chromatography in combination with high-resolution mass spectrometry (radio-UPLC-HRMS) to analyse NbV4m119 prior to and after derivatisation/radiolabelling. An Acquity UPLC BEH C18 column

(1.7 µm, 2.1 mm x 150 mm, Waters) and a Zorbax SB-C3 column (1.8 µm, 3.0 mm x 100 mm, Agilent) were compared. First the MS settings and LC-parameters for a solution of the unlabelled NbV4m119 were optimised. Gradients, flow rates and column temperatures were varied. The best analysis results were obtained with a Zorbax SB-C3 column at a flow rate of 0.3 ml/min with a column temperature of 40 °C (**Figure 1**).

The theoretical average neutral molecular mass of unlabelled NbV4m119 is 14577.85 Da [M] (calculated for $C_{643}H_{950}N_{188}O_{196}S_4$) and the observed mass after deconvolution was 14577.61 ± 0.02 Da [M]. We also observed the presence of a deamination product with an observed mass of 14560.76 ± 0.02 Da (calculated for $C_{643}H_{947}N_{187}O_{196}S_4$ [M]: 14560.82). This deamination product was expected and can be formed spontaneously during manipulation and storage of the protein. This radio-LC-HRMS method allows detecting whether the disulfide bonds are still intact after the derivatisation procedure. Proteins with intramolecular disulfide bonds will shift two daltons when a disulfide is converted to two sulfhydryl groups. Disulfide bonds play an important role in the folding and stability of proteins which is crucial to assure that the nanobody retains its antigen affinity. After the successful characterisation of the unlabelled NbV4m119 with our LC-HRMS method, we derivatised the nanobody using the bifunctional chelator RESCA1-TFP and labelled the conjugate with $\{Al^{18}F\}^{2+}$ (**Figure 2**). NbV4m119 possesses five lysine residues in its amino acid sequence, therefore several lysine groups can react with the active ester *via* the free amino functionalities. RESCA1-TFP ester was efficiently conjugated to NbV4m119 providing RESCA1-V4m119 Nb with a chelator-to-protein ratio of 1.5, estimated by ESI-TOF-HRMS analysis and no aggregates or degradation products were formed. The theoretical average neutral molecular masses for single and dual conjugation are 14979.2602 Da and 15397.7014 Da [M], respectively. The observed masses for RESCA1-NbV4m119 after deconvolution were 14979.35 ± 0.02 Da and 15397.69 ± 0.02 Da [M], respectively.

RESCA1-V4m119 Nb was labelled with $\{Al^{18}F\}^{2+}$ in good radiochemical yield (RCY) in mild conditions (12 min, 25 °C, pH 4.5). The crude reaction mixture was purified using three or four Hitrap desalting columns in series yielding the purified batch [^{18}F]AlF-RESCA1-NbV4m119 (eluting at 5-7 min) with a radiochemical yield of 45-53% (n=3). The best separation between [^{18}F]AlF-RESCA1-V4m119 Nb and non-reacted $Al^{18}F$-species was obtained using four Hitrap desalting columns in series.

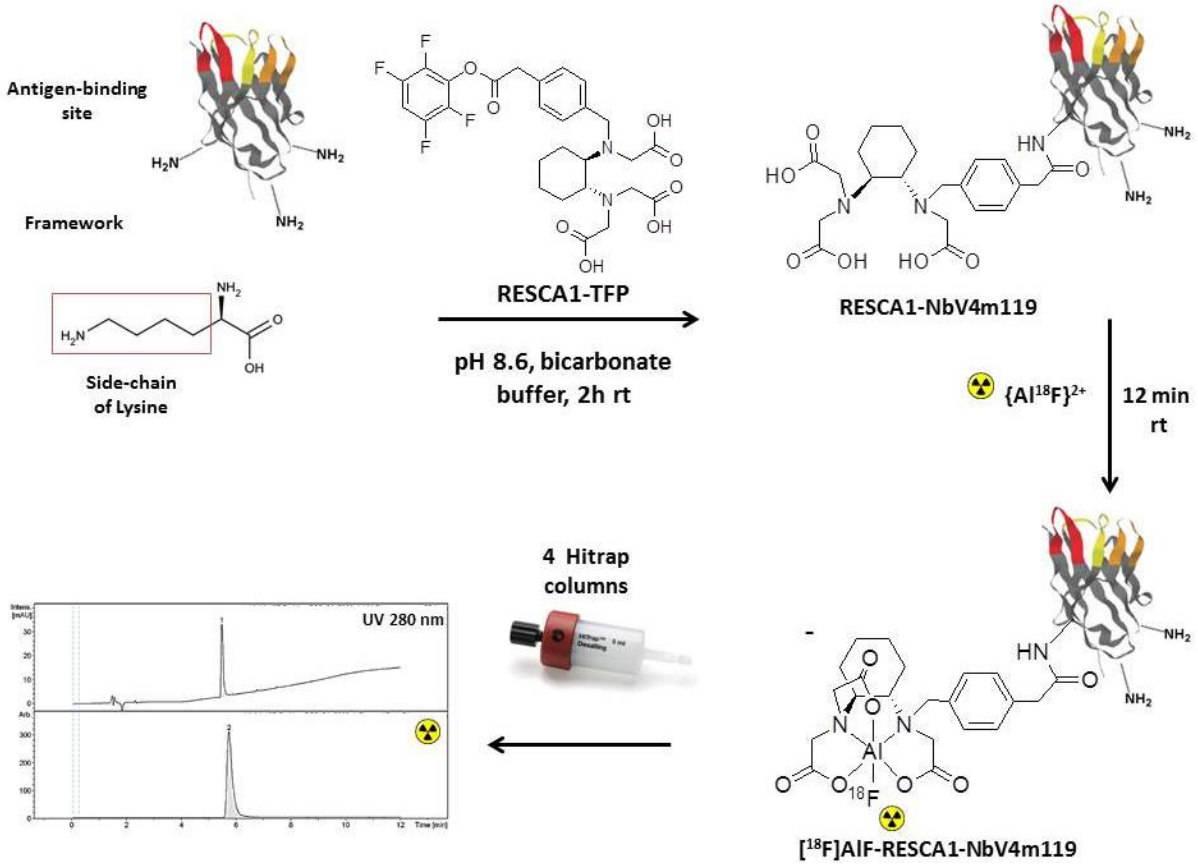

Figure 2: *Synthesis and radiolabelling of RESCA1-NbV4m119 with {Al^{18}F}$^{2+}$. RESCA1-TFP ester was conjugated to NbV4m119 providing RESCA1-NbV4m119 with a chelator-to-protein ratio of 1.5, estimated by ESI-TOF-HRMS analysis. The conjugate was purified by gel filtration (PD-10 desalting column). [^{18}F]AlF-RESCA-NbV4m119 was prepared in high RCY (>45%). Purification was accomplished with preparative HPLC using 4 Hitrap desalting columns in series, resulting in the final product (2 GBq) with a high purity (>97%) in less than 35 min (starting after elution of fluorine-18 from the anion exchange QMA cartridge). LC-UV280 nm chromatogram and radio-chromatogram of purified Al^{18}F-RESCA1-NbV4m119 with a retention time of 5.6 min and 5.9 min respectively.*

Al^{18}F-RESCA-NbV4m119 was thus obtained with a batch activity of about 2 GBq and a radiochemical purity higher than 97% in less than 35 min starting from the elution of fluorine-18 from the anion exchange cartridge. The specific activity ranged from 80 to 85 GBq/µmol. [^{18}F]AlF-RESCA-NbV4m119 was analysed with the optimised radio-LC-HRMS method, eluting at a retention time of 5.6 min. The UV detector and radiometric detector are coupled in series, which explains the minor delay in the radiometric signal. [^{18}F]AlF-RESCA-NbV4m119 showed excellent stability *in vitro*. Analysis with size exclusion chromatography (SEC) revealed that 96% of the Al^{18}F-tracer was still intact after 6 h incubation in the storage buffer (Na_2HPO_4 0.01M pH 7.4 + 0.14M NaCl) at room temperature and 91.5% of the Al^{18}F-tracer was still intact after 4 h incubation in rat plasma at 37°C (**Figure 3**).

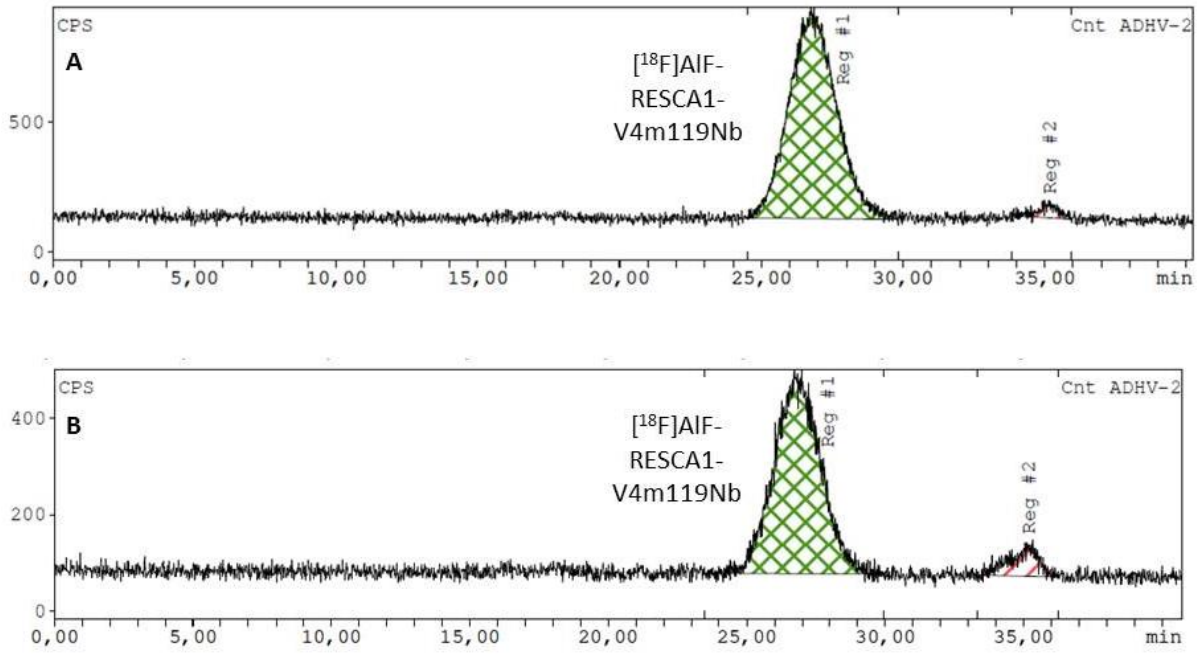

Figure 3: ***A:*** *Radio-chromatogram of [^{18}F]AlF-RESCA1-NbV4m119 after 2 minutes incubation in rat plasma at 37°C,* ***97.9%*** *of [^{18}F]AlF-RESCA1-NbV4m119 (Rt 26.8 min) and 2.1% free Al^{18}F-species,$^{18}F^-$ and/or ^{18}F-labelled degradation fragments (Rt 35.1 min) are observed* ***B:*** *Radio-chromatogram of [^{18}F]AlF-RESCA1-NbV4m119 after 4 hours incubation in rat plasma at 37°C, 91.5% [^{18}F]AlF-RESCA1-NbV4m119 (Rt 26.8 min) and 8.5% free Al^{18}F-species,$^{18}F^-$ and/or ^{18}F-labelled degradation fragments (Rt 35.1 min) are observed*

A biodistribution study with [^{18}F]AlF-RESCA1-NbV4m119 was carried out in healthy wild-type (WT) mice at 1 h and 3 h p.i., the results are expressed as percentage of injected dose (%ID) (**Figure 4**). Since the molecular size of nanobodies is below the threshold for renal glomerular filtration, nanobodies are generally cleared fast from blood, mainly *via* renal clearance. High uptake in kidneys (27.5 ± 1.8%ID and 9.8 ± 1.8%ID at 1 h and 3 h p.i. respectively) and urine/bladder (23.0 ± 2.9%ID and 46.5 ± 6.2%ID at 1 h and 3 h p.i. respectively) were observed. Only 0.7 and 1.6%ID of the radioactivity was observed in blood after 1 h and 3 h p.i. respectively, indicating fast blood clearance.

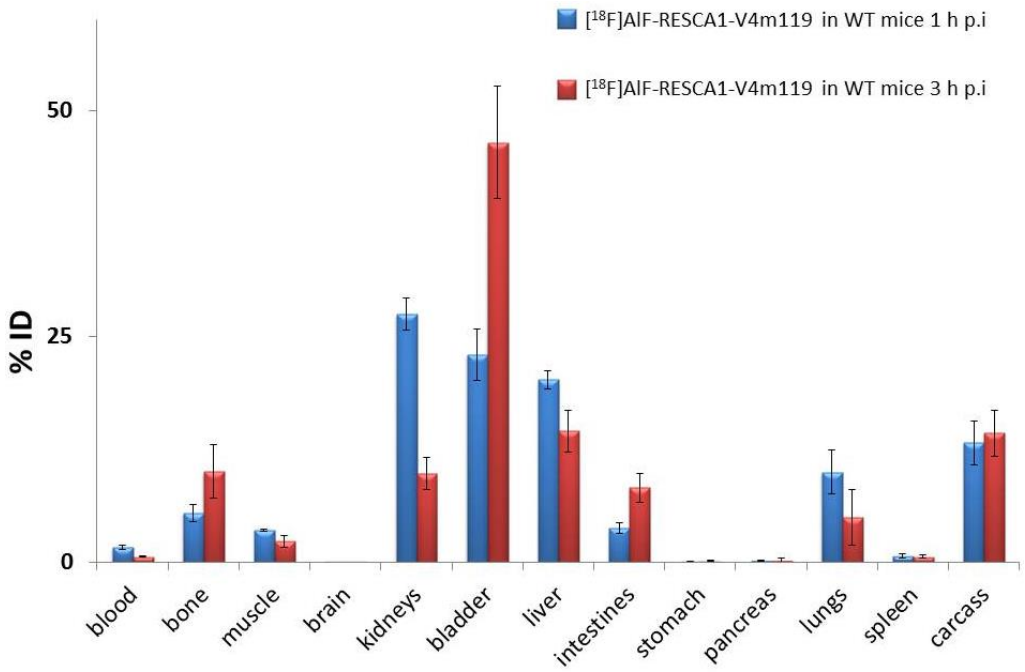

Figure 4: *Biodistribution of [^{18}F]AlF-RESCA1-NbV4m119 in naïve wild-type mice (WT, n=3/group; 22-26 g) at 1 h and 3 h p.i. Results are presented as percentage of injected dose (%ID).* For calculation of *total radioactivity in blood, bone and muscle, tissue mass was assumed to be, respectively, 7, 12 and 40% of the total body mass.*

Zheng et al. investigated CRIg mRNA levels in collagen-induced arthritis (CIA) mice to determine whether this marker is expressed homogeneously in the body or specifically in certain tissues during inflammation.[15] High CRIg mRNA levels were found in liver (the CRIg receptor has a pronounced expression on Kupffer cells) and low or undetectable quantities in bone marrow, lymph nodes, spleen and lungs. In accordance with the tissue mRNA studies performed by Zheng et al., [^{18}F]AlF-RESCA1-NbV4m119 showed high uptake in liver (20.2 ± 1.0%ID and 14.5 ± 2.3%ID at 1 h and 3 h p.i. respectively), but low uptake in other organs. Fluorine-18 in the form of fluoride as well as {Al^{18}F}$^{2+}$ are known to accumulate in bone.[20,21] Although we showed excellent *in vitro* stability of [^{18}F]AlF-RESCA1-NbV4m119 in rat plasma, relative high bone uptake was observed *ex vivo* at 3 h p.i. (10.1 ± 3.0%ID), indicating demetallation or defluorination of the compound. Another explanation for the increased bone uptake could be that [^{18}F]AlF-RESCA1-NbV4m119 or small ^{18}F-labelled degradation fragments have specific retention in bone marrow, resulting in bone accumulation. Non-specific bone accumulation might compromise the utility of this tracer for noninvasive quantification of joint inflammation *in vivo*. To confirm the specificity of our Al^{18}F-labelled nanobody targeting CRIg, we performed a biodistribution study at 3 h p.i on naïve CRIg$^{-/-}$ (CRIg knockout) mice.

Figure 5 shows the results of the biodistribution study presented in standardised uptake values (SUV) in the different organs. The highest activity concentration at 3 h p.i. was observed in kidneys indicating renal clearance of the radiolabelled ligand. In CRIg$^{-/-}$ mice no specific uptake of [^{18}F]AlF-

RESCA1-NbV4m119 could be observed in the liver (SUV: 0.27 ± 0.1) or other organs. Liver uptake of [^{18}F]AlF-RESCA1-NbV4m119 3 h p.i. in WT mice was significantly higher with a SUV value of 2.31 ± 0.2, indicating excellent *in vivo* specificity of the tracer. Higher kidney uptake in the CRIg$^{-/-}$ mice at 3 h p.i compared with the kidney uptake in the WT mice at 3 h p.i. might be explained by the lower liver uptake in CRIg$^{-/-}$ mice, resulting in higher availability of [^{18}F]AlF-RESCA1-NbV4m119 towards the renal elimination pathway. Furthermore, a relatively high bone uptake was observed in CRIg$^{-/-}$ mice, comparable to the observed bone uptake in WT mice, indicating that [^{18}F]AlF-RESCA1-NbV4m119 as such does not show specific binding in bone tissue. Whole-body PET imaging clearly showed specific uptake of Al^{18}F-RESCA1-NbV4m119 in the liver, whereas no liver uptake was observed in the CRIg knockout mice (**Figure 5**).

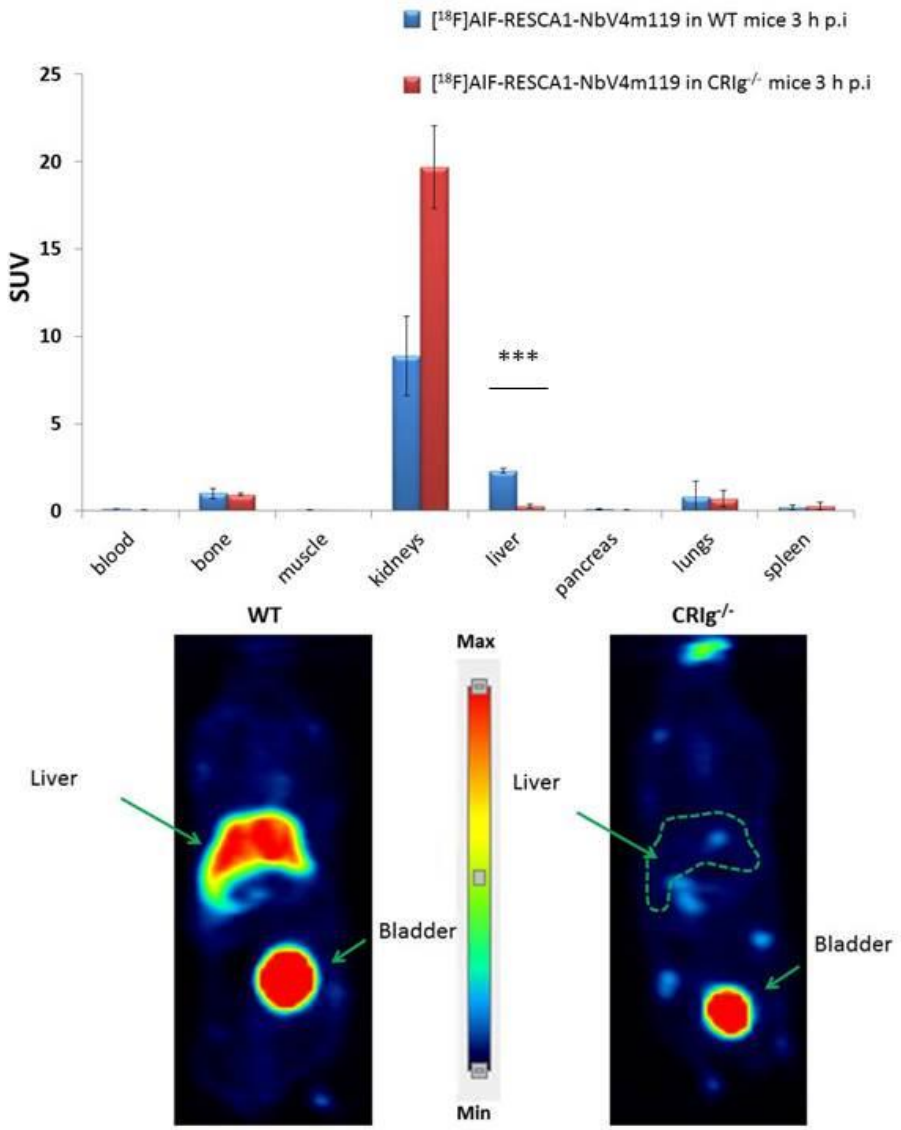

Figure 5: *Biodistribution of [^{18}F]AlF-RESCA1-NbV4m119 in naïve wild-type mice (WT, n=3/group; 20-23 g) mice and CRIg$^{-/-}$ mice (n=3/group; 19-21 g) at 3 h p.i. and coronal views of microPET imaging. Biodistribution results are presented as standardised uptake value (SUV).***P < 0.001. Summed images (30-60 min p.i., average volume time weighted) performed on naïve WT and CRIg$^{-/-}$ mice.*

To further investigate the unexpected bone uptake, we analysed a urine sample of naïve WT mouse 3 h after i.v. injection of [^{18}F]AlF-RESCA1-NbV4m119. Surprisingly, size exclusion chromatography showed that urine contained only 2.2% of the intact compound [^{18}F]AlF-RESCA1-NbV4m119, the rest of activity (97.9%) eluted at later time points under the form of small ^{18}F-labelled degradation products, $^{18}F^-$ and/or different Al^{18}F-species (**Figure 6**). Comparable results were obtained in urine samples of CRIg$^{-/-}$ mice 3 h p.i. of [^{18}F]AlF-RESCA1-NbV4m119.

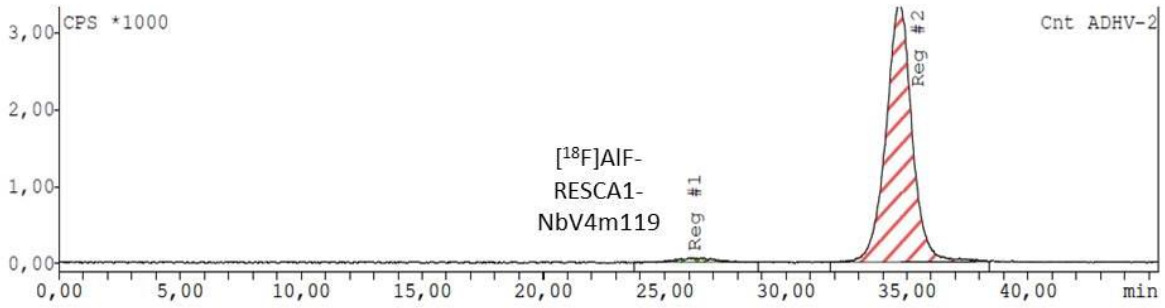

Figure 6: *Radio-chromatogram of urine sample of naïve WT mouse 3 h after i.v. injection of [^{18}F]AlF-RESCA1-NbV4m119. Only 2.2% of [^{18}F]AlF-RESCA1-NbV4m119 (Rt 26.2 min) is still intact, the rest of activity (97.9%) elutes under the form of small ^{18}F-labelled degradation products, $^{18}F^-$ and/or different Al^{18}F-species (Rt 34.7 min)*

This high rate of *in vivo* degradation was unexpected. It seems that severe demetallation or defluorination occurs in the kidneys and that {Al^{18}F}$^{2+}$ or $^{18}F^-$ as such is released back into circulation, resulting in increased bone uptake values. However, further analysis of the degradation products in urine samples with reverse phase or ion exchange chromatography is necessary to identify the degradation products. Also *ex vivo* determination of blood metabolites would be interesting to find out if degradation of the Al^{18}F-tracer occurs in blood or after glomerular filtration. Nevertheless, the calculated bone uptake is still limited and could be overestimated. Indeed, to calculate this parameter we assumed that 12 % of the body mass exists out of bone, which might be an overestimation in these mice. The *in vivo* PET imaging did not show significant bone uptake after 1 h and high liver-to background images were obtained, indicating favourable *in vivo* imaging properties of [^{18}F]AlF-RESCA1-NbV4m119 with high specificity for CRIg. We successfully labelled for the first time a nanobody via the Al^{18}F-method with high radiochemical yields. However, the first step of this approach is a non-specific derivatisation of the nanobody with one or more Al^{18}F-chelators, resulting in batch-to-batch differences. Therefore site-specific incorporation of the chelator into the nanobody would even further improve this promising radiolabelling approach.

4. CONCLUSIONS

Nanobodies are promising tools in molecular imaging and have many advantages in comparison with full-size antibodies. Fluorine-18 is the radionuclide of choice in view of the short biological half-life of

nanobodies. We demonstrated that the Al^{18}F-method using our recently developed chelator RESCA1 provides an efficient approach to radiolabel nanobodies with fluorine-18 at ambient temperature. We successfully derivatised nanobodies targeting the CRIg receptor with RESCA1 and labelled the conjugate with {Al^{18}F}$^{2+}$ in good radiochemical yields at ambient temperature. [^{18}F]AlF-RESCA1-NbV4m119 was purified with preparative HPLC resulting in the Al^{18}F-tracer with a radiochemical purity higher than 97% and the compound showed excellent *in vitro* stability. Furthermore, we successfully optimised a generic radio-HPLC-HRMS system for the analysis and quality control of radiolabelled nanobodies. Biodistribution studies in mice showed that [^{18}F]AlF-RESCA1-NbV4m119 was mainly excreted *via* the renal pathway but also high liver uptake was observed in normal WT mice, which is expected because CRIg receptors are highly expressed on Kupffer cells. Biodistribution and microPET studies in CRIg$^{-/-}$ mice demonstrated absence of significant uptake in liver, indicating excellent specificity of the Al^{18}F-labelled tracer. Unexpectedly, almost no intact [^{18}F]AlF-RESCA1-NbV4m119 was found in urine at 3 h p.i. and relatively high bone uptake was observed, indicating *in vivo* instability of the tracer. However, *in vivo* PET imaging in mice did not show significant bone uptake at 1 h p.i. and high liver-to background images were obtained, indicating favourable *in vivo* imaging properties of [^{18}F]AlF-RESCA1-NbV4m119 with high specificity for CRIg. This tracer will be further evaluated in CIA mice for quantification of joint inflammation. This generic radiolabelling, purification and characterisation method provides a general approach for radiolabeling of nanobodies with fluorine-18.

5. ACKNOWLEDGMENTS

The authors thank Ann Van Santvoort and Tine Buelens from the Department of Nuclear Medicine and Julie Cornelis, Ivan Sannen, Pieter Haspeslagh and Jana Hemelaers from the Laboratory for Radiopharmacy for their assistance. RESCA-TFP was synthesised by Dr. Joan Lecina. This research has received support within the SBO project MIRIAD, funded from the IWT Flanders.

6. REFERENCES

(1) Vaneycken, I., Matthias, D., Hernot, S., Vos, J. De, Xavier, C., Devoogdt, N., Caveliers, V., and Lahoutte, T. (2011) Immuno-imaging using nanobodies. *Curr. Opin. Biotechnol. 22*, 877–881.

(2) De Meyer, T., Muyldermans, S., and Depicker, A. (2014) Nanobody-based products as research and diagnostic tools. *Trends Biotechnol. 32*, 263–270.

(3) Harmsen, M. M., and De Haard, H. J. (2007) Properties, production, and applications of camelid single-domain antibody fragments. *Appl. Microbiol. Biotechnol. 77*, 13–22.

(4) Muyldermans, S., Baral, T. N., Retamozzo, V. C., De Baetselier, P., De Genst, E., Kinne, J., Leonhardt, H., Magez, S., Nguyen, V. K., Revets, H., Rothbauer, U., Stijlemans, B., Tillib, S., Wernery, U., Wyns, L., Hassanzadeh-Ghassabeh, G., and Saerens, D. (2009) Camelid immunoglobulins and nanobody technology. *Vet. Immunol. Immunopathol. 128*, 178–183.

(5) Vosjan, M. J. W. D., Perk, L. R., Roovers, R. C., Visser, G. W. M., Walsum, M. S., and Bergen, P. M. P. Van. (2011) Facile labelling of an anti-epidermal growth factor receptor Nanobody with ^{68}Ga via a novel bifunctional desferal chelate for immuno-PET. J*. Nucl. Med.* 753–763.

(6) Chakravarty, R., Goel, S., and Cai, W. (2014) Nanobody : The " Magic Bullet " for Molecular Imaging ? *Theranostics 4*, 386–398.

(7) Huyvetter, M. D., Xavier, C., Caveliers, V., Lahoutte, T., Muyldermans, S., and Devoogdt, N. (2014) Radiolabeled nanobodies as theranostic tools in targeted radionuclide therapy of cancer. *Expert Opin. Drug Deliv. 11*, 1939–1954.

(8) Xavier, C., Devoogdt, N., Hernot, S., Vaneycken, I., Huyvetter, M. D., Vos, J. De, Massa, S., Lahoutte, T., and Caveliers, V. (2012) Site-Specific Labeling of His-Tagged Nanobodies with ^{99m} Tc : A Practical Guide, in *Methods in Molecular Biology 30*, 485–490.

(9) Serdons, K., Verbruggen, A., and Bormans, G. M. (2009) Developing new molecular imaging probes for PET. *Methods 48*, 104–111.

(10) Vaneycken, I., Devoogdt, N., Van Gassen, N., Vincke, C., Xavier, C., Wernery, U., Muyldermans, S., Lahoutte, T., and Caveliers, V. (2011) Preclinical screening of anti-HER2 nanobodies for molecular imaging of breast cancer. *FASEB J. 25*, 2433–2446.

(11) Verbruggen, A., and Bormans, G. (2015) Course notes on Radiopharmaceuticals.

(12) Laverman, P., McBride, W. J., Sharkey, R. M., Goldenberg, D. M., and Boerman, O. C. (2014) Al$^{(18)}$ F labeling of peptides and proteins. *J. Labelled Comp. Radiopharm. 57*, 219–223.

(13) Thonon, D., Goblet, D., Goukens, E., Kaisin, G., Paris, J., Aerts, J., Lignon, S., Franci, X., Hustinx, R., and Luxen, A. (2011) Fully Automated Preparation and Conjugation of N-Succinimidyl 4-[^{18}F]Fluorobenzoate ([^{18}F]SFB) with RGD Peptide Using a GE FASTlab^{TM} Synthesizer. *Mol. Imaging Biol 13*, 1088-1095.

(14) Bilzer, M., Roggel, F., and Al, G. (2006) Role of Kupffer cells in host defense and liver disease. *Liver Int. 26*, 1175–1186.

(15) Zheng, F., Bouwens, L., Lahoutte, T., Matthys, P., Muyldermans, S., De, P., Devoogdt, N., Raes, G., and Schoonooghe, S. (2014) Nanobodies for Early and Preclinical Diagnosis in a Mouse Model of Rheumatoid Arthritis. *J. Nucl. Med. 55*, 824–830.

(16) Fritzberg, A. R., Whitney, W. P., Kuni, C. C., and Klingensmith, W. (1982) Biodistribution and renal excretion of ^{99m}Tc-N,N'-bis-(Mercaptoacetamido) ethylenediamine. Effect of renal tubular transport inhibitors. *Int. J. Nucl. Med. Biol. 9*, 79–82.

(17) Mitterhauser, M., Toegel, S., Wadsak, W., Lanzenberger, R. R., Mien, L.-K., Kuntner, C., Wanek, T., Eidherr, H., Ettlinger, D. E., Viernstein, H., Kluger, R., Dudczak, R., and Kletter, K. (2007) Pre vivo, ex vivo and in vivo evaluations of [^{68}Ga]-EDTMP. *Nucl. Med. Biol. 34*, 391–397.

(18) Le Bars, D. (2006) Fluorine-18 and medical imaging: Radiopharmaceuticals for positron emission tomography. *J. Fluor. Chem. 127*, 1488–1493.

(19) Blykers, a., Schoonooghe, S., Xavier, C., D'hoe, K., Laoui, D., D'Huyvetter, M., Vaneycken, I., Cleeren, F., Bormans, G., Heemskerk, J., Raes, G., De Baetselier, P., Lahoutte, T., Devoogdt, N., Van Ginderachter, J. a., and Caveliers, V. (2015) PET Imaging of Macrophage Mannose Receptor-Expressing Macrophages in Tumor Stroma Using ^{18}F-Radiolabeled Camelid Single-Domain Antibody Fragments. *J. Nucl. Med. 56*, 1265–1271.

(20) Jadvar, H., Desai, B., and Conti, P. S. (2015) Sodium ^{18}F-fluoride PET/CT of bone, joint, and other disorders. *Semin. Nucl. Med. 45*, 58–65.

(21) Chatalic, K. L. S., Franssen, G. M., van Weerden, W. M., McBride, W. J., Laverman, P., de Blois, E., Hajjaj, B., Brunel, L., Goldenberg, D. M., Fehrentz, J.-A., Martinez, J., Boerman, O. C., and de Jong, M. (2014) Preclinical comparison of Al^{18}F- and ^{68}Ga-labeled gastrin-releasing peptide receptor antagonists for PET imaging of prostate cancer. *J. Nucl. Med. 55*, 2050–2056.

GENERAL DISCUSSION AND FUTURE PERSPECTIVES

1. GENERAL DISCUSSION

Positron emission tomography (PET) is a sensitive, non-invasive imaging technology that produces three-dimensional images showing the dynamic *in vivo* concentration of radiotracers, which are labelled with positron emitting radioisotopes. Among β^+-emitting radioisotopes, the halogen fluorine-18 is the most commonly used due to its optimal chemical properties, almost ideal nuclear decay characteristics and ease of production of high activity batches with a cyclotron.

Most methods for radiolabelling biomolecules with fluorine-18 are laborious and require multistep procedures with moderate overall labelling yields. Besides conventional carbon-fluorine radiolabelling methods, different inorganic approaches can be used for labelling of biomolecules with fluorine-18. Several non-carbon elements favour strong bonds (*i.e.* high bond enthalpy) with fluorine, preserve high kinetic stability of the fluorine containing compounds formed and have a lower activation energy for their formation in comparison to carbon-fluorine bonds. These chemical properties were the basis for a new field in ^{18}F-radiochemistry. Currently, boron, silicon and aluminium are three elements under investigation. The strength of the inorganic approach is that it can entail only one, potentially very fast, radiochemical reaction step, which can be easily automated for routine production. Furthermore, time-consuming and rather complex drying steps are avoided since the reaction can take place in, at least partially, aqueous media.

The Al^{18}F-labelling strategy involves chelation of aluminium mono[^{18}F]fluoride ({Al^{18}F}$^{2+}$) in aqueous medium by a suitable chelator conjugated to a biomolecule. McBride *et al.* published the first study using a chelator for {Al^{18}F}$^{2+}$ labelling in 2009. Numerous studies demonstrated the versatility of the Al^{18}F approach to radiolabel peptides using macrocyclic complexing agents such as NOTA and NODA. However, this approach has up to now limited applicability for heat sensitive biomolecules due to high temperatures required (≥ 100 °C) for the complexation of {Al^{18}F}$^{2+}$ by macrocyclic chelators.

Therefore the objective of this thesis was to develop new polydentate ligands that allow chelation of {Al^{18}F}$^{2+}$ at moderate temperatures (<40 °C), whilst maintaining *in vivo* stability. The availability of new Al^{18}F-chelators may have a great impact on PET radiochemical space as it provides a versatile platform for fluorine-18 labelling of peptides and heat-sensitive biomolecules. Ultimately, this approach could result in a kit-based radiolabelling method that reduces the radiolabelling procedure to the simple addition of an aqueous {Al^{18}F}$^{2+}$ solution to a lyophilised kit. Kit preparation of ^{18}F-labelled PET tracers has the potential to substitute current technetium-99m tracers considering that (1) PET is a superior imaging technology over single photon emission computed tomography (SPECT), (2) recent problems with availability of technetium-99m generators due to molybdenum-99

disruptions is affecting the continuity of patient care worldwide, and (3) growing availability of compact cyclotrons.

The first set of new chelators that we developed are acyclic ligands with an N_2O_3 coordinative set or N_3O_2 bis-phenol structure (**Chapter II, Figure 1**). It was observed that only ligands containing the fragment ethylenediamine-*N*,*N*'-diacetic acid (H_3L1-L4) were able to efficiently chelate aluminium fluoride. Ligands without this arrangement of functional groups (H_3L5-8) did not complex aluminium fluoride with good radiochemical yield (RCY) under the conditions tested. Successful labelling of two compounds, (H_3L1) and (H_3L3) was established. H_3L1 and H_3L3 both have excellent labelling properties but, unfortunately, $Al^{18}F$-L1 was not stable *in vitro*. On the other hand, $Al^{18}F$-L3 showed good stability in rat plasma up to 2 h but suffered from decomplexation after extended incubation times (**Chapter II, Figure 2**). Hence, there is still room for improvement regarding the stability of these $\{Al^{18}F\}^{2+}$-chelator complexes.

We explored whether incorporation of a *trans*-cyclohexyl moiety into H_3L1, to form restrained complexing agent 1 (RESCA1, **Chapter III, Figure 1**), would increase steric rigidity of the chelator, improving the orientation of the chelating groups and as a result improving the stability of the resulting AlF-complex. RESCA1 is an acyclic pentadentate ligand with an N_2O_3 coordinative set and the first results revealed that RESCA1 was as efficient as H_3L1 to chelate $\{Al^{18}F\}^{2+}$, with high reactivity (RCY ≥85%) at room temperature (rt). Encouraged by these promising results and in an attempt to broaden the range of chelators, we decided to develop more derivatives of RESCA1 with refined changes in the backbone (RESCA 2-5, **Chapter III**, **Figure 1**). However, small changes in the backbone of RESCA1, to form RESCA2-5, resulted in minor to major loss of stability of the corresponding $Al^{18}F$ complexes and thus, RESCA1 was found to be the most promising lead candidate for radiolabelling heat-sensitive biomolecules *via* the $Al^{18}F$-method.

This metal chelating agent becomes a bifunctional chelator (BFC) when it accommodates another reactive functional group for stable attachment to biomolecules. Different RESCA1 based BFCs were synthesised for conjugation to various biomolecules (**Figure 1**). RESCA1-tetrafluorophenyl ester (RESCA1-TFP) and RESCA1-maleimide (RESCA1-mal) have already been synthesised and can be used to conjugate the chelator with the biomolecule via the side-chain of a lysine or to conjugate the chelator in a site-specific way with a biomolecule via a maleimide-thiol reaction, respectively. However, it would be interesting to develop more BFCs, based on RESCA1 to create a broad generic platform **(Figure1).** RESCA1-KYGGG can potentially be used for site-specific labelling of proteins using sortase-mediated reactions and RESCA1-tetrazine (RESCA1-Tz) can potentially be used for

conjugation to a biomolecule via inverse-electron-demand Diels-Alder (IEDDA) "click" reaction between tetrazines (Tz) and *trans*-cyclooctene (TCO) derivatives (**Future perspectives**).

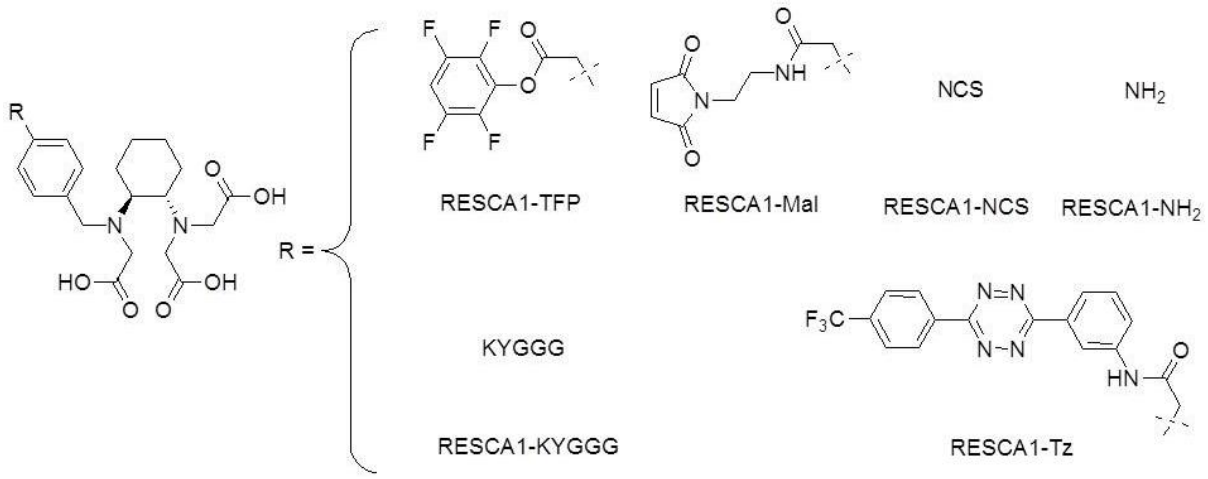

Figure 1: *Chemical structures of RESCA1-TFP, RESCA1-mal, RESCA1-NCS, RESCA1-NH_2, RESCA1-KYGGG and RESCA1-Tz*

To demonstrate the generic applicability of the proposed method we successfully labelled the heat-sensitive biomolecule human serum albumin (HSA) at ambient temperature with $\{Al^{18}F\}^{2+}$ with high radiochemical purity in less than 30 minutes. HSA (66.5 kDa) is a globular protein with a primary sequence made up of 585 amino acid residues and is the most abundant protein in human plasma (3.5-5 g/dl). Its high solubility, stability and circulatory half-life of approximately 16-18 h, make HSA the ideal vector for PET blood pool imaging applications and to evaluate the stability and kinetic inertness of the chelate *in vivo*. To our knowledge this was the first time that a heat-sensitive biomolecule was labelled via the $Al^{18}F$-method in one radiolabelling step. A patent was filed to protect this innovative method which may have a great impact on PET radiochemical space as it will facilitate the development of new fluorine-18 labelled heat-sensitive biomolecules. It would be interesting to implement the $Al^{18}F$-radiolabelling process on automated kit based synthesis modules (eg the "All-in-One module" (Trasis)) to further optimise and fully automate the $Al^{18}F$-radiolabelling method, allowing to produce multiple $Al^{18}F$ labelled compounds with a single batch of $\{Al^{18}F\}^{2+}$.

The pH of the labelling buffer is critically important for the formation of $\{Al^{18}F\}^{2+}$-chelates. If the pH is too low, the carboxyl groups are protonated which will hinder the coordination of aluminium and moreover the dominant fluoride species in equilibrium is likely to be HF. The optimal pH range for labelling *N*-benzyl-NODA was found to be between 3.8 and 4.2, whereas the optimal pH range for H_3L3 and RESCA1 lies somewhat higher between 4.5 and 5. Even at pH 5.5-6 high RCYs were still observed, indicating that also acid-sensitive proteins can be labelled with the proposed method. At even higher pH values, aluminium tends to form insoluble aluminium hydroxide. This results in lower

RCYs and therefore it is of great importance that the pH of the reaction mixture is carefully controlled by a suitable buffer.

As it was stated before, we aim to push the $Al^{18}F$-approach to a kit-based strategy for radiolabelling heat-sensitive biomolecules. This assertion is backed up by the similarity of the labelling methodology of other radiometals (^{68}Ga, ^{99m}Tc, etc…). McBride *et al.* reported a lyophilised kit for rapid radiofluorination of heat-stable peptides, based on the aluminium-fluoride procedure.[1] The formulation was optimised for pH, buffer, peptide to Al^{3+} ratio, bulking agent and radioprotectant. However, a final purification step using solid-phase extraction was still needed to obtain the final product with sufficient radiochemical purity for injection. Moreover, organic solvents and high temperatures (≥ 100 °C) were required for the complexation reaction, harsh conditions which are not compatible with heat-sensitive biomolecules. In an ideal situation, the labelling is carried out in water or saline, at room temperature, in less than 20 minutes, using a minimal amount of precursor (biomolecule conjugated to a chelator). Moreover, almost quantitative conversion (RCYs >95%) would allow to skip the final purification step, thus simplifying the method. Unfortunately, unlike radiolabelling with radiometals that are carrier-free (no presence of a stable isotope of the radiometal), fluorine-18 is heavily contaminated with stable fluorine-19 (up to 1000-fold relative to fluorine-18 mass) causing a drop in the chelation yield and requiring a higher amount of precursor.

A possible explanation for the decreased radiochemical yield as a function of the mass amount of fluorine could be the formation of other aluminum-fluoride $Al^{18/19}F_n^{(3-n)+}{}_{(aq)}$ (n = 1-6) species. Among all the metal-fluoride species, only the mono-fluoride can be efficiently chelated. Certainly, the addition of more aluminium in solution will lead to the formation of mainly aluminium mono-fluoride but as a consequence, more precursor would be required since there would be more “free” aluminium as well. With an excess of Al^{3+} relative to chelator, most likely the corresponding $\{AlOH\}^{2+}$ complex is formed and as a consequence there is less ligand available for chelation of $\{Al^{18}F\}^{2+}$. The presence of increased amounts of precursor will have a negative impact on the specific activity since, ideally in a kit-based labelling no purification step is applied. The specific activity of fluorine-18 thus proves to be an important parameter for the $Al^{18}F$ chelation yield. In order to enhance the radiolabelling conditions, finding the sources of the ^{19}F contamination is crucial. It has been reported that the main origin of fluorine-19 is the [^{18}O]water dispensing (loading) and delivery (unloading) system of the target, which often contains teflon (PTFE) tubings. This will be thoroughly investigated, but also solvents (H_2O), reagents (e.g. NaCl) anion-exchange columns and glasswork should be evaluated in an attempt to minimise ^{19}F contamination.

Important to discuss is the difference between residualising and non-residualising radiolabels and its effect on kidney retention and tumor uptake of protein-based radiotracers. Most peptides and small proteins (< 60 kDa) are excreted via the renal elimination pathway. After glomerular filtration these compounds might undergo receptor-mediated reabsorption in the renal tubuli cells. This process is mainly mediated by the endocytic megalin and cubulin receptors that are highly expressed on the apical side of proximal tubule cells.[2] Both receptors can interact with protein-based radioligands, followed by internalisation, transfer to the lysosomal compartment and degradation by proteolytic enzymes into amino acids and other (radio)catabolites. Lipophilic (radio)catabolites are able to diffuse through lysosomal and cellular membranes and thus leak out from cells, which is called the non-residualising effect.[3] Therefore radiocatabolites are cleared faster from the kidneys when peptides or small proteins are labelled using non-residualising halogens such as fluorine-18, bromine-86 or different iodine radioisotopes. In contrast, the use of residualising radiometals, including AlF-NODA complexes[4], results in extended retention of radioactivity in kidneys because these stable radiocomplexes are not able to diffuse out of the cells. We expect that the Al^{18}F-RESCA complex will behave like most other residualising radiometals, however it could occur that the Al^{18}F-complex is prone to degradation in the harsh environment of lysosomes and thus might behave rather as a non-residualising radiolabel. The residualising effect is not only important regarding kidney retention but might also occur in target cells of interest (e.g. cancer cells) if there is a high rate of internalisation. In this case the residualising effect is beneficial as tumor uptake may be higher and last longer.

Prostate-specific membrane antigen (PSMA) is overexpressed in a majority of primary and metastatic prostate cancer patients and is a promising target for specific prostate cancer imaging and therapy. Currently, [^{68}Ga]Ga-PSMA-HBEDD-CC is the most widely used PSMA-ligand. This urea-based PSMA inhibitor demonstrates excellent pharmacokinetics as well as stability *in vivo*, leading to its clinical applications worldwide for imaging of prostate cancer. However, labelling with fluorine-18 would offer advantages with respect to availability, batch size, and image resolution compared to labelling with gallium-68. In **chapter III and IV** we have developed three new Al^{18}F-labelled urea-based PSMA inhibitors, [^{18}F]AlF-PSMA-L3, [^{18}F]AlF-PSMA-NODA-MPAA and [^{18}F]AlF-PSMA-RESCA1. The urea-based inhibitor of PSMA, Glu-NH-CO-NH-Lys, can tolerate high temperature radiolabelling procedures, therefore NODA was suitable as chelator. The process of radiosynthesis and purification with preparative radio-HPLC was performed using a home-built remotely controlled system. However, it would be interesting to translate the synthesis of the most promising Al^{18}F-tracer, [^{18}F]AlF-PSMA-RESCA1 into a “kit”-preparation for further clinical studies. We found out that the purification strategy using an alumina-*N* cartridge is not suitable in this case because of low recovery. However,

this purification strategy might be very useful for more lipophilic radiotracers labelled via the Al^{18}F-method.

The Al^{18}F-tracers were evaluated in a preclinical setup and the results were compared with those of [^{68}Ga]Ga-HBEDD-CC-PSMA. Cell uptake and internalisation experiments with LNCaP (PSMA^{+}) and PC-3 (PSMA^{-}) cells revealed similar PSMA-specific internalisation and cell accumulation for [^{18}F]AlF-PSMA-RESCA1 and [^{68}Ga]Ga-PSMA-HBED-CC. Interestingly, [^{18}F]AlF-PSMA-L3 showed considerably lower uptake in LNCaP cells but demonstrated high LNCaP tumour uptake *in vivo*. Aware of the limited stability of [^{18}F]AlF-PSMA-L3 in rat plasma, we tested the stability of [^{18}F]AlF-PSMA-L3 in the cell culture medium that was used for cell uptake and internalisation experiments. Indeed, cell culture medium contains metal ions, amino acids, vitamins and proteins that could hamper the stability of the Al^{18}F-complex. As a consequence, this could influence results of cell uptake and internalisation experiments. After 45 min incubation in cell culture medium at 37 °C, only 67% of [^{18}F]AlF-PSMA-L3 was still intact as assessed by instant thin layer chromatography (iTLC), indicating demetallation and/or defluorination. This instability explains partially the lower *in vitro* cell binding of [^{18}F]AlF-PSMA-L3. In LNCap inoculated mice [^{18}F]AlF-PSMA-L3 showed high LNCaP tumour uptake but also increased bone uptake was observed over time. Non-specific bone accumulation might compromise the utility of the tracer for non-invasive imaging of prostate cancer metastasis, because most metastatic lesions occur in lymph nodes and in the bone. Therefore [^{18}F]AlF-PSMA-L3 is not the imaging tool of choice for early detection of prostate cancer recurrence.

[^{68}Ga]Ga-HBEDD-CC-PSMA, [^{18}F]AlF-PSMA-NODA-MPAA and [^{18}F]AlF-PSMA-L3 were cleared fast by the kidneys and almost no liver uptake was observed. In contrast, [^{18}F]AlF-PSMA-RESCA1 was cleared fast from plasma and PSMA-negative tissue by the kidneys but also hepatobiliary excretion was observed, which is consistent with the biodistribution data. Blocking studies with 2-PMPA proved that the observed retention in kidneys is predominatly due to PSMA-specific binding of the radiotracers rather than megalin/cubulin mediated residualising effect after glomerular filtration. Comparable specific tumor uptake was observed for [^{18}F]AlF-PSMA-RESCA1 and [^{68}Ga]Ga-HBEDD-CC-PSMA in a head-to-head comparison. To conclude, [^{18}F]AlF-PSMA-RESCA1 might be a promising tool for early detection of prostate cancer recurrence. It would be interesting to evaluate the pharmacokinetics of [^{18}F]AlF-PSMA-RESCA1 in primates and finally, clinical evaluation is needed to compare the sensitivity of [^{18}F]AlF-PSMA-RESCA1 with that of the established tracer [^{68}Ga]Ga-HBEDD-CC-PSMA in prostate cancer patients.

Immuno-PET combines selective localisation of antibodies or antibody-fragments at their target *in vivo* and high resolution and sensitivity of PET. Immuno-PET might play an important role as a

diagnostic tool in cancer staging but also as dosimetry tool to predict the optimal doses of subsequent radioimmunotherapy (RIT). Nanobodies are the smallest antigen-binding antibody fragments available and interact fast and with nanomolar affinity with their target. In **Chapter V** we demonstrated that the $Al^{18}F$-method using our chelator RESCA1, provides an efficient approach to radiolabel nanobodies with fluorine-18 at ambient temperature. We successfully derivatised (in a non-site-specific way) nanobodies targeting the CRIg receptor with RESCA1 and labelled it with $\{Al^{18}F\}^{2+}$ in good radiochemical yields in less than 30 minutes. Biodistribution studies showed that [^{18}F]AlF-RESCA1-NbV4m119 was mainly excreted *via* the renal pathway but also high liver uptake was observed in normal WT mice, which is expected because CRIg receptors are highly expressed on Kupffer cells. Biodistribution and microPET studies in $CRIg^{-/-}$ mice demonstrated absence of liver uptake, indicating excellent specificity of the $Al^{18}F$-labelled tracer. However, a relatively high bone uptake was observed in $CRIg^{-/-}$ mice, comparable to the observed bone uptake in WT mice, indicating *in vivo* instability of the tracer. To further investigate the unexpected bone uptake, we analysed urine samples using size exclusion chromatography 1 h and 3 h after i.v. injection of [^{18}F]AlF-RESCA1-NbV4m119. Only 11% and 2% of ^{18}F-activity respectively, corresponded to intact [^{18}F]AlF-RESCA1-NbV4m119. This shows that although $Al^{18}F$-RESCA1-NbV4m119 is stable *in vitro* in rat plasma, the radiotracer is metabolised to some extent in the kidneys. This high rate of *in vivo* degradation was also reported previously for ^{99m}Tc-labelled nanobodies targeting the epidermal growth factor receptor (EGFR). In this study the authors found that only 10% of labelled nanobody was intact in urine at 1 h p.i. indicating that this degradation is specific for nanobodies rather than to be dependent on the radiolabelling method. Nanobodies are efficiently reabsorbed in the renal proximal tubuli. Gainkam et al. showed elegantly that the megalin receptor plays an important role in this mechanism using megalin-knockout mice.[2]

Figure 2A shows an *ex vivo* autoradiogram of a renal tissue slice of a naïve WT mouse injected with [^{18}F]AlF-RESCA1-NbV4m119 and sacrificed at 1 h p.i.. The radioactivity is mainly concentrated in the renal cortex indicating that the kidney retention might be caused by tubular reabsorption and subsequent internalisation. One should consider the harsh environment in kidney lysosomes as a possible explanation for the observed elevated bone uptake. Indeed, after glomerular filtration [^{18}F]AlF-RESCA1-NbV4m119 is internalised and transported to lysosomes. Here, AlF-RESCA1 might be degraded and as a result $\{Al^{18}F\}^{2+}$ or $^{18}F^-$ as such could be recycled back into circulation, resulting in increased bone uptake values. If above assumption is correct, bone uptake could be lowered by preventing tubular reabsorption of the tracer (**Future perspectives**).

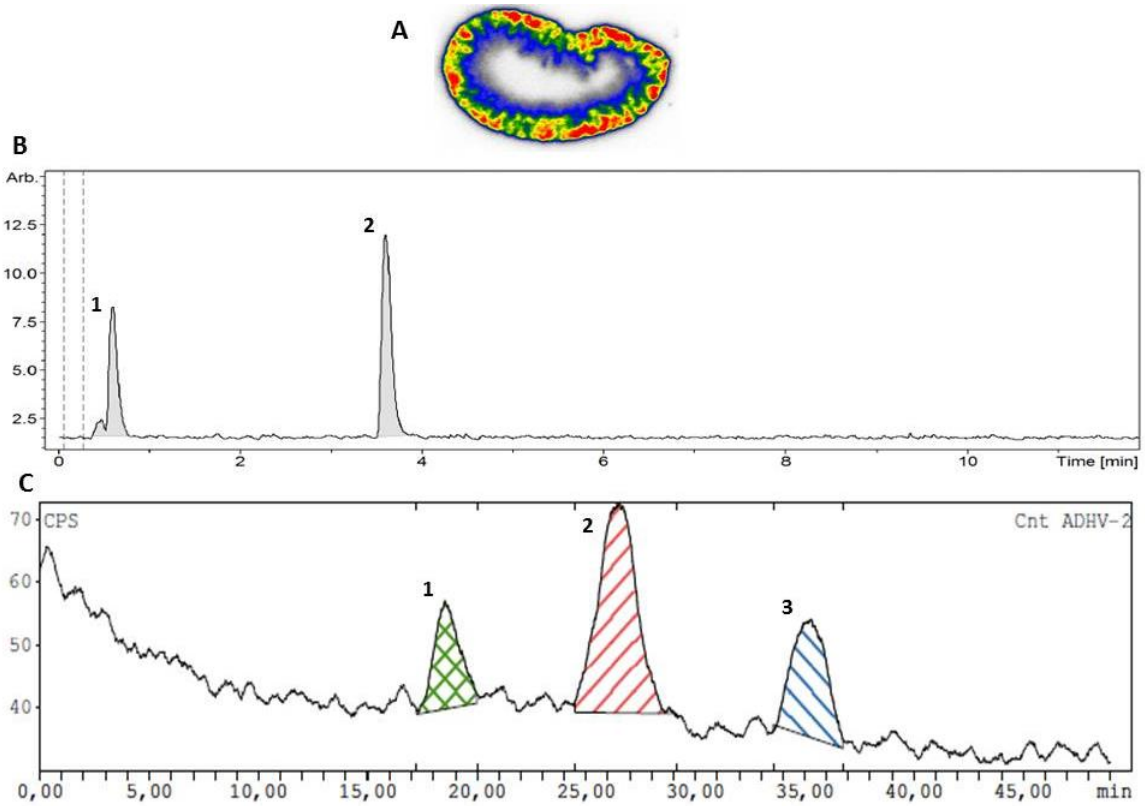

Figure 2: A: *Ex vivo autoradiography on renal tissue of naïve WT mouse injected with [^{18}F]AlF-RESCA1-NbV4m119 and sacrificed at 1 h after i.v. injection* ***B:*** *RP-HPLC analysis of the radiometabolite fraction eluting at 34.7 min on size exclusion HPLC of urine obtained from naïve WT mouse 1 h after i.v. injection of* [^{18}F]AlF-RESCA1-NbV4m119 *(**Chapter V, Figure 6**)*. An Acquity UPLC BEH C18 column (1.7 µm, 2.1 mm x 150 mm, Waters) was used with following method. Solvent A (H_2O) and solvent B (acetonitrile), flow rate 0.3 ml/min. The elution gradient was: 0-1 min: 99% A; 1-7 min: from 99% A to 1% A; 7-10 min: 1% A; 10.1-12 min: 99% A. Two major peaks are observed: peak 1, (Rt 0.6 min, 40 %) and peak 2 (Rt 3.6 min, 60%). **C:** *Radio-chromatogram of plasma sample of naïve WT mouse 1 h after i.v. injection of [^{18}F]AlF-RESCA1-NbV4m119 using size exclusion chromatography. A* Superdex 75 10/300 GL column (GE Healthcare) using sodium phosphate buffer (0.01M, pH 7.4, 0.14 M NaCl), as eluent at a flow rate of 0.5 ml/min was used. Three major peaks are observed: peak 1, protein-bound fraction (Rt 18.4 min, 19%), peak 2, *[^{18}F]AlF-RESCA1-NbV4m119 (Rt 26.8 min, 54%) and peak 3, free Al^{18}F-species,$^{18}F^-$ and/or ^{18}F-labelled degradation fragments (Rt 35.1 min, 27%)*

In an attempt to further identify the radiometabolites in urine, we collected the metabolite fraction eluting at 34.7 min (**Chapter V, Figure 6**) and analysed it using reverse phase chromatography (**Figure 2B**). The radiometabolites eluting at the void volume (peak 1, 40%) are probably $\{Al^{18}F\}^{2+}$, $^{18}F^-$ and/or very polar fluorine-18 containing degradation fragments of [^{18}F]AlF-RESCA1-NbV4m119. The remaining fraction (60%) elutes later (peak 2) which indicates that this fraction consist out of a somewhat more lipophilic radiometabolite of [^{18}F]AlF-RESCA1-NbV4m119. The *in vivo* stability of the tracer in blood was tested by analysing plasma 1 h after i.v. injection of [^{18}F]AlF-RESCA1-NbV4m119 using size exlusion chromatography (**Figure 2C**). The tracer was partially bound to other proteins present in plasma (peak 1, 19%), 54% of tracer was observed as intact [^{18}F]AlF-RESCA1-NbV4m119 (peak 2) and 27% of tracer was degraded in low molecular weight radiometabolites (peak 3). This

indicates good *in vivo* stability in blood of [^{18}F]AlF-RESCA1-NbV4m119. Studies with [^{18}F]AlF-RESCA1-HSA, which is not excreted by the kidneys due to the high molecular weight of albumin, confirms the high *in vivo* stability in blood of the Al^{18}F-RESCA1 complex because only minor increase in bone uptake was observed over time. PET imaging with [^{18}F]Al^{18}F-RESCA1-NbV4m119 did not show severe bone uptake at 1 h p.i. and images with high liver-to background ratios were obtained, indicating good *in vivo* imaging properties of Al^{18}F-RESCA1-NbV4m119 with high specificity for CRIg.

2. FUTURE PERSPECTIVES

The acyclic chelator RESCA1 demonstrated to be a good lead candidate for labelling of heat-sensitive biomolecules with fluorine-18, however more basic research is needed before this method can be used as a generic tool to radiolabel a diversity of biomolecules for PET applications.

Further fundamental research is needed in order to fully understand the different factors that influence the radiolabelling yield of the $Al^{18}F$-method. Among all the different aluminium-fluoride species, only mono-fluoride can be efficiently chelated by the proposed chelators. The identification of the different aluminium-fluoride species might be carried out by radio/UV-HPLC based on a methodology previously described.[5] The development of an analysis method would also allow us to further investigate the stability of the new complexes and determine whether the loss of the radionuclide is due to defluorination (breaking of the Al-F bond) or demetallation.

As derived from the molecular ion mass, the AlF-complexes formed with ligands H_3L3 and RESCA1 have a negative overall charge. The synthesis of new ligands with another coordinative set that would result in neutral or cationic complexes would allow us to understand how the net overall charge is affecting the biodistribution profile of $Al^{18}F$-labelled peptides and more specifically if it affects the uptake and retention in kidneys. Additional information on the structure of AlF-RESCA1 is necessary to understand the orientation of the chelating moieties and to rationally design new ligands. Therefore, single-crystal X-ray diffraction study of $Al^{19}F$-RESCA1 is desired. Synthesis and purification of the "cold" aluminium fluoride RESCA1 complex should be improved and different conditions should be tested to obtain a single crystal suitable for X-ray diffraction studies.

Uptake and retention in kidneys is often a problem for radiolabelled peptides and smaller proteins, with a molecular weight less than 60 kDa, which can pass the glomerular basement membrane. A substantial part of these radiolabelled peptides or proteins may be reabsorbed and retained in the proximal tubule of the kidneys after glomerular filtration. This causes a high radiation burden for the kidneys, hinders diagnostic accuracy and limits radionuclide therapy applications. In many cases kidney retention might be reduced by (partially) blocking tubular reabsorption after pre- or co-injection of basic amino acids and other reagents such as gelatin-based plasma expanders like Gelofusine. Another interesting approach to reduce radioactivity accumulation in the kidneys is based on conjugation of chelators to peptides or proteins by cleavable linkers. The radionuclide, together with the chelator will be cleaved off by specific brush-border enzymes in kidneys before internalisation in the proximal tubule. In the design of tracers with cleavable linkers, the linkers should be stable against enzymes in plasma and should be cleaved off specifically by the renal brush

border enzymes. It was shown that the use of glycyl-L-lysine or glycyl-L-tyrosine containing linkers provides impressive reduction of renal uptake of ^{125}I-labelled antibody fragments.[6] Both strategies for reducing renal accumulation could be explored for different Al^{18}F-labelled peptides and proteins.

In **Chapter V** we demonstrated that our Al^{18}F-chelator RESCA1 provides an efficient approach to radiolabel nanobodies with fluorine-18 at ambient temperature. However, the first step of this approach is a non-specific derivatisation of the nanobody with one or more Al^{18}F-chelators, resulting in potential batch-to-batch differences due to degree and site of derivatisation. Therefore, site-specific incorporation of the chelator into the nanobody would even further improve this promising radiolabelling approach. A possible strategy is using the site-specific maleimide-thiol reaction for derivatisation of nanobodies. Another promising approach is combining the Al^{18}F-method with the sortase-mediated conjugation method **(Figure 2).**[7,8]

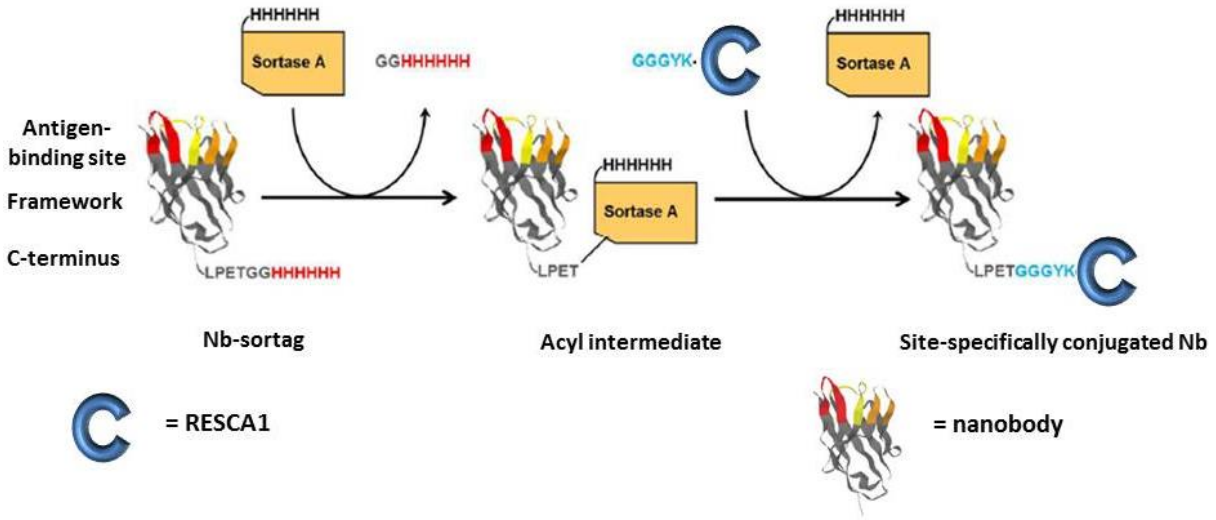

Figure 2: *Sortase-mediated site-specific conjugation method. S. aureus sortase A recognises the C-terminal sortag (LPETGG) of the nanobody and cleaves the peptide bond between T and G, with release of the downstream His-tag. Next, a nucleophilic attack of the triglycine-functionalised chelator (RESCA1-KYGGG) on the acyl-enzyme intermediate leads to the formation of a new peptide bond with the nanobody, resulting in the site-specifically conjugated nanobody. (adjusted from Massa et al.)*[9]

In cancer research, pretargeted PET imaging has emerged as an effective two-step approach that combines the affinity and selectivity of antibodies with the rapid pharmacokinetics and favourable dosimetry of smaller molecules radiolabelled with short-lived radionuclides (e.g. fluorine-18). This approach can be based on a bioorthogonal inverse-electron-demand Diels-Alder (IEDDA) "click" reaction between tetrazines and *trans*-cyclooctene (TCO) derivatives. Recently, new [^{18}F]TCO-dienophiles and tetrazines with high reactivity for the IEDDA reaction, improved *in vivo* stability and favourable pharmacokinetics were developed in the laboratory of Radiopharmacy. However, the synthesis of a ^{18}F-labelled variant of tetrazine, which to date has eluded researchers, would be an

especially useful development in the field of the pretargeting approach.[10] Standard radiolabelling approaches (harsh reaction conditions) cannot be used to introduce fluorine-18 in the tetrazine moiety because of the limited chemical stability. The proposed $Al^{18}F$-method might be an ideal approach to overcome these problems. Therefore it would be interesting to conjugate a tetrazine moiety with RESCA1 and radiolabel this RESCA1-tetrazine (RESCA1-Tz) fragment with $\{Al^{18}F\}^{2+}$. Tetrazine-moieties are known to give solubility issues, therefore it may be necessary to introduce polar linkers (PEG-linkers) to counteract this problem.

3. REFERENCES

(1) McBride, W. J., D'Souza, C. a, Karacay, H., Sharkey, R. M., and Goldenberg, D. M. (2012) New lyophilized kit for rapid radiofluorination of peptides. *Bioconjug. Chem. 23*, 538–47.

(2) Olive, L., Gainkam, T., Caveliers, V., Devoogdt, N., Vanhove, C., Xavier, C., Boerman, O., Muyldermans, S., Bossuyt, A., and Lahoutte, T. (2011) Localization , mechanism and reduction of renal retention of technetium-99m labeled epidermal growth factor receptor-specific nanobody in mice. *Contrast Media Mol. Imaging 6*, 85–95.

(3) Strand, J., Nordeman, P., Honarvar, H., Altai, M., and Orlova, A. (2015) Site-Specific Radioiodination of HER2-Targeting Affibody Molecules using 4-Iodophenethylmaleimide Decreases Renal Uptake of Radioactivity. *ChemistryOpen 4*, 174–182.

(4) McBride, W. J., Sharkey, R. M., and Goldenberg, D. M. (2013) Radiofluorination using aluminum-fluoride ($Al^{18}F$). *EJNMMI Res. 3*, 36–47.

(5) Frankowski, M. (2012) Simultaneous determination of aluminium , aluminium fluoride complexes and iron in groundwater samples by new HPLC – UVVIS method. *Microchem. J. 101*, 80–86.

(6) Akizawa, H., Imajima, M., Hanaoka, H., Uehara, T., Satake, S., and Arano, Y. (2013) Renal brush border enzyme-cleavable linkages for low renal radioactivity levels of radiolabeled antibody fragments. *Bioconjug. Chem. 24*, 291–299.

(7) Guimaraes, C. P., Witte, M. D., Theile, C. S., Bozkurt, G., Kundrat, L., Blom, A. E. M., and Ploegh, H. L. (2013) Site-specific C-terminal and internal loop labeling of proteins using sortase-mediated reactions. *Nat. Protoc. 8*, 1787–1799.

(8) Paterson, B. M., Alt, K., Jeffery, C. M., Price, R. I., Jagdale, S., Rigby, S., Williams, C. C., Peter, K., Hagemeyer, C. E., and Donnelly, P. S. (2014) Enzyme-mediated site-specific bioconjugation of metal complexes to proteins: Sortase-mediated coupling of copper-64 to a single-chain antibody. *Angew. Chemie - Int. Ed. 53*, 6115–6119.

(9) Massa, S., Vikani, N., Betti, C., Ballet, S., Vanderhaegen, S., Steyaert, J., Descamps, B., Vanhove, C., Bunschoten, A., Leeuwen, F. W. B., Hernot, S., Caveliers, V., Lahoutte, T., Muyldermans, S., Xavier, C., and Devoogdt, N. (2016) Sortase A-mediated site-specific labeling of camelid single-domain antibody-fragments: a versatile strategy for multiple molecular imaging modalities. *Contrast Media Mol. Imaging*. (Epub ahead of print)

(10) Reiner, T., and Zeglis, B. M. (2014) The inverse electron demand Diels-Alder click reaction in radiochemistry. *J. Label. Compd. Radiopharm. 57*, 285–290.

SUMMARY

Positron emission tomography (PET) is a sensitive, non-invasive imaging technology that produces three-dimensional images showing the *in vivo* concentration of radiotracers, which are usually labelled with short-lived positron emitting radioisotopes. Among β^+-emitting radioisotopes, fluorine-18 is currently the radionuclide of choice for PET because of its favourable nuclear decay characteristics and ease of production. Clinicians in the molecular imaging community are not only interested in in using small organic molecules but also high molecular weight biomolecules and peptides are increasingly being considered for use as PET-radiopharmaceuticals. However, the incorporation of fluorine-18 into heat-sensitive and complex biomolecules creates substantial challenges for radiochemists.

The $Al^{18}F$-labelling method is a relatively new approach that allows radiofluorination of biomolecules such as peptides and proteins in a one-step procedure and in aqueous solution. McBride *et al.* published the first study using a chelator for $\{Al^{18}F\}^{2+}$ labelling in 2009. Although many studies demonstrated the versatility of the $Al^{18}F$ approach to radiolabel peptides, the approach has limited applicability for heat sensitive biomolecules due to high temperatures required for the complexation reaction (≥ 100 °C) when used with macrocyclic complexing agents such as NOTA and NODA. Therefore the objective of this thesis was to develop new polydentate ligands that allow chelation of $\{Al^{18}F\}^{2+}$ at moderate temperatures (<40 °C), whilst maintaining *in vivo* stability. In this thesis, we identified new chelators that allow efficient complexation of $\{Al^{18}F\}^{2+}$ using mild labelling conditions, whilst maintaining *in vivo* stability.

The first set of chelators that we developed are acyclic ligands with an N_2O_3 coordinative set or N_3O_2 bis-phenol structure. It was observed that only ligands containing the fragment ethylenediamine-*N*,*N*'-diacetic acid (H_3L1-L4) were able to efficiently chelate aluminium fluoride. Ligands without this arrangement of functional groups (H_3L5-8) did not complex aluminium fluoride with good RCY under the conditions tested. Successful labelling of two compounds, (H_3L1) and (H_3L3) was established. H_3L1 and H_3L3 both have excellent labelling properties but, unfortunately, [^{18}F]AlF-L1 was not stable *in vitro*. [^{18}F]AlF-L3 complex demonstrated a stability in PBS and in rat plasma comparable to that of the previously reported [^{18}F]AlF-*N*-benzyl-NODA complex, up to 60 minutes, but suffered from decomplexation after extended incubation times. Although *in vitro* incubation in rat plasma showed slow decomposition, biodistribution of [^{18}F]AlF-L3 showed absence of bone uptake indicating that *in vivo* defluorination or demetalation if any, is limited. Optimal labelling results were obtained at pH 4.5-5 and it has been shown that the specific activity of fluorine-18 proves to be an important parameter for the $Al^{18}F$ chelation yield. The acyclic chelator H_3L3 demonstrated to be a good lead

candidate for labelling of heat-sensitive biomolecules with fluorine-18. However, there was still room for improvement regarding the stability of the [^{18}F]AlF-L3 complex, so that the synthesis of improved derivatives was warranted.

We explored whether incorporation of a *trans*-cyclohexyl moiety into H_3L1, to form restrained complexing agent 1 (RESCA1), would increase steric rigidity of the AlF-complex, improving the orientation of the chelating groups and as a result improving the stability of the resulting AlF-complex. RESCA1 is an acyclic pentadentate ligand with an N_2O_3 coordinative set of donor atoms and was synthesised starting from commercially available chemicals. RESCA1 as such showed excellent labelling properties and its Al^{18}F-complex demonstrated high *in vitro* and *in vivo* stability. Small changes in the backbone of RESCA1, to form RESCA2-5, resulted in minor to major loss of stability of the corresponding Al^{18}F-complexes and thus, RESCA1 was found to be the most promising lead candidate for radiolabelling heat-sensitive biomolecules *via* the Al^{18}F-method. To demonstrate the generic applicability of the proposed method we successfully labelled the heat-sensitive biomolecule Human Serum Albumin (HSA) at ambient temperature with {Al^{18}F}$^{2+}$ with high radiochemical purity in less than 30 minutes. [^{18}F]AlF-RESCA1-HSA showed excellent *in vitro* and *in vivo* stability. Moreover, [^{18}F]AlF-RESCA1-HSA showed favourable properties for PET blood pool imaging applications.

Prostate-specific membrane antigen (PSMA) is overexpressed in a majority of primary and metastatic prostate cancer patients and is a very promising target for specific prostate cancer imaging and therapy. Currently, [^{68}Ga]Ga-PSMA-HBEDD-CC is the most widely used PSMA-ligand. This urea-based PSMA inhibitor demonstrates excellent pharmacokinetics as well as stability *in vivo*, leading to its clinical applications worldwide for imaging of prostate cancer. However, labelling with fluorine-18 would offer advantages with respect to availability, batch size, and image resolution compared to labelling with gallium-68. In this thesis we have developed three new Al^{18}F-labelled urea-based PSMA inhibitors, [^{18}F]AlF-PSMA-L3, [^{18}F]AlF-PSMA-NODA-MPAA and [^{18}F]AlF-PSMA-RESCA1. Cell uptake and internalisation experiments with LNCaP (PSMA$^+$) and PC-3 (PSMA$^-$) cells revealed similar specific internalisation and cell accumulation for [^{18}F]AlF-PSMA-RESCA1 and [^{68}Ga]Ga-PSMA-HBED-CC. In contrast, [^{18}F]AlF-PSMA-NODA-MPAA and [^{18}F]AlF-PSMA-L3 showed considerable lower uptake in LNCaP cells. Moreover, [^{18}F]AlF-PSMA-L3 suffers from instability over time which compromises the utility of this tracer. All tracers were cleared fast from plasma and PSMA-negative tissue mainly by the kidneys but also hepatobiliary excretion was observed in the case of [^{18}F]AlF-RESCA1-PSMA. High specific accumulation of all tracers was observed on PSMA$^+$ LNCaP tumour slices and autoradiography on human prostate tumour tissue showed specific affinity for the human PSMA receptor. Comparable specific tumor uptake was observed for [^{18}F]AlF-PSMA-RESCA1 and [^{68}Ga]Ga-HBEDD-CC-

PSMA in a head-to-head comparison in $PSMA^+$ tumor bearing mice. To conclude, [^{18}F]AlF-PSMA-RESCA1 might be a promising tool for early detection of prostate cancer recurrence.

Nanobodies are promising tools in molecular imaging and have many advantages in comparison with full-size antibodies. We demonstrated that the Al^{18}F-method using RESCA1 provides an efficient approach to radiolabel nanobodies with fluorine-18 at ambient temperature. We successfully derivatised nanobodies targeting the CRIg receptor with RESCA1 and labelled the conjugate with $\{Al^{18}F\}^{2+}$ in good radiochemical yields at ambient temperature. [^{18}F]AlF-RESCA1-NbV4m119 was purified with preparative HPLC resulting in the Al^{18}F-tracer with a radiochemical purity higher than 97% and the compound showed excellent *in vitro* stability. Furthermore, we successfully optimised a generic radio-HPLC-HRMS system for the analysis and quality control of radiolabelled nanobodies. Biodistribution studies in mice showed that [^{18}F]AlF-RESCA1-NbV4m119 was mainly excreted *via* the renal pathway but also high liver uptake was observed in normal WT mice, which is expected because CRIg receptors are highly expressed on Kupffer cells. Biodistribution and microPET studies in $CRIg^{-/-}$ mice demonstrated absence of significant uptake in liver, indicating excellent specificity of the Al^{18}F-labelled tracer. Almost no intact [^{18}F]AlF-RESCA1-NbV4m119 was found in urine at 3 h p.i. and relatively high bone uptake was observed, indicating *in vivo* instability of the tracer. However, *in vivo* PET imaging in mice did not show significant bone uptake at 1 h p.i. and high liver-to background images were obtained, indicating favourable *in vivo* imaging properties of [^{18}F]AlF-RESCA1-NbV4m119 with high specificity for CRIg. This generic radiolabelling, purification and characterisation method provides a general approach for radiolabelling of nanobodies with fluorine-18.

In conclusion, the acyclic chelator RESCA1 demonstrated to be a good lead candidate for labelling of heat-sensitive biomolecules with fluorine-18. This new class of AlF-chelators may have a great impact on PET radiochemical space as it will stimulate the rapid development of new fluorine-18 labelled peptides and other heat-sensitive biomolecules. However, more basic research is needed before this method can result in a kit-based, radiolabelling strategy.

SAMENVATTING

Positron emissie tomografie (PET) is een gevoelige, niet-invasieve beeldvormingstechniek die toelaat de verdeling van een radioactief gemerkte ligand *in vivo* te visualiseren. Deze radioliganden zijn meestal gemerkt met kortlevende radionucliden zoals koolstof-11, gallium-68 of fluor-18. Fluor-18 is dankzij zijn bijna ideale vervaleigenschappen en eenvoudige productiemethode het meest gebruikte radionuclide voor PET. Er is tegenwoordig steeds meer interesse om ook hitte-gevoelige en complexe peptiden en biomoleculen te merken met fluor-18. Omdat de traditionele manier om fluor-18 in organische moleculen in te bouwen strenge condities vereist die niet compatibel zijn met fragiele biomoleculen, moeten andere methoden ontwikkeld worden.

De $Al^{18}F$-merkingsstrategie is een relatief nieuwe methode die kan gebruikt worden om fluor in peptiden en biomoleculen in slechts één synthesestap in te bouwen. Het eerste raport van zo'n merking die gebruik maakt van de $Al^{18}F$-strategie werd in 2009 gepubliceerd door McBride et al. Op dit ogenblik heeft de $Al^{18}F$-strategie slechts een beperkte toepasbaarheid omdat hoge temperaturen (≥ 100 °C) noodzakelijk zijn voor de complexatiereactie indien gebruikt gemaakt wordt van de reeds gekende macrocyclische chelatoren NODA en NOTA. Daarom was het hoofddoel van deze thesis het ontwikkelen van nieuwe chelatoren die wel toelaten om $\{Al^{18}F\}^{2+}$ te cheleren op kamertemperatuur. Een belangrijke vereiste is dat de gevormde $Al^{18}F$-complexen voldoende stabiel zijn *in vivo* gedurende enkele uren.

De eerste set van chelatoren die ontwikkeld werd gedurende deze thesis zijn alle acyclische chelatoren die bestaan uit een N_2O_3 coördinatieve set of een bis-fenol structuur. Het werd duidelijk dat enkel liganden (H_3L1-L4) die een ethyleendiamine-N,N-diazijnzuur fragment bezitten in hun structuur efficiënt $\{Al^{18}F\}^{2+}$ kunnen complexeren. Bij de liganden (H_3L5-8) die dit motief niet bezitten werd geen efficiënte complexatie waargenomen in deze studie. De liganden (H_3L1) en (H_3L3) konden beide succesvol gebruikt voor de complexatie van $\{Al^{18}F\}^{2+}$, maar helaas bleek reeds uit *in vitro* stabiliteitstesten dat het gevormde [^{18}F]AlF-L1 niet stabiel was, dit in tegenstelling tot het gevormde [^{18}F]AlF-L3. De *in vitro* stabilieteitstesten in ratplasma toonden aan dat [^{18}F]AlF-L1 een gelijkaardige stabiliteit vertoont als [^{18}F]AlF-*N*-benzyl-NODA tot 1 uur na incubatie. Op latere tijdstippen werd echter significante instabiliteit aangetoond voor [^{18}F]AlF-L3. Desondanks bleek uit de resultaten van de *ex vivo* biodistributie in gezonde muizen met [^{18}F]AlF-L3 dat er slechts in beperkte mate *in vivo* defluorinering of decomplexering plaatsvindt, aangezien er slechts beperkte botopname geobserveerd werd. De nieuw ontwikkelde acyclische chelator H_3L3 heeft goede eigenschappen maar aangezien er nog ruimte is voor verbetering aangaande de stabiliteit, is de ontwikkeling van nieuwe derivaten noodzakelijk.

Er werd een *trans*-cyclohexyl fragment ingebouwd in H_3L1 om zo "restrained complexing agent 1" (RESCA1) te vormen. We onderzochten of de sterische rigiditeit van het AlF complex en de oriëntatie van de chelerende groepen hierdoor zouden verbeteren om zo het gevormde AlF complex stabieler te maken.

RESCA1 is een acyclisch pentadentaatligand (N_2O_3) en werd gesynthetiseerd uitgaande van commerciëel beschikbare chemicaliën. RESCA1 vertoonde uitstekende complexeringseigenschappen en *in vitro* en *in vivo* stabiliteitsstudies toonden aan dat het resulterende $Al^{18}F$-complex zeer stabiel was. Kleine wijzigigen in de structuur van RESCA1 (RESCA2-5), leidden in mindere of meerdere mate tot stabiliteitsverlies van de overeenkomstige $Al^{18}F$-complexen. Bijgevolg is RESCA1 tot dusver de meest geschikte chelator om hitte-gevoelige biomoleculen te merken met $\{Al^{18}F\}^{2+}$. De generische toepasbaarheid van deze methode werd aangetoond door het hitte-gevoelige proteïne Humaan Serum Albumine (HSA) succesvol met $\{Al^{18}F\}^{2+}$ te merken bij kamertemperatuur. [^{18}F]AlF-RESCA1-HSA werd geproduceerd in minder dan 30 minuten met een hoge radiochemische zuiverheid. Het $Al^{18}F$-gemerkte biomolecule vertoonde uitstekende *in vitro* en *in vivo* stabiliteit.

Prostaat-specifiek membraan antigen (PSMA) wordt overvloedig tot expressie gebracht bij de meeste vormen van primaire en gemetastaseerde prostaatkanker en is daardoor een veelbelovend doelwit voor beeldvorming en therapie van prostaatkanker. De PSMA inhibitor [^{68}Ga]Ga-PSMA-HBEDD-CC is, dankzij zijn gunstige farmacokinetiek, specificiteit, sensitiviteit en *in vivo* stabiliteit, momenteel wereldwijd het meest gebruikte ligand voor beeldvorming van prostaatkanker met PET. Een fluor-18-derivaat zou echter significante voordelen kunnen opleveren.

In deze thesis hebben we drie $Al^{18}F$-gemerkte PSMA inhibitors ontwikkeld: [^{18}F]AlF-PSMA-L3, [^{18}F]AlF-PSMA-NODA-MPAA en [^{18}F]AlF-PSMA-RESCA1. Experimenten met LNCaP ($PSMA^+$) en PC-3 ($PSMA^-$) cellen toonden vergelijkbare celopname en internalisatie aan voor [^{18}F]AlF-PSMA-RESCA1 en [^{68}Ga]Ga-PSMA-HBED-CC. [^{18}F]AlF-PSMA-NODA-MPAA en [^{18}F]AlF-PSMA-L3 daarentegen werden significant minder opgenomen in LNCaP cellen. Bovendien is [^{18}F]AlF-PSMA-L3 instabiel, wat zijn bruikbaarheid beperkt. Alle radioliganden werden snel renaal geklaard uit plasma en PSMA-negatief weefsel. Bij [^{18}F]AlF-RESCA1-PSMA werd ook hepatobiliaire klaring waargenomen. Autoradiografiestudies toonden hoge opstapeling van alle radioliganden aan in $PSMA^+$ LNCaP tumorcoupes en studies op humaan prostaatkankerweefsel wezen op specifieke affiniteit voor de humane PSMA receptor. Vergelijkbare tumoropname werd waargenomen voor [^{18}F]AlF-PSMA-RESCA1 en [^{68}Ga]Ga-HBEDD-CC-PSMA in $PSMA^+$ xenograftmuizen. We kunnen dus besluiten dat [^{18}F]AlF-PSMA-RESCA1 een beloftevolle PET-ligand zou kunnen zijn voor het vroegtijdig opsporen van prostaatkanker.

Nanobodies bezitten een hoge affiniteit en selectiviteit voor hun doelwit en hebben bovendien een korte biologische halfwaardetijd, vergelijkbaar met de fysische halfwaardetijd van fluor-18. Er werd aangetoond dat nanobodies doeltreffend kunnen gemerkt worden met fluor-18 op kamertemperatuur via de $Al^{18}F$-methode met RESCA1. We derivatiseerden nanobodies gericht tegen de CRIg receptor met RESCA1 en merkten dit derivaat succesvol met $\{Al^{18}F\}^{2+}$. [^{18}F]AlF-RESCA1-NbV4m119 werd opgezuiverd met preparatieve hoge druk vloeistofchromatografie (HDVC) en leverde een $Al^{18}F$-ligand op met een radiochemische zuiverheid van meer dan 97% en een uitstekende *in vitro* stabiliteit. Daarnaast optimaliseerden we een generisch radio-HDVC-HRMS (hoge resolutie massaspectrometrie) systeem voor de analyse en kwaliteitscontrole van de gemerkte nanobodies. Biodistributiestudies in muizen toonden aan dat [^{18}F]AlF-RESCA1-NbV4m119 voornamelijk uitgescheiden werd via de nieren. In gezonde muizen werd zoals verwacht ook hoge leveropname gezien, aangezien CRIg receptoren veel voorkomen op Kupffer cellen. Met biodistributie- en microPET studies in $CRIg^{-/-}$ muizen werd geen leveropname gezien, wat een uitstekende specificiteit van de $Al^{18}F$-gemerkte radiotracer aantoonde. Tegen de verwachtingen in werd quasi geen intact [^{18}F]AlF-RESCA1-NbV4m119 gevonden in de urine drie uur na injectie en biodistributie studies toonden een relatief hoge botopname aan, wat wijst op enige *in vivo* instabiliteit. Deze merkings-, karakterisatie- en opzuiveringsmethode kan generisch gebruikt worden voor het labelen van nanobodies met fluor-18.

We kunnen besluiten dat de chelator RESCA1 tot dusver de beste ligand is voor het merken van hitte-gevoelige biomoleculen en we zijn ervan overtuigd dat deze nieuwe klasse van chelatoren een belangrijke rol kan spelen in de verdere ontwikkeling van fluor-18 gemerkte PET liganden. Er moet echter nog bijkomend fundamenteel onderzoek uitgevoerd worden vooraleer deze strategie kan evolueren naar een klinisch bruikbare merkingskit.

CURRICULUM VITAE

Personal information

Name:	Cleeren Frederik
E-mail:	Frederik.cleeren@pharm.kuleuven.be
Phone number:	+32 485 08 26 41
Date of Birth	August 23th, 1989
Place of Birth	Gent, Belgium

Education

2012-2016	PhD in Pharmaceutical Sciences Laboratory for Radiopharmacy, KU Leuven, Leuven, Belgium *Promoter*: Prof. Guy Bormans
2010-2012	Master in drug development, Pharmaceutical sciences Faculty of Pharmaceutical Sciences, KU Leuven, Leuven, Belgium *Thesis: Development of PET tracers for the visualisation of PD10A* *Internship*: Pharmacy Kinget, Bertem, Belgium
2007-2010	Bachelor in pharmaceutical science, Pharmaceutical sciences Faculty of Pharmaceutical Sciences, KU Leuven, Belgium
Secondary School	Latin – Mathematics KSO Glorieux, Ronse, Belgium

Grants/awards

- The article *"New chelators for low temperature Al^{18}F-labeling of biomolecules"* has been selected to be featured in ACS Editors' Choice in addition to being published in Bioconjugate Chemistry.
- The article "PET imaging of MMR-expressing macrophages in tumor stroma using ^{18}F-radiolabeled camelid single-domain antibody fragments" has received the Alavi–Mandell award.
- FWO travel grant, June 2016, International Scientific Contacts (San Diego)

Additional courses during doctoral training

- Laboratory Animal Science module I and II (*certificate of 'expert laboratory animal leader'*, FELASA C)
- INMiND training course. *PET and SPECT Radiopharmaceuticals Preparation: Design, Radiolabelling Strategy, Radiosynthesis and Drug Development.*

- INMiND training course. *GMP and Radiopharmaceuticals*
- EMIDS Workshop 'Nanobody Theranostics'
- Online Excel course VIB (advanced)
- Medical Writing (Sven Deferme)
- Radiopharmaceuticals

Teaching experience

Representative:
- Member as academic staff (representative AAP-BAP) of the board of the Faculty of Pharmaceutical Sciences (2014-present)

Teaching:
- Practical course Radiopharmaceuticals (Master after master clinical Pharmacist) - 2013-present
- Practical course complex matrices (Bachelor Pharmaceutical science) - 2013-present
- Assistent of the year 2013

Master students:
- Inias Demunynck, Masterthesis Pharmaceutical science, "Low temperature fluorine-18 radiolabelling of exendin-4: new chelator for the [^{18}F]AlF method", 2014-2015
- Joey Amankwah, Masterthesis Pharmaceutical science, "Radiolabelling of biomolecules with [Al^{18}F]$^{2+}$", 2013-2014

Skills and techniques

- Languages:
  - Dutch: native language
  - English
  - French (basic knowledge)

- Software:
  - Microsoft Office: Excel, Word and PowerPoint
  - Optiquant
  - PMOD (basic knowledge)

- Techniques:
  - Organic chemistry (basic knowledge)
  - Analytical and preparative HPLC
  - Standard ^{18}F-labelling
  - Al^{18}F-labelling
  - ^{89}Zr-labelling of biomolecules
  - ^{68}Ga-labelling
  - ^{99m}Tc-labelling
  - Digital autoradiography
  - µPET
  - Small animal handling
  - Tumor models

- LC-HRMS (small organic molecules and proteins)
- Protein separation techniques (SEC chromatography)
- Peptide synthesis (basic knowledge)

LIST OF PUBLICATIONS

Papers in international peer-reviewed journals

- **Cleeren, F.**, Lecina, J., Billaud, E. M., Ahamed, M., Verbruggen, A., and Bormans, G. M. (2016) New chelators for low temperature Al^{18}F-labeling of biomolecules. Bioconjug. Chem. 27, 790–798.

- Blykers, a., Schoonooghe, S., Xavier, C., D'hoe, K., Laoui, D., D'Huyvetter, M., Vaneycken, I., **Cleeren, F.**, Bormans, G., Heemskerk, J., Raes, G., De Baetselier, P., Lahoutte, T., Devoogdt, N., Van Ginderachter, J. a., and Caveliers, V. (2015) PET imaging of MMR-expressing macrophages in tumor stroma using ^{18}F-radiolabeled camelid single-domain antibody fragments. J. Nucl. Med. 56, 1265-1271

- Ory, D., Van den Brande, J., de Groot, T., Serdons, K., Bex, M., Declercq, L., **Cleeren, F.**, Ooms, M., Van Laere, K., Verbruggen, A., and Bormans, G. (2015) Retention of [^{18}F]fluoride on reversed phase HPLC columns. J. Pharm. Biomed. Anal. 111, 209–214.

Patents

- **Cleeren, F.**, Lecina, J., Billaud, E. M., Ahamed, M., Verbruggen, A., and Bormans, G. M. (2016) Methods for low temperature fluorine-18 radiolabelling of biomolecules (WO/2016/065435)

Conference presentations

- SNMMI 2016, San Diego, USA, June (oral presentation)
  New complexing agent for one-step Al^{18}F-labeling of heat-sensitive biomolecules: RESCA1

- SNMMI 2016, San Diego, USA, June (oral presentation)
  Radiosynthesis and preclinical evaluation of Al^{18}F-RESCA1-PSMA for PET imaging of prostate cancer

- ESSR Salzburg 2016, Austria, April (oral presentation)
  New complexing agent for Al^{18}F-labelling of heat-sensitive biomolecules: Synthesis and preclinical evaluation of Al^{18}F-RESCA1-HSA

- ISRS Columbia 2015, USA (poster presentation)
  Radiosynthesis and preclinical evaluation of new Al^{18}F-labelled Urea-based PSMA inhibitors for PET imaging of prostate cancer

- Belnuc Maastricht 2015, The Nederlands (poster presentation)
  Al^{18}F-labelled Urea-based PSMA inhibitors for PET imaging of prostate cancer

- ESSR Pamplona 2014, Spain (oral presentation)
  Analysis of [^{18}F]-labelled nanobodies with radio-UPLC-HRMS

- ESSR Pamplona 2014, Spain (poster presentation)
  Validation of the Thermo Fisher Carbopac PA20 column for quality control of 2-[^{18}F]fluoro-2-deoxy-D-glucose

- Belgian Society of Pharmaceutical Sciences 2013, Belgium (oral presentation)
  ^{18}F-labeling of biomolecules: [Al^{18}F]$^{2+}$ chelation-based radiolabeling method

- Ulla Summer School London 2013, UK (poster presentation)
  ^{18}F-labeling of biomolecules: [Al^{18}F]$^{2+}$ chelation-based radiolabeling method